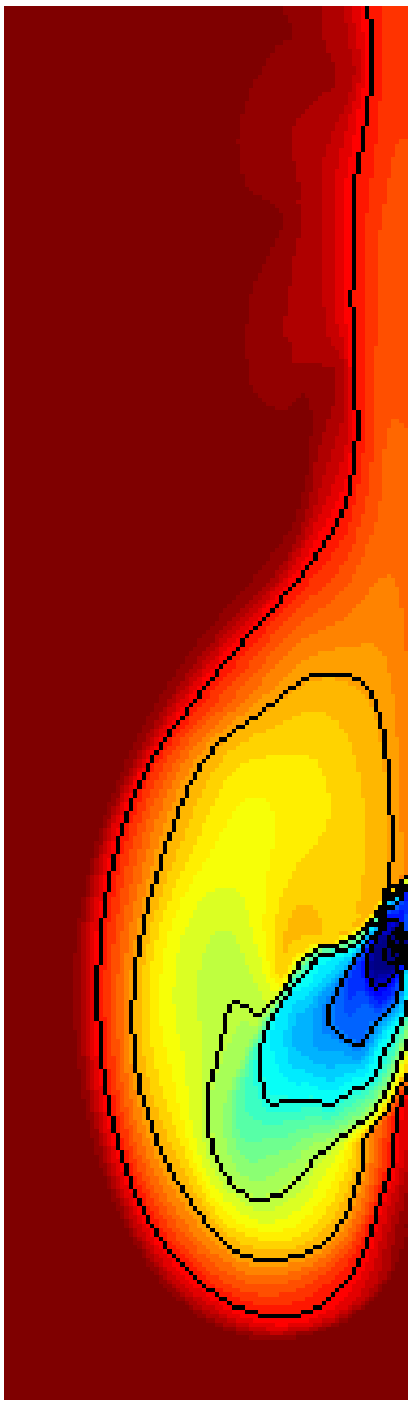

Modelling the Rhine Region Of Freshwater Influence on a non-straight coast

Additional MSc Thesis

Matthijs R.A. Gensen

21st of September 2016

TU Delft Delft University of Technology

Modelling the Rhine Region Of Freshwater Influence on a non-straight coast

Exploring the effect of the Sand Engine on the Rhine ROFI

September 2016

Additional MSc Thesis

Assessment by:

Prof.dr. J.D. Pietrzak – Delft University of Technology

Ir. S. Rijnsburger – Delft Univeristy of Technology

Student:

Matthijs Robert Alexander Gensen, BSc

Abstract

The Rhine river outflow has a major impact on the North Sea in front of the Dutch coast. It creates the Rhine ROFI (region of freshwater influence), a very complex three-dimensional volume of water with a relatively low salinity. Many researches have been conducted on this phenomenon. Now another complex factor is added: a non-straight coastline. The specific case of the Sand Engine, a sandbar-shaped peninsula in front of the Holland coast, is studied. The objective is to identify changes in the Rhine ROFI caused by the Sand Engine and their possible causes.

Simpson (Simpson, et al., 1993) and De Boer (2008) have identified several mechanisms influencing the shape and size of the Rhine ROFI. The major ones are: the deflection of the fresh water jet from the river Rhine through the Coriolis force towards the north forming a 'coastal river' of fresh water, advection due to tidal propagation, density currents as a consequence of horizontal density gradients, tidal straining and tidal mixing. Fortnightly and semidiurnal variations of velocities and stratification can be expected within the Rhine ROFI.

Signell (1989) has had major contributions to the understanding of tidal propagation around coastal headlands. In his work a categorization is made for different combinations of tidal conditions and headland shapes. Within this categorization the Sand Engine is seen as a rather small and streamlined headland. Flow separation may be expected with a stagnant lee-side eddy forming each tidal period.

These researches cover the main domain of interest of this thesis. An extension is made by exploring the baroclinic effects of the perturbation of the coast to the Rhine ROFI. For this purpose a numerical model was set up. In essence the original model De Boer used in his dissertation was applied. The Sand Engine was added as a blunt rectangular shape at the same distance from the river mouth as in reality. No numerical problems were found after adapting the model. The performance of the model was successfully verified by comparing time-averaged salinity distributions to figures in De Boer's work.

The Rhine ROFI and the 'coastal river' remain largely unchanged, comparing outcomes of the models with and without the Sand Engine. On a more detailed scale some interesting phenomena can be distinguished. During both neap and spring tide a fresh water feature forms ahead of high tide at the location of the Sand Engine. The offset of the fresh water feature has a barotropic origin, being generated by a strong current at the southwest corner of the Sand Engine. Under neap tide conditions this fresh water feature grows in the offshore direction, whereas this does not occur for spring tide conditions. This offshore advection is a baroclinic effect as such widespread offshore velocities involved with the offshore advection of fresh water were not found under barotropic conditions. A possible explanation of the offshore velocities is the strength of the tidal straining effect, being enforced by the stronger vertical density gradient when the fresh water is located at the Sand Engine. Tidal mixing is larger under spring conditions, preventing tidal straining from happening, explaining why offshore-directed velocities and subsequent offshore fresh water advection are not found in the results.

In this thesis a simplified approach has been applied. Therefore the results must be treated with care under the likely possibility that flow mechanisms have been altered, enhanced or ruled out. However, the results do show the likely importance of baroclinic effects. These effects may have large consequences on the hydrodynamics in the area surrounding the Sand Engine. Therefore it is recommended to perform additional research on this topic.

Preface

This additional thesis is performed as part of the curriculum of the Master Hydraulic Engineering at the Delft University of Technology. The thesis represents 10 ECTS, which entails a workload of approximately 300 hours. This report concludes the additional thesis. The main aim of the thesis is exploring the effects of the Sand Engine on the Rhine ROFI. As of such this report could be of interest for scientists, researchers and students in the field of oceanography.

Words of gratitude go out to:

Julie Pietrzak of the department of Environmental fluid mechanics at the TUDelft for providing the topic of the research, Sabine Rijnsburger for her support, help and feedback during the entire course of the thesis, Gerben de Boer for allowing the use of his model and Mark Voorendt and Deltares for providing me with a license of Delft3D.

Delft, September 2016

Matthijs Gensen

Contents

1. Introduction

The Rhine Region of Freshwater Influence (Rhine ROFI) is a large region in the North Sea with relatively fresh water. The existence of the Rhine ROFI was first described by Simpson (Simpson, et al., 1993). The term ROFI describes the complex three-dimensional volume of fresh water. The Rhine ROFI has a major influence on the currents in front of the South-Holland coast. The fresh water originates mainly from the river Rhine except for a small fraction with its origin from the river Meuse. The inflow into the North Sea is located at the artificial channel *Nieuwe Waterweg.* This channel is a very busy shipping route as it is the primary access to the Port of Rotterdam.

Figure 1.1: Artificial '*Nieuwe Waterweg'* (Van Eyck, 1997)

In 2011 the coast northwards of the Nieuwe Waterweg has undergone a major change. This coast is prone to beach erosion. The coast requires regular nourishments in order to maintain the current coastline and to guarantee the safety of the low-lying areas in the west of the Netherlands. In 2011 the Sand Engine was constructed as an experiment to replace the regular replenishments. 21 million cubic meters of sand were placed in front of the coast. Its initial area was 128 hectares, extending one kilometre into the North Sea and an alongshore width of two kilometres. Currents are ought to spread the sand along the coast, creating a more sustainable and natural self-managing system.

The Rhine ROFI is known to have a major impact on the nearshore hydrodynamics. The ROFI itself extends over an area of 50 kilometres offshore and 100 kilometres alongshore. The effects are however found along the entire Dutch coast and even in Denmark the coastal waters of the North Sea are slightly fresher (Simpson, et al., 1993). It can also be described as a 'coastal river'. The Sand Engine is near the origin of this 'coastal river', with its location only six kilometres north of the Nieuwe Waterweg, see Figure 1.3. Besides local changes to the currents the Sand Engine may have an impact on a much larger area.

Figure 1.2: The Sand Engine on 1st October 2013 (Van Houdth, 2013)

Figure 1.3: Location of the Sand Engine shown (Google Maps, 2016)

2. Problem statement and research goals

In this research it is attempted to model the impact of the Sand Engine on the Rhine ROFI. Previous work on modelling the Rhine ROFI was done by Gerben de Boer in his doctoral dissertation (De Boer, 2008). His effort resulted in a large increase of knowledge on dominant processes playing a role in the Rhine ROFI. The flow patterns he found can be used to roughly predict the propagation of floating, suspended and dissolved substances. With the artificial channel Nieuwe Waterweg containing high concentrations of pollutions this is highly relevant with the densely populated Dutch coast in its near vicinity.

With the changed coastline the flow patterns are likely to have changed. The Sand Engine is not the only change of the coastline; in the last decade Maasvlakte 2 has been constructed. Maasvlakte 2 is the large land reclamation project accommodating the capacity increase of the Port of Rotterdam. For the obvious reason of these perturbations not having been built yet, these have not been taken into account in De Boer's original research. This thesis will only look into the effects of the Sand Engine. Modelling the effects of Maasvlakte 2 on the Rhine ROFI could be a topic of further research.

The goal of this research is to explore the effects of the Sand Engine on the Rhine ROFI. The main research question is expressed as follows:

Does the Sand Engine have an influence on the velocity and salinity distributions in the Rhine ROFI?

This research limits itself to the global changes in flow patterns and salinity distribution due to the Sand Engine. An attempt is made to gain valuable conclusions whether the Sand Engine does or does not have a major impact on the Rhine ROFI. It can be regarded as follow-up research on De Boer's research and an exploratory research for detailed modelling of the processes in the Rhine ROFI in the vicinity of the Sand Engine. Modelling and understanding the detailed physics induced by disturbances in the coastline is thus outside the scope of the project. Additional research questions are:

1. Can the Sand Engine be implemented into the original model of De Boer?
    - How can the Sand Engine be included in the model?
    - Does the inclusion of the Sand Engine impact the boundary conditions and functioning of the model?
2. Is there a change in the current pattern in the Rhine ROFI when the Sand Engine is present?
    - Are the effects similar during neap and spring tide?
    - Do the changes in the velocity patterns have a more barotropic or baroclinic origin?
3. Is there a change in the salinity distribution in the Rhine ROFI when the Sand Engine is present?
    - Are the effects similar during neap and spring tide?
    - Can these changes be explained by the changes of the current patterns?
4. If there are changes in the Rhine ROFI: does the interaction between salinity distribution and currents play a role?

3. Theory

3.1. Scope of the thesis

The Rhine ROFI governs for a large part the currents in front of the South-Holland coast. The density gradients between the fresh and salt water drive currents. The lighter freshwater acts as a buoyancy term on a wide-spread area of 50 kilometres offshore and 100 kilometres alongshore. This spreading is caused by tidal currents and the Coriolis Effect. Temporal and spatial scales vary significantly in the process. The main time scale is the semi-diurnal tide. De Boer concluded that the fortnightly variation of the tide, spring and neap tides, is also highly relevant. Both time scales have to be taken into account.

The scales used in this thesis are kept similar to De Boer's. As the goal of this thesis is to explore the effects of the Sand Engine, it is not necessary to increase accuracy. This is beyond the scope of the project. Furthermore the model outcomes of De Boer's model will be helpful to explain differences when the Sand Engine is included. The area of study is 50x100 km^2 where the three-dimensional character of the ROFI is taken into account. Fortnightly variability is taken into account by using separate models for neap tide and spring tide.

The next sections will go deeper into the theory concerning the Rhine ROFI. Firstly, section 3.2 will look into the area of study and its surroundings. It will for instance explain the tidal currents along the Dutch coast. Section 3.3 will describe the basics of density-driven currents. Section 3.4 will look at the phenomena of tidal straining and tidal mixing. Finally section 3.5 discusses the work of Signell (1989) and follow up work on the topic of tidal propagation around coastal headlands. With this theoretical base the model will be set up and used from Chapter 4 onwards.

3.2. Characteristics of the North Sea and its tidal wave

The North Sea is a shelf sea with an area of 575,000 km^2. The average depth is over 90 meters, but in the southern part the sea is much shallower. In a wide stretch along the Dutch coast the water depth is approximately 20 meters. The water in the North Sea has multiple origins, with the most important being the inflow from the ocean's tide around the tip of Scotland and river inflows.

The largest tides in the North Sea are the M2 lunar component and S2 solar component. Together these two components create a semi-diurnal tide with fortnightly variation. The tide along the Dutch coast can be classified as a (propagating) Kelvin wave. The Kelvin wave was first described by Taylor (1921). The entire North Sea consists of multiple amphidromic systems with several amphidromic points of zero tidal amplitude (Figure 3.1). With deflection of currents through Coriolis to the right in the Northern Hemisphere it follows that the tide propagates in an anti-clockwise sense around the amphidromic points. The tidal amplitude increases towards the coast. Along the Dutch coast the tidal wave thus propagates from South to North. Near the coast the average tidal amplitude is approximately one meter. One of the characteristics of a Kelvin wave is its propagating character. In a propagating wave velocities and water levels are nearly synchronized: high water and maximum velocity in the direction of propagation occur nearly at the same time. Without the effect of the Rhine ROFI the velocities would almost only be alongshore.

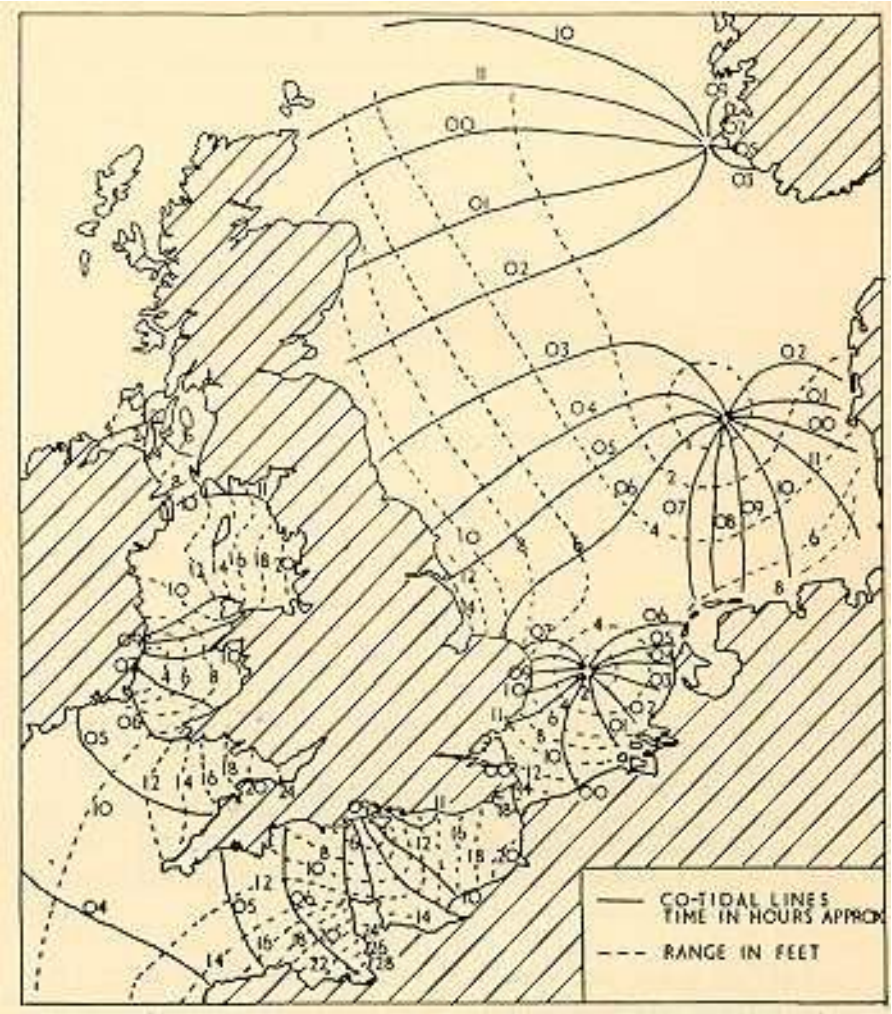

Figure 3.1: Amphidromic system of tides in the North Sea with the tidal Kelvin wave travelling in anti-clockwise direction around the amphidromic points with 0 amplitude. Shown are the amphidromic points, co-tidal lines (line with locations where high tide occurs at the same time) and co-tidal range circles. Source: Oostdam (2001)

When density variations are taken into account, things change. Water densities are very non-uniform throughout the North Sea. Stratification of water masses occurs both due to temperature and salinity variations. Temperature variations are mostly relevant in the central North Sea and salinity variations are more relevant in coastal areas. De Kok et al. (2001) stated that only salinity anomalies govern the density differences in the Rhine ROFI. Temperature differences are solely a response to salinity distributions. This was also found by De Boer as he showed that to a great extent temperature can be regarded as a passive tracer in the Rhine ROFI. As the fresh water travels with the Kelvin wave, density gradients are mainly in the cross shore direction with the saltier water further offshore. The interaction between the alongshore velocities and cross shore density gradients has been studied extensively, as will be discussed in the next paragraphs.

3.3. Density-driven currents

Most of the density-driven current field in the Rhine ROFI can be described in a simplified case. In this case the governing relation is the thermal wind balance. This equation combines the geostrophic balance with the hydrostatic pressure assumption. It reads as follows for a density gradient in one of the horizontal dimensions:

$$\rho_0 f \frac{\partial v}{\partial z} = -g \frac{\partial \rho}{\partial x}$$

In the Rhine ROFI the cross shore density gradient is governing as explained before. In this case the thermal wind balance predicts a current near the surface towards the north.

When adding the vertical dimension the formula does not balance equally. This is illustrated in Figure 3.2. The horizontal hydrostatic pressure forces balance each other out, but their working lines are not equal. This creates a momentum imbalance, which drives shear flow circulation. In this circulation an offshore current with lighter water is found near the surface and an onshore current with heavier water near the bottom. This mechanism is often addressed to as estuarine circulation.

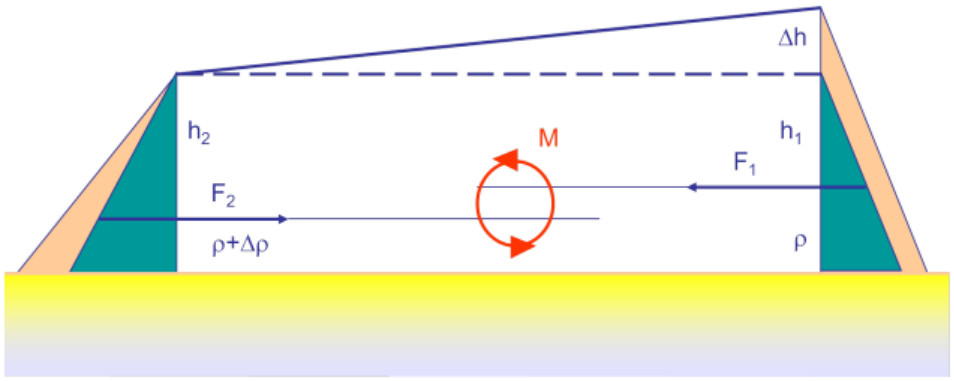

Figure 3.2: Resultant hydrostatic forces create a horizontal balance of forces. However due to the indifference in working line a momentum is added to the system resulting in two opposing flows at the surface and the bottom (Savenije, 2012)

In the case of the Rhine ROFI the salinity distribution is not uniform in space. The density distribution in the cross-shore direction can be seen as an S-shape instead (Visser, 1993). This results in a Gaussian distribution of the density gradient. The strongest currents are found where the density gradients are largest (De Boer, 2008). This follows from the thermal wind balance. The highest density gradients are at the boundary of the Rhine ROFI, so this is where flow velocities are expected to be relatively large. Also in the alongshore direction the salinity distribution is non-uniform. Near the mouth the freshwater reaches further offshore. This width decreases in upstream direction. Obviously this has consequences for the flow field. However the same equations and phenomena as before are still governing. These can be defined in a different system of axis where the lines of same density (isopycnals) are the y-direction with perpendicular the x-direction. The expected current field can then be visualized as is done by De Boer (2008).

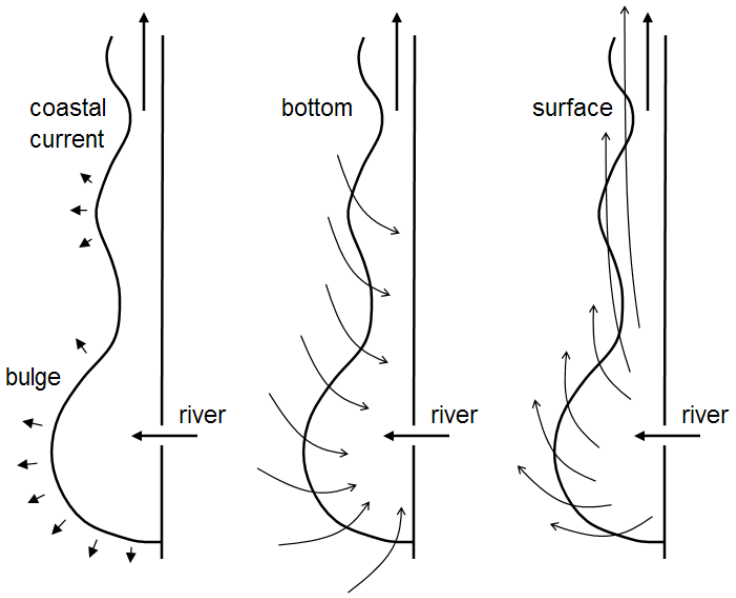

Figure 3.3: Sketch by De Boer (2008) showing the river plume. Near the mouth currents are mainly cross shore. These currents are expected when modelling the Rhine ROFI.

3.4. Tidal straining and tidal mixing

In the previous two sections the tidal propagation (3.2) and density-driven currents (3.3) have been discussed. In this section the interaction between those two will be discussed. This topic was the key element of De Boer's doctoral dissertation (De Boer, 2008). Earlier work on the interplay between tides and salinities centers mainly around estuaries, e.g. "*Tidal straining, Density currents, and stirring in the Control of Estuarine Stratification*" (Simpson, Brown, Matthews, & Allen, 1990).

Stratification and destratification are the key elements of the interaction between tides and densities. The wind and tide are both sources of mixing the water column; in different circumstances the one or the other is dominant (Simpson, Brown, Matthews, & Allen, 1990). Generally the source of stratification is an external input. This can for instance be solar heat input or freshwater buoyancy from a river. When tides do not play a role a stratified situation will be found in which the buoyant river water floats on top of the salty sea water.

When tides become more dominant, tidal mixing is able to diminish the vertical stratification and the horizontal density-driven currents. With higher tidal energy, viscosity increases. A higher viscosity will counteract the vertical shear exerted by the horizontal density gradient. Therefore in cases of large tidal amplitudes no stratifaction will occur, but instead a well-mixed situation will be found. Once tidal mixing decreases the water column will return to its stratified state.

Furthermore the tidal straining effect also comes into play when tides interact with stratified water bodies. This tidal straining effect was first described for estuaries by Simpson et al. (1990). During ebb conditions water flows out of the estuary with the largest flow velocities at the surface. This flow draws along fresh water, thus increasing stratification. Contrary, during flood conditions, water is drawn into

the estuary, pushing back the fresh water at the surface, thus destratifying the estuary. This creates a semidiurnal period of stratification and destratification.

The same phenomenon occurs in the Rhine ROFI, although it is not in an enstuary. This was first discovered by Simpson and Souza (Simpson & Souza, 1995). Similar to the situation in estuaries the buoyancy of the freshwater and the mixing by winds, tides and waves compete for dominance. During periods of mean stratification cross-shore tidal straining causes a semi-diurnal period of stratification and destratification. Mean stratification is onset by gravitational circulation as a consequence of horizontal density gradients (see 3.3). This can only occur when mixing is rather low, so during spells of low wind input and a low tidal range, i.e. neap tide.

When a stratified situation is present viscosities are low, allowing the decoupling of velocities above and below the pycnocline (the line along which the density gradient is largest and thus divides the water column into a part with low densities and a part with high densities). This decoupling is essential for the existence of cross-shore tidal straining. When the surface and bottom layer are decoupled, they have the tendency to rotate in a clockwise (anti-cyclonic) and anti-clockwise (cyclonic) sense respectively. The exact cause of the onset of the tidal ellipses can be explained in multiple ways (De Boer, 2008). One possible explanation can be found in the logarithmic velocity profile under the tidal wave with the largest velocities at the surface. The Coriolis force is lineary dependent on the velocity and thus it exerts a larger force on the surface layer forcing it in an anti-cyclonic direction. At the land boundary zero flux is required. Therefore the bottom layer has to rotate in the other direction.

The cross-shore velocities during certain stages of the tidal cycle cause stratification and destratification. For a perfect Kelvin wave (no phase shift due to friction) the highest flood velocities (towards the North along the Dutch coast) are found at high tide. Figure 3.4 to Figure 3.6 show the typical displacement distribution, velocity distribution and cross-shore salinity distribution for the tidal straining process.

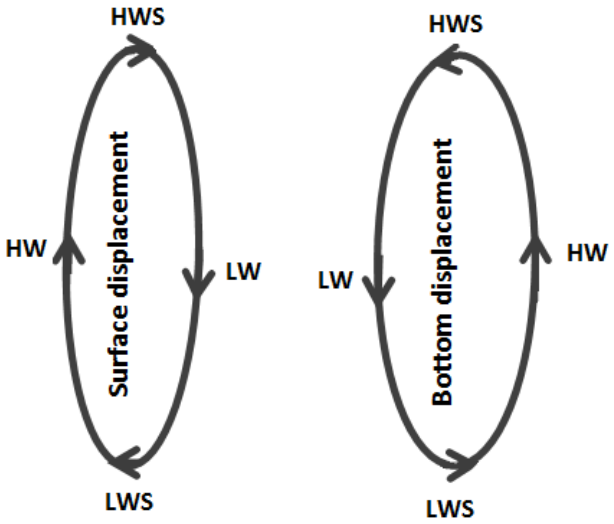

Figure 3.4: Tidal ellipses: particle displacement for the bottom and surface layer during stratified conditions. HW and LW are High Water and Low Water respectively and HWS and LWS are the slack times after high water and low water respectively.

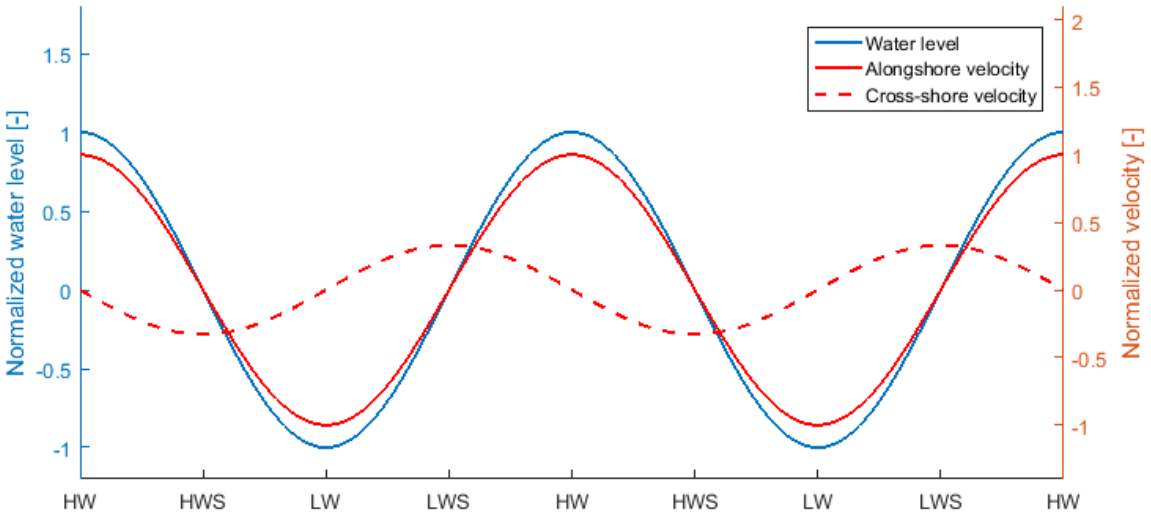

Figure 3.5: Water levels and velocities for a pure Kelvin wave (no time lag between water levels and velocities) and the cross-shore velocities during stratified flow conditions. Positive directions are northwards (flood) and eastwards (offshore). Offshore flow is thus found in the period between Low Water and High Water with a maximum at Low Water Slack.

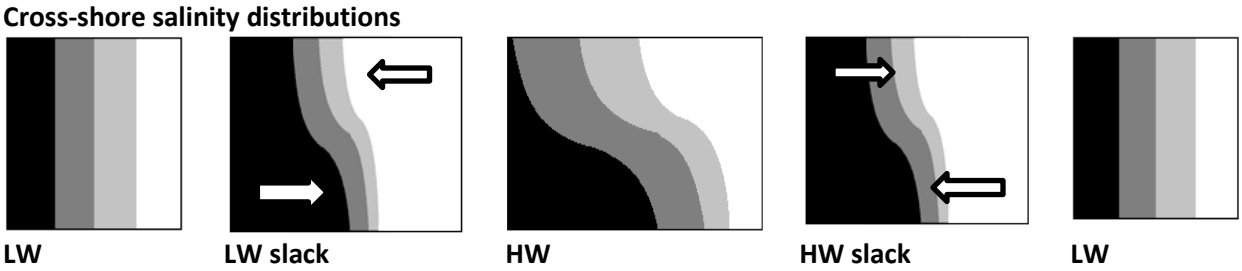

Figure 3.6: Theoratical cross-shore salinity distributions during one tidal period illustrating tidal straining on a semi-diurnal timescale.

It can thus be concluded that the tidal straining in the Rhine ROFI exists due to the interaction between salinities and the tide. Without a horizontal density gradient tidal straining cannot occur. In the end it is a self-retaining system as long as a mean stratification is present. Without this mean stratification tidal ellipses cannot develop, preventing semi-diurnal stratification due to tidal straining from occuring.

To summarize, all dominant mechanisms controlling the size and shape of the Rhine ROFI are shown in Figure 3.7 (De Boer, Pietrzak, & Winterwerp, 2009).

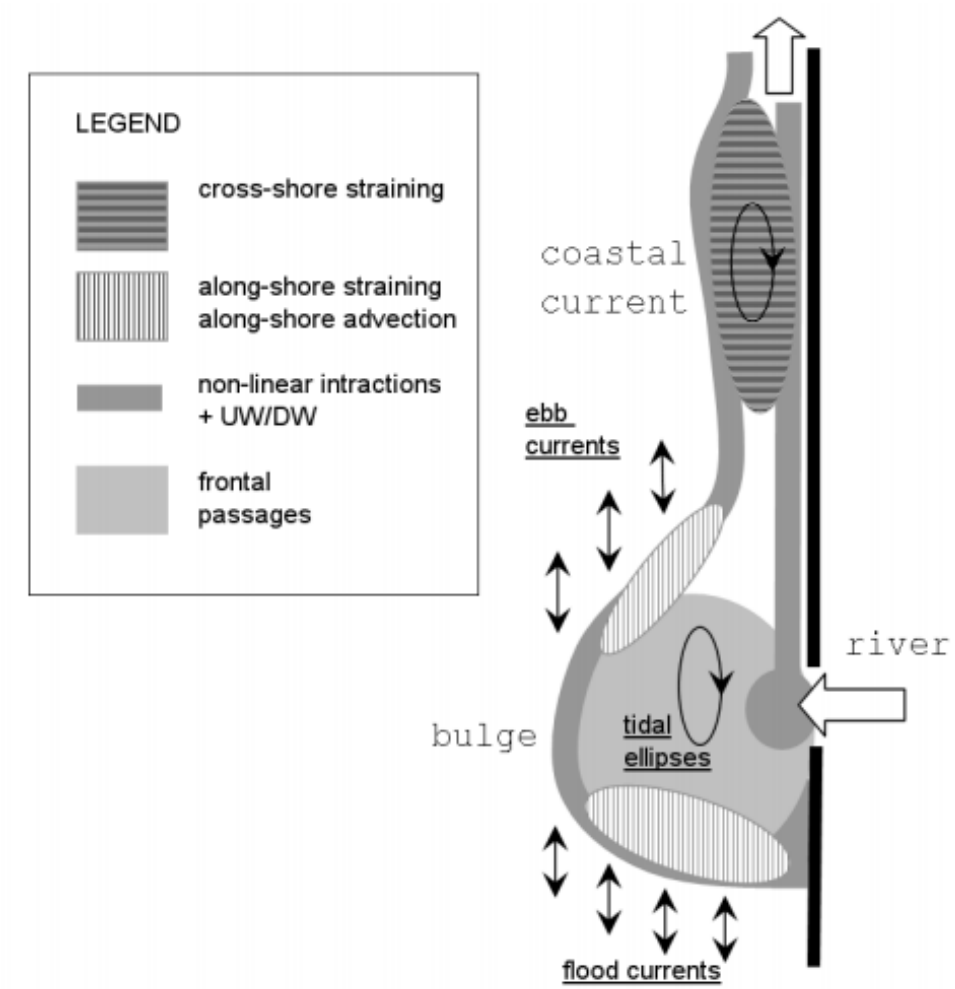

Figure 3.7: Sketch from De Boer, Pietrzak, & Winterwerp (2011) showing the dominant mechanisms involved with the shape, stratification and size of the Rhine ROFI.

3.5. Tidal propagation around headlands

With the Kelvin wave propagating around the North Sea basin, the tide propagates in alongshore direction along the Dutch coast. The Sand Engine is a perturbation in the coast. Important theory on tidal propagation around such perturbations is described by Richard Signell (Signell R. , 1989) (Signell & Geyer, 1991). This theory describes under which circumstances tidal flow separation can be expected and which type of separation will occur. The dominant parameters are the ratios of the advection terms over the friction terms and the inertia terms. Signell summarizes his theory in a figure (Signell & Geyer, 1991), this figure is shown in Figure 3.8 below.

The four cases Signell defines are as follows:

1. A lee-side eddy forms at the tip of the headland during each half-period of the tidal cycle. It dissipates quickly as friction is relatively high. The alongshore length of the eddy is

approximately equal to the tidal excursion. The cross-shore length is approximately twice the headland's cross-shore width.

2. Lee-side eddies again form during each half-period of the tidal cycle. Friction is lower, such that eddies dissipate much slower and interaction between subsequent eddies is made possible.
3. Tidal excursion is much larger and now large scale tidal flow separation results in a steady flow approximately parallel to the shore. Dissipation is rather high so recirculation is weak.
4. A high tidal excursion with low friction results in a steady flow with a propagating eddy at the tip.

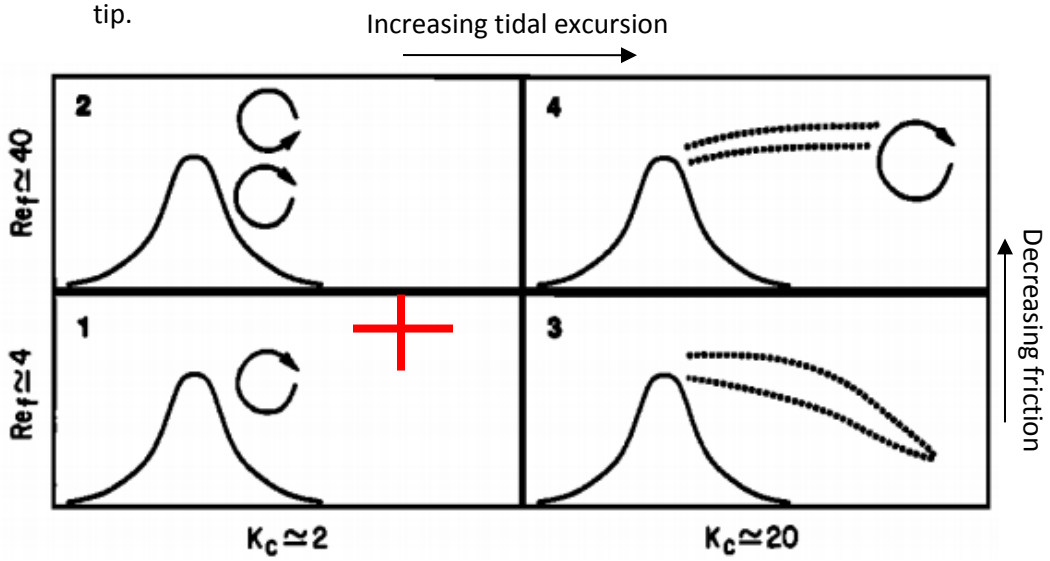

Figure 3.8: Figure summarizing the Signell's theory (Signell R. , 1989) (Signell & Geyer, 1991). Four types of tidal flow separation are shown. The vertical axis indicates the importance of the advection terms over the inertia term. The horizontal axis indicates the importance of the advection term over the fricition terms. As will be shown by the simple calculation below the Sand Engine case can likely be categorized as the first class as is indicated by the red cross

With the implementation of the Sand Engine into the numerical model (Chapter 4), the case of the Sand Engine can be fitted into this theory from Signell (Signell R. , 1989) (Signell & Geyer, 1991). The vertical axis in the figure above describes the importance of the advection term over the friction term. It is defined as the following non-dimensional parameter:

$$Re_f \equiv \left[\frac{H}{C_D a}\right]$$

With the following parameters for the case of the Sand Engine:

- H = Water depth = 20 m (see chapter 4.1: Basic model)
- C_D = Depth-averaged drag coefficient = $2.5*10^{-3}$ (Signell & Geyer, 1991)
- a = Characteristic length scale of the perturbation = 1 km (see chapter 4.3)

The horizontal axis in Figure 3.8 describes the importance of the advection term over the local acceleration term (inertia). It is defined as a non-dimensional parameter, equivalent to the Keulegan-Carpenter number. Keulegan and Carpenter (1958) have shown this number to be an indicator for the nature of oscillatory flows around cylinders.

$$K_C \equiv \left[\frac{U_0}{\sigma a}\right]$$

With the following parameters:

- U_0 = Tidal flow velocity amplitude ≈ 1 m/s, typical value according to Savenije (2012)
- σ = Frequency of the (S2) tide = $1.45*10^{-4}$ s^{-1}
- a = Characteristic length scale of the perturbation = 1 km

The two dominant parameters have the following magnitudes in the case of the Sand Engine:

$$Re_f = \left[\frac{H}{C_D * a}\right] \approx \frac{20}{2.5 * 10^{-3} * 1000} = 8$$

$$K_C = \left[\frac{U_0}{\sigma * a}\right] \approx \frac{1}{1.45 * 10^{-4} * 1000} = 7$$

These values place the Sand Engine into class 1 of Signell's theory, see the red cross in Figure 3.8. This means one would expect a rather stationary lee-side eddy which dissipates completely during a half tidal cycle.

4. Model set-up

In this chapter the model set-up will be described. This research makes use of the original model of De Boer (2008). An outline of his model is sketched in the next section. In section 4.2 the model outcomes will be verified using the model outcomes of De Boer. Finally, section 4.3 describes how the Sand Engine is implemented in the model.

4.1. Basic model

This research makes use of the original model of De Boer (2008). He used this model to determine detailed physics playing a role in the formation, stability and dynamics of the Rhine ROFI. This research will attempt to use the same model with adjustments to the coastline profile to find the main changes to the Rhine ROFI. Modelling and understanding the detailed physics induced by the disturbances in the coastline is outside the scope of the project. For a detailed description and explanation of the model set-up reference is made to De Boer's doctoral dissertation (De Boer, 2008).

The model of De Boer is a highly simplified model of the Dutch part North Sea. It focusses on three driving components in the Rhine ROFI: the buoyant fresh water term, the Kelvin wave and Coriolis. The main interest lies in a 50x100 km^2 area which includes the major part of the Rhine ROFI. The southern North Sea is rather shallow with water depths ranging from 10 meters to maxima of 60 meters. The Rhine ROFI area is in the shallowest parts of the North Sea. In the simplified model no complex bathymetry is required. Introducing a realistic bathymetry will induce complex current patterns which are difficult to separate from the density-driven currents that are of interest. The same 20 meters constant water depth as De Boer used, will be used in the adapted model.

The grid has 155x235 cells. The resolution of the main cells is 500x500 meters. This is rather course, but supposed to be sufficiently accurate. The main cells cover the area of interest of 50x100 km^2 plus a margin of 15 km in the cross shore direction and 5 km in the alongshore direction. Towards the model boundaries the cell size increases by a factor 1.2 with every remaining cell (Figure 4.1). This results in model boundaries far away from the area of interest.

The river discharge is located 30 km north of the southern boundary of the model, leaving just enough space for the ROFI to develop in the southern direction. The fresh water inflow is set to a constant river discharge of 2500 m^3/s with a salinity of 0 ppt. Naturally there is severe variability of the river discharge, but 2500 m^3/s coincides with the long term average discharge of the Rhine plus the Meuse. For this model with its focus on the ROFI this approach is sufficient.

The model boundaries are kept equal to De Boer's model with a trapped S2-type Kelvin wave on the Southern border. Figure 4.3 shows the theoretical twelve hour tidal signal. The near-coast amplitudes of the tidal waves are 0.75m and 1.25m for neap tide and spring tide respectively. Figure 4.2 displays the amplitudes of the Kelvin wave during neap and spring tide on the southern border.

The model is run separately for spring and neap tide conditions. The amplitude of the wave is set at every grid point on the southern border, so that every grid point has a different value. The western and northern model boundaries are Riemann boundaries with zero amplitude. This makes them weakly

reflective. But as they are located far away from the area of interest any reflection will be damped before it reaches the area of interest.

Spin-up time of the model is taken into account in two steps: barotropic and baroclinic spin-up. The first 2.5 days the model is run without fresh water discharge, thus tides only. Subsequently the fresh water is released upstream and the ROFI is being developed. After approximately 15 days a stable ROFI can be distinguished; after every 12 hours it returns to nearly the same form. Slight changes can be found as there is an ongoing input of fresh water.

A summary of the settings discussed with the addition of some other parameters is found in Table 4.1.

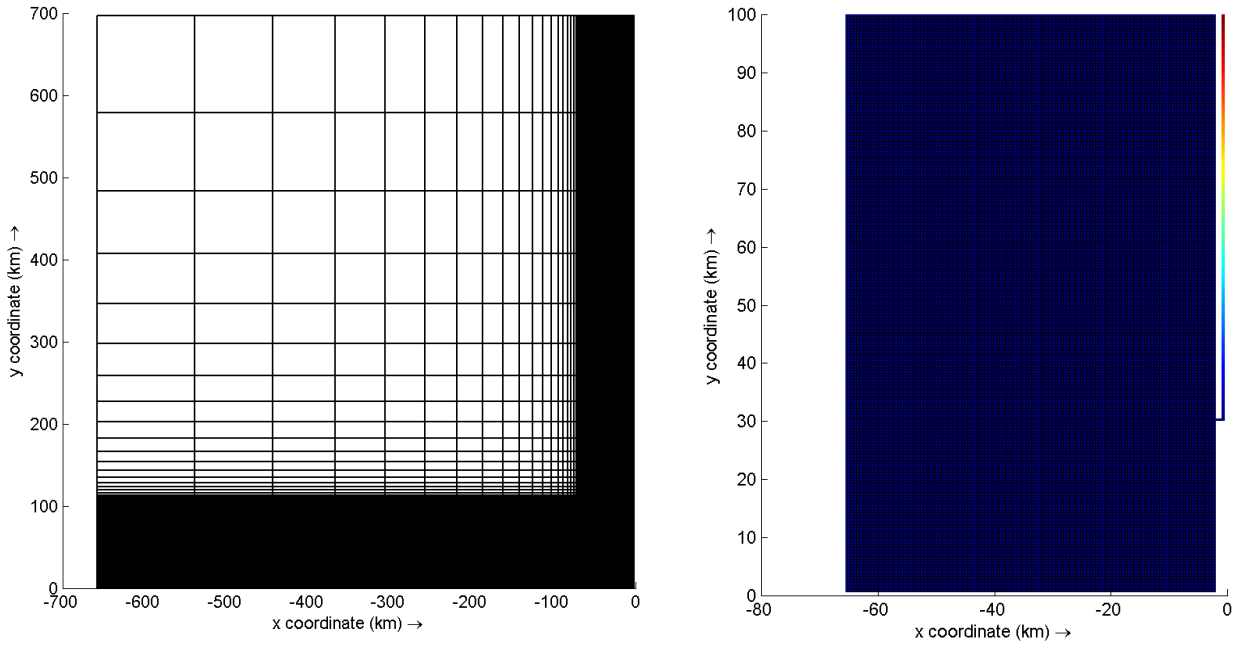

Figure 4.1: Left: Full hydrodynamic grid. Right: Main high resolution grid; location of river discharge shown to be 30 km from the southern boundary

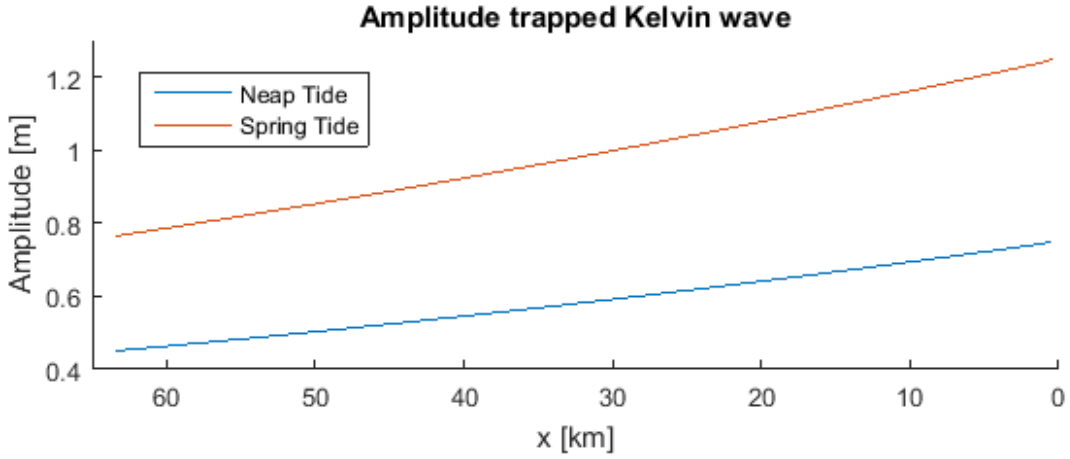

Figure 4.2: Amplitudes of the trapped Kelvin Wave on the Southern border

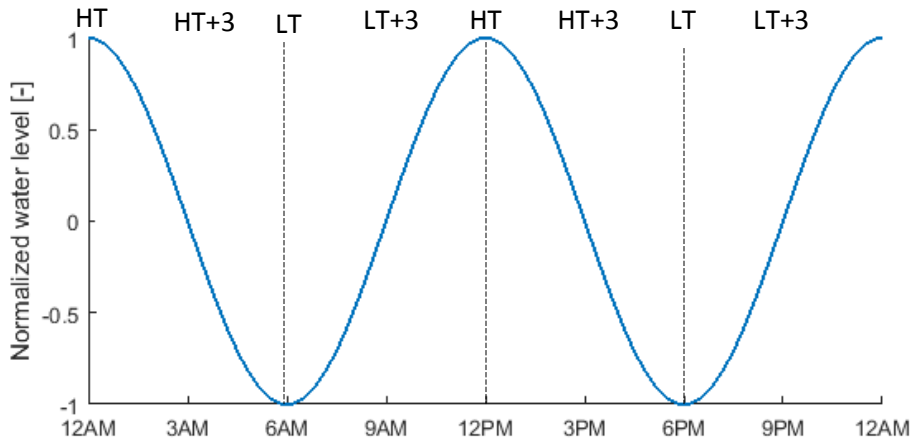

Figure 4.3: Two tidal cycles plotted for one day. Times in the graph correspond to those of the model. The vertical axis gives the normalized water level (normalized with the tidal amplitude). Locally this water level graph will be shifted as it takes time for the tidal wave to travel to a location away from the southern boundary, also deforming along the way.

Table 4.1: Overview model settings

Variable	Value	Unit
Main grid size	130x210	Cells
Main cell dimensions	500x500	M
Number of σ-layers	16	
Latitude	52.5	° North
Near-coast spring amplitude	1.25	M
Near-coast neap amplitude	0.75	m
Initial salinity	34.5	PSU
Water temperature (invariable)	15	°C
River discharge	2500	m^3/s
River salinity	0	PSU
Time step	2	Min
Barotropic spin-up time	2.5	Days
Baroclinic spin-up time	15	Days
Final simulation time	1.5	Days
Total simulation duration	19	Days
White-Colebrook Roughness	0.0025	
Background horizontal eddy viscosity	1	m^2/s
Background horizontal eddy diffusivity	1	m^2/s
3D turbulence model	k-ε	
Background vertical eddy viscosity	1e-4	m^2/s
Background vertical eddy diffusivity	1e-4	m^2/s

4.2. Model verification

To verify the model outcomes of the basic model a comparison is made to De Boer's model outcomes. Model verification is done by plotting time- and depth averaged salinities of the Rhine ROFI which De Boer has done in the middle panels of figures 4.4 and 4.5 of his doctoral dissertation. Below these two figures are shown with the outcomes of the re-run next to it. Furthermore also a comparison is made between the salinities in four cross-sections respectively 15, 30, 45 and 60 kilometres from the river mouth.

The figures show both distinct similarities and differences. When looking at the neap tide simulations the magnitudes of the salinities seem to be right. Furthermore the shape of the initial bulge stretching from kilometre 10 to 60 is very similar. Both simulations show a 'coastal river'; a narrow 15 kilometre wide flow of fresher water. Differences between the results are rather subtle. Firstly the stratification near the river mouth seems to be stronger than in the original run. This can be concluded from the salinities in the cross-section 15 kilometres upstream of the river mouth where the salinities are lower over a much larger cross-shore distance. The neap simulations seem to correspond well enough to each other and it is thus not expected that minor differences influence the conclusions in this report.

The spring simulations bear more distinct differences. The first tidal bulge near the river mouth between kilometre 10 and 40 is nearly similar. Further upstream correspondence between the two models is less clear. In both models the band of lower salinities widens when moving away from the river mouth. However this process goes much faster in the original run where the maximum width is reached at kilometre 80, compared to beyond kilometre 110 in the rerun. The widening of the plume northwards is a result of residual velocities in the offshore direction at the surface and onshore direction near the bottom, most probably due to gravitational circulation as these residual currents are only found inside the freshwater plume (see Figure 4.13 in De Boer's doctoral dissertation (2008)). When the maximum width of the plume is reached, in both cases approximately 35 kilometres, salinities increase quickly to the original 34.5 PSU as a result of strong mixing. The process of residual velocities is captured well in the rerun, but it most likely is weaker. As the process itself is captured well it should not harm the conclusions of this report.

4.3. Implementation of the Sand Engine

The implementation of the Sand Engine into the model is rather straightforward, as only the geometry has to be adapted. However, there are some important aspects to take into account. The same standard model set-up is used as was described before.

On the coarse grid with cells of 500x500 meters it is hard to accurately represent the Sand Engine. It will always end up being a blunt shaped object. The original Sand Engine as it was built in 2011 extended 1 kilometre offshore at maximum. Its original width was approximately 2 kilometres. In the model the Sand Engine will be represented by a rectangle of 1x2km. Its location is 6 kilometres north of the river mouth. The location and size is shown in Figure 4.8.

Neap Tide

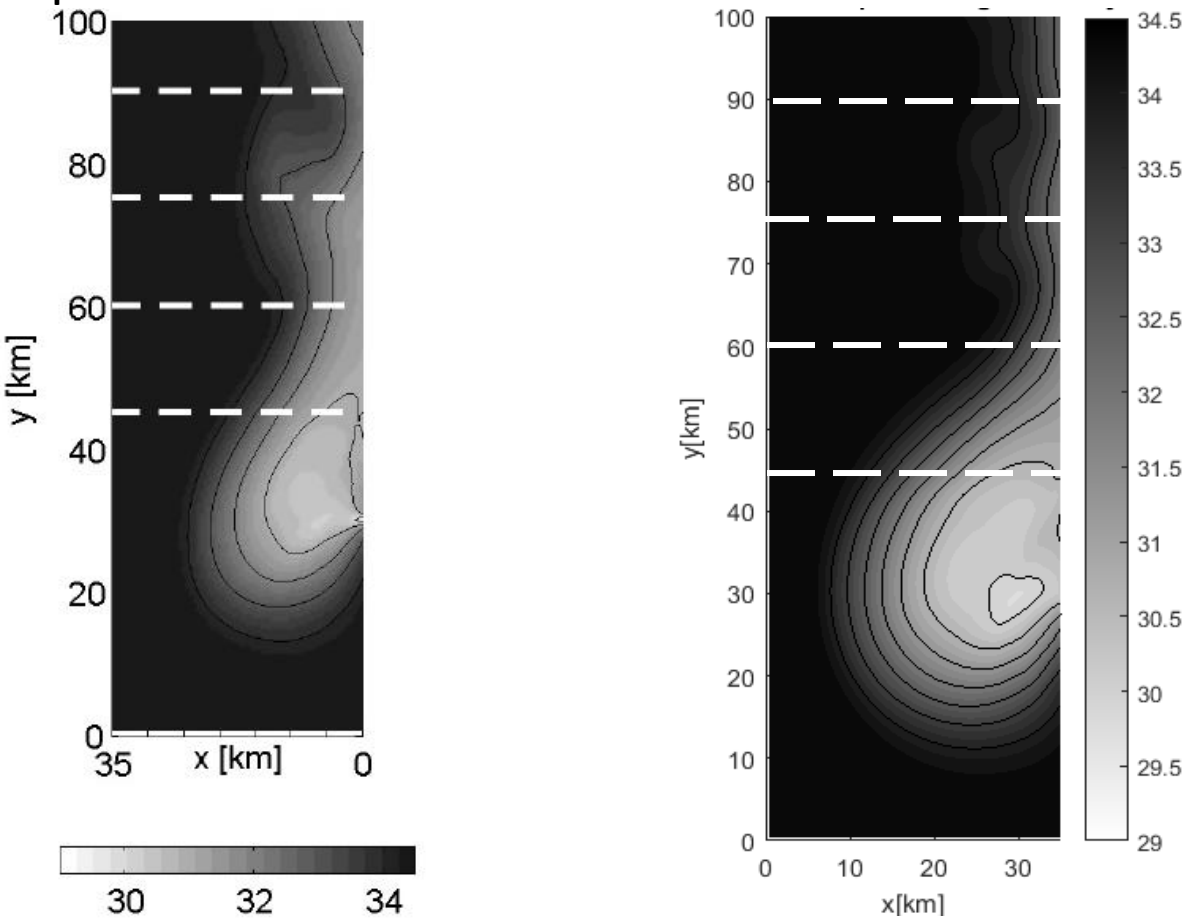

Figure 4.4: Both panels show the time- and depth averaged salinities during neap tide. Left panel: As is found in De Boer's Doctoral dissertation on page 78 (De Boer, On the interaction between tides and stratification in the Rhine Region of Freshwater Influence, 2008). Right panel: As is found in the re-run of the model.

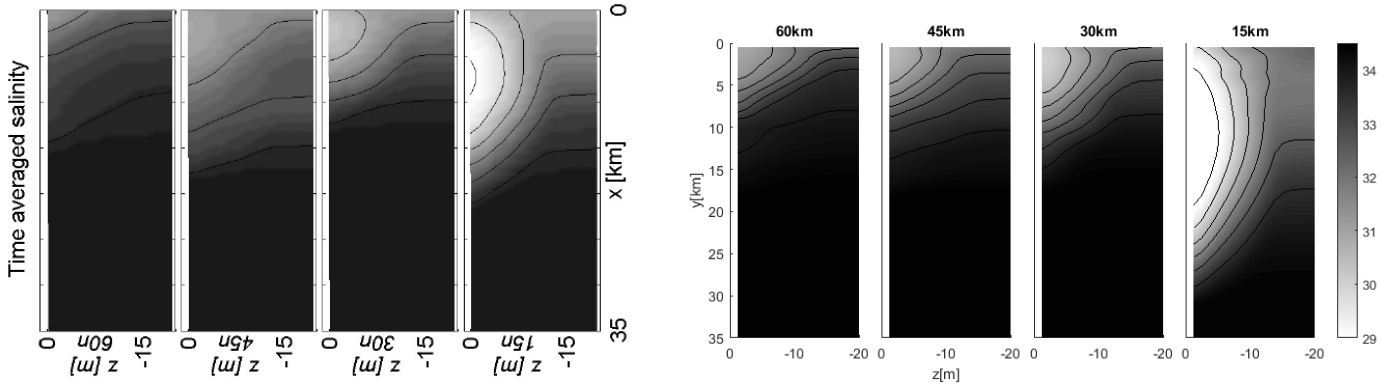

Figure 4.5: Both panels show the time-averaged salinities for neap tide in several cross-sections indicated by the dashed white lines in Figure 4.4. As is found in De Boer's Doctoral dissertation on page 78 (De Boer, 2008). Right panel: As is found in the re-run of the model.

Spring tide

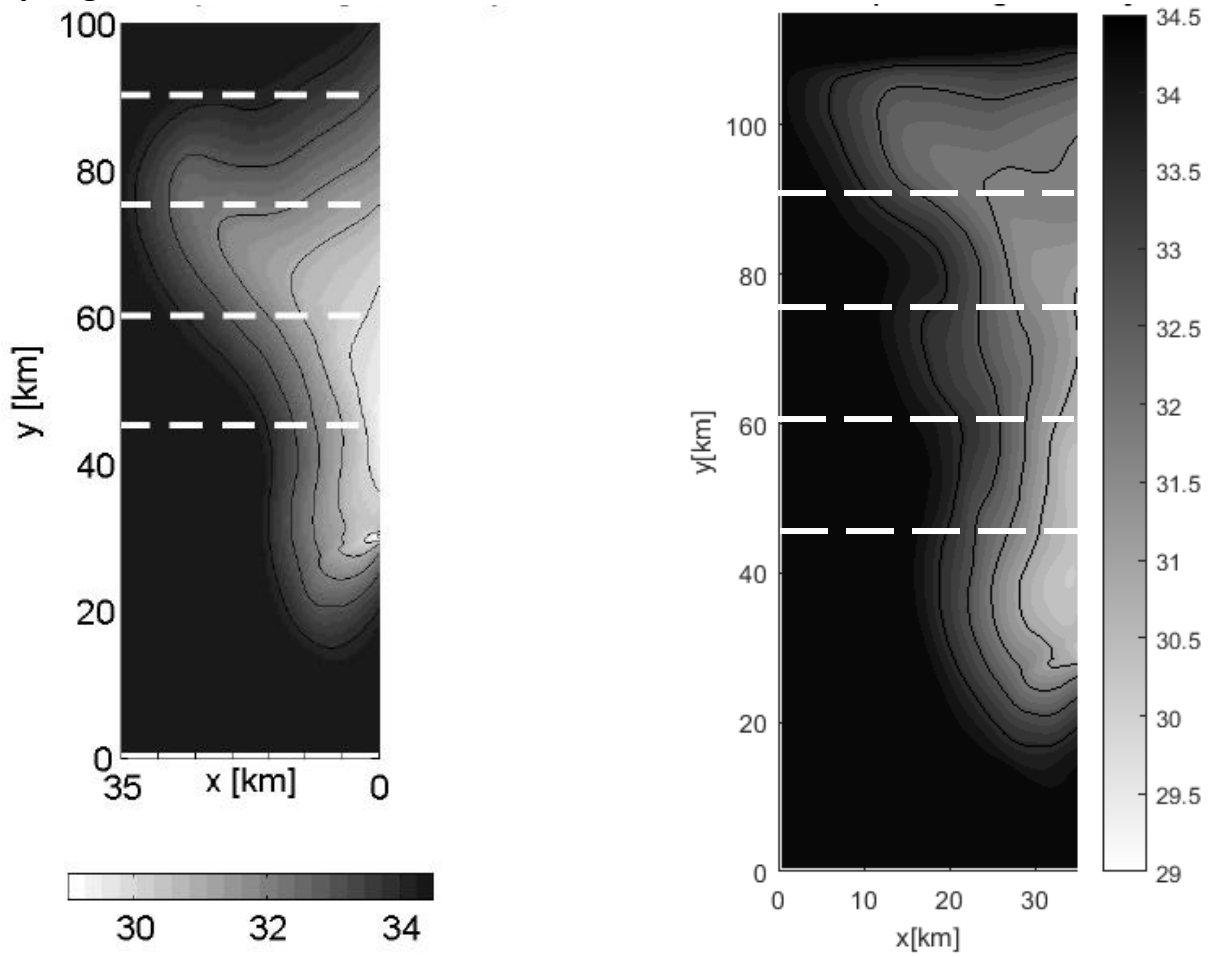

Figure 4.6: Both panels show the time- and depth averaged salinities during spring tide. Left panel: As is found in De Boer's Doctoral dissertation on page 79 (De Boer, 2008). Right panel: As is found in the re-run of the model.

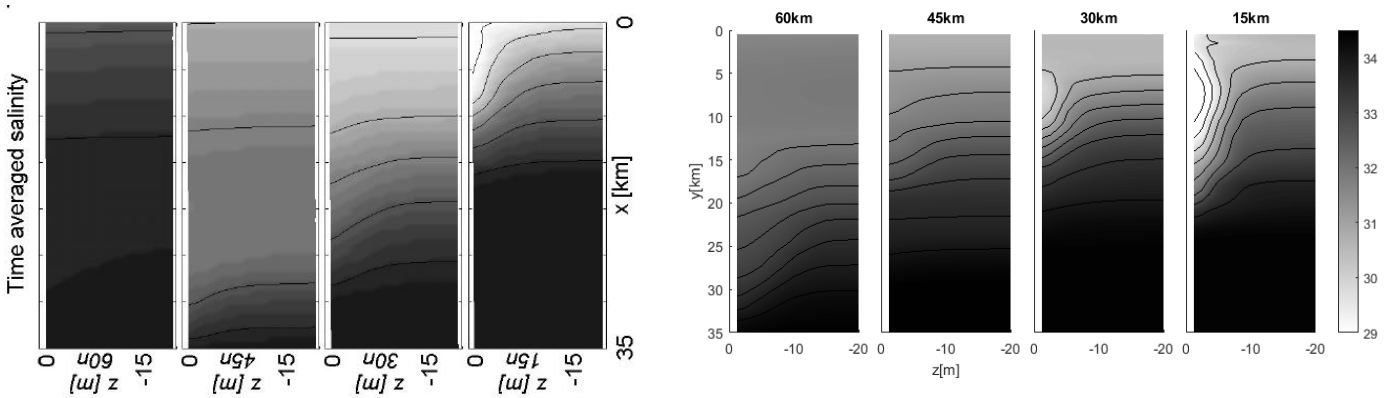

Figure 4.7: Both panels show the time-averaged salinities for spring tide in several cross-sections indicated by the dashed white lines in Figure 4.6. As is found in De Boer's Doctoral dissertation on page 79 (De Boer, 2008). Right panel: As is found in the re-run of the model.

The Sand Engine is set as dry points, preventing any flooding of the relevant cells. The Sand Engine is rather over-dimensioned, but it is the best way it can be represented on this grid. Together with the effect of the blunt shape it can be expected that the found results will be exaggerated significantly compared to reality. However, the changes between the original geometry and the geometry with the Sand Engine might lead to insights into the type of effects of the Sand Engine.

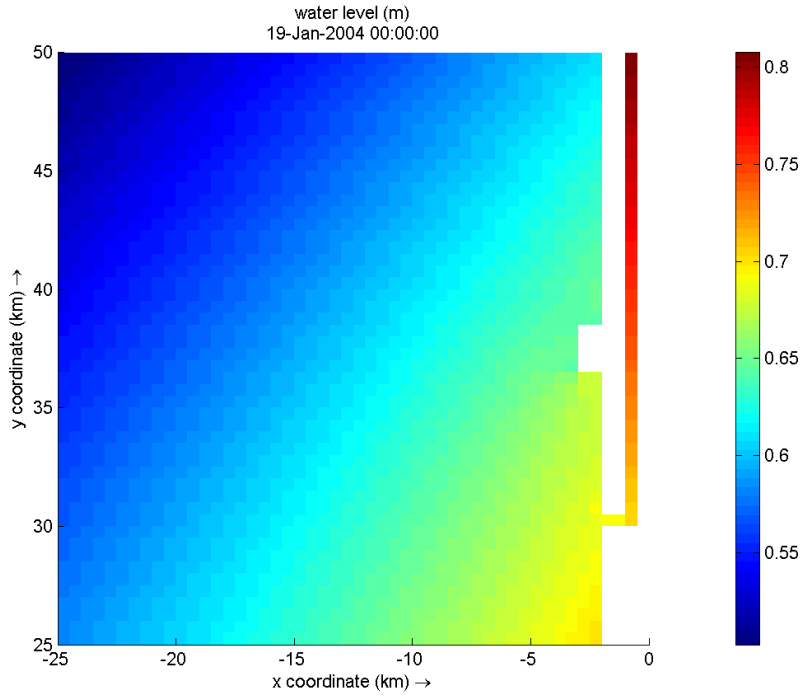

Figure 4.8: Location of the Sand Engine shown in a water level plot at high water

A further aspect to take into account when analysing the results, is that drying and flooding is disabled, as the Sand Engine is set as a dry point. It is thus represented as a straight wall. In reality the edges of the Engine slope downwards. In the case of a vertical wall introduced mechanisms will again be enlarged as the water has to flow around the object creating strong currents and possibly strong vorticities in the lee-side.

Finally it must be mentioned that the Sand Engine might create strong currents in its near vicinity. This may lead to longer spin-up times. During the set spin-up periods of 2.5 days (baroptropic) and 15 days (baroclinic) the results must be closely monitored to see if any spin-up effect persists.

5. Results

In this chapter the results will be discussed. The model has been split into a neap tide and spring tide simulation to take the fortnightly variation into account. Therefore the outcomes will also be split into two sections. First of all the neap tide simulations will be discussed in 5.1. Subsequently the spring tide simulations will be discussed in paragraph 5.2. For both neap and spring tide simulations the results will be discussed in three steps. Firstly the original case without the Sand Engine will be briefly discussed to find out the dominant mechanisms. Secondly the area of interest of 40x90 kilometres capturing the largest part of the Rhine ROFI is looked at for the case when the Sand Engine is included. Possible large scale features may be distinguished. Finally the results are tried to be explained by taking a closer look at an area of 10x20 kilometres which includes both the river mouth and the Sand Engine. Smaller scale features could be found at this figure scale.

5.1. Neap tide simulations

The neap tide simulations have a tidal boundary condition with an amplitude of 0.75 meters. This results in low energy conditions creating ideal conditions for the Rhine ROFI to exist and persist. It is found (section 5.1.2) that by including the Sand Engine a remarkable fresh water feature with strong offshore currents will appear. To support this conclusion a barotropic model run is also performed; this will be discussed in section 5.1.3.

5.1.1. Original neap tide simulation

This section discusses the original model outcomes. The time- and depth averaged salinities resulting from this model run have been shown in the model verification (section 4.2). In this paragraph these results will be discussed in more detail. Figure 5.1 on the next page gives distributions of salinities in the surface layer. These figures capture an entire tidal cycle with high tide at twelve a.m. and p.m. and low tide at six p.m. (in correspondence with Figure 4.3).

It can be seen that the Rhine ROFI is very stable as it more or less keeps its original shape throughout the entire tidal cycle. The entire ROFI travels in southern direction from 4 p.m. (HT+4) until 10 p.m. (LT+4). It reaches its southernmost position at slack time when flow reversal occurs. Apparently, this occurs two hours before high tide. In the remaining part of the tidal cycle it travels the same distance northwards with its northernmost position two hours before low tide. The tidal excursion is approximately ten kilometres, which is a typical value for the tidal excursion (Savenije, 2012).

In the upper halves of the figures the ‘coastal tidal river’ can clearly be distinguished. This coastal river is expected from theory and is also found in salinity measurements along the entire Dutch North Sea coast (De Boer, Pietrzak, & Winterwerp, 2011). It is an important feature of the ROFI and may be affected by the Sand Engine as it interrupts the coast in the early stages of the ‘river’ formation. This will be addressed in the next paragraph.

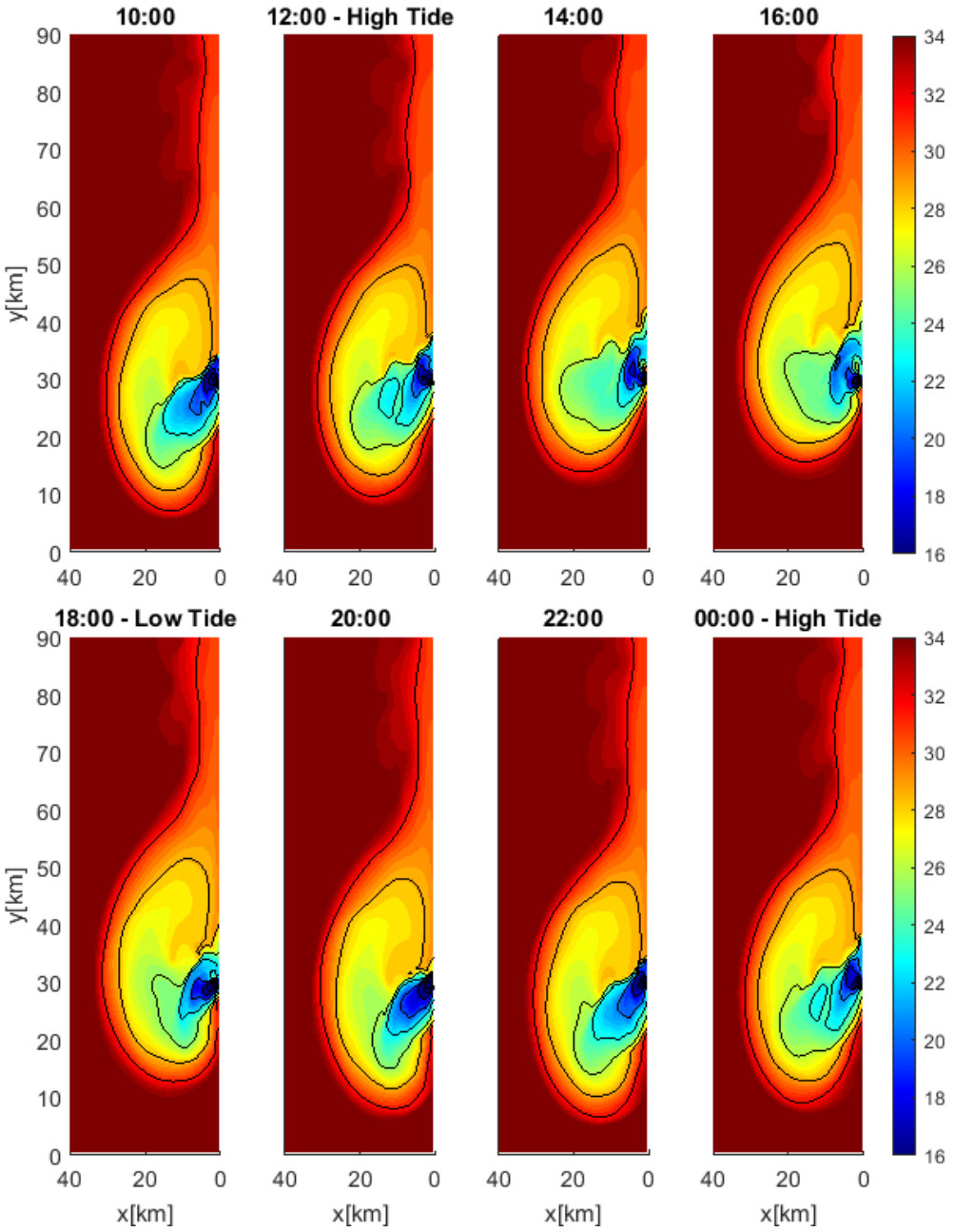

Figure 5.1: Salinity distribution in the surface layer for neap tide simulation without the Sand Engine. The time step between the figures is two hours as is shown in the titles and they capture an entire tidal cycle.

In general, the most important mechanisms determining the shape of the ROFI are tidal straining and mixing. Inside the ROFI tidal straining is one of the mechanisms that causes semi-diurnal stratification and destratification, see chapter 3.4. That indeed stratification occurs can be derived from Figure 5.2. This figure plots the salinities in the eight sigma layer (at around 10 meters water depth). It can be seen that salinities are severely lower than in the surface layer in all subplots, from which it can be concluded that stratification occurs throughout the entire tidal cycle. There is a high chance that this stratification

is caused by tidal straining. An elaboration on this statement is given in Attachment A: "*Tidal straining in the 'Coastal river' during neap tide*"

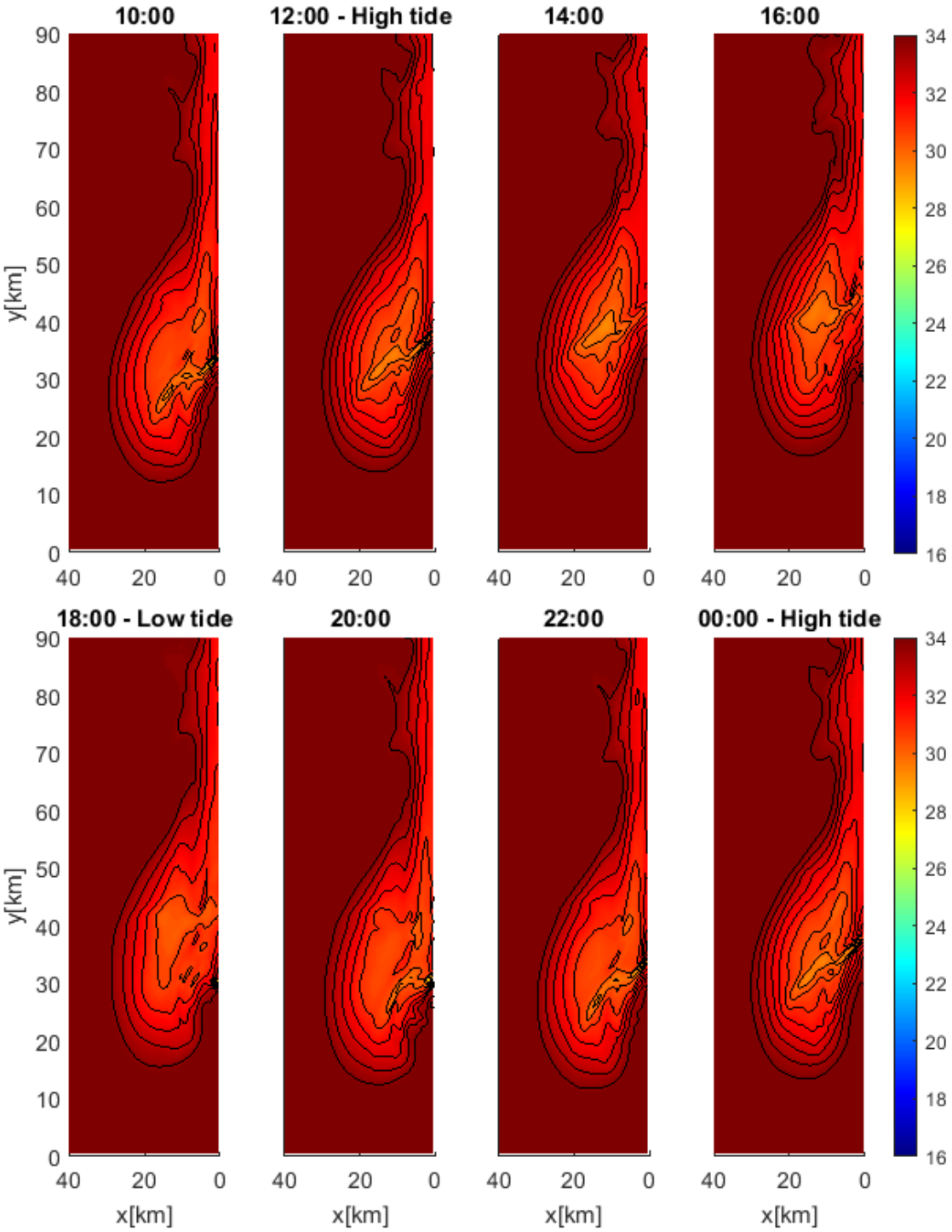

Figure 5.2: Salinity distributions in the eighth sigma-layer for neap tide simulation without the Sand Engine. Comparing these figures to the plots of the surface layer, it can be concluded that the Rhine ROFI is highly stratified

5.1.2. Neap tide with Sand Engine

In this paragraph the results are discussed when the Sand Engine is included. The method for creating this model has been explained in paragraph 4.3. Figure 5.4 shows distributions of salinity in the surface layer for this model at different points in time. No visible problems with boundary conditions can be distinguished and therefore the results of the two separate runs can be compared without numerical constraints.

It can be seen that very large scale differences are not found in the Rhine ROFI. This can be expected as the ROFI's area is much larger than the size of the disturbance. The 'coastal river' is thus also left unchanged. However, looking in more detail a remarkable difference can be distinguished. The Sand Engine seems to attract fresh water. This effect is indicated in Figure 5.3.

When zooming in on this area surrounding the Sand Engine a phenomena can be seen which is related to the presence of the Sand Engine. In the hours ahead of high tide, with high tide occurring at 12 a.m., a coastal fresh water feature starts forming at the head of the Sand Engine. After formation it grows in size and is advected along the coast in northern direction. This can be seen in Figure 5.5.

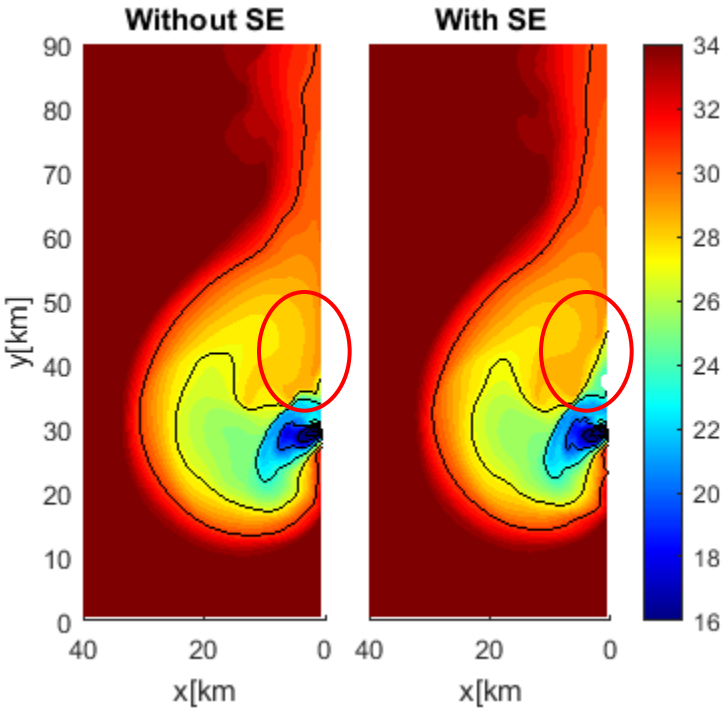

Figure 5.3: Salinities are plotted at low tide; 6 p.m. The red circle indicates the location where a difference between the two models can be seen. When the Sand Engine is included in the model fresher water is found near the coast.

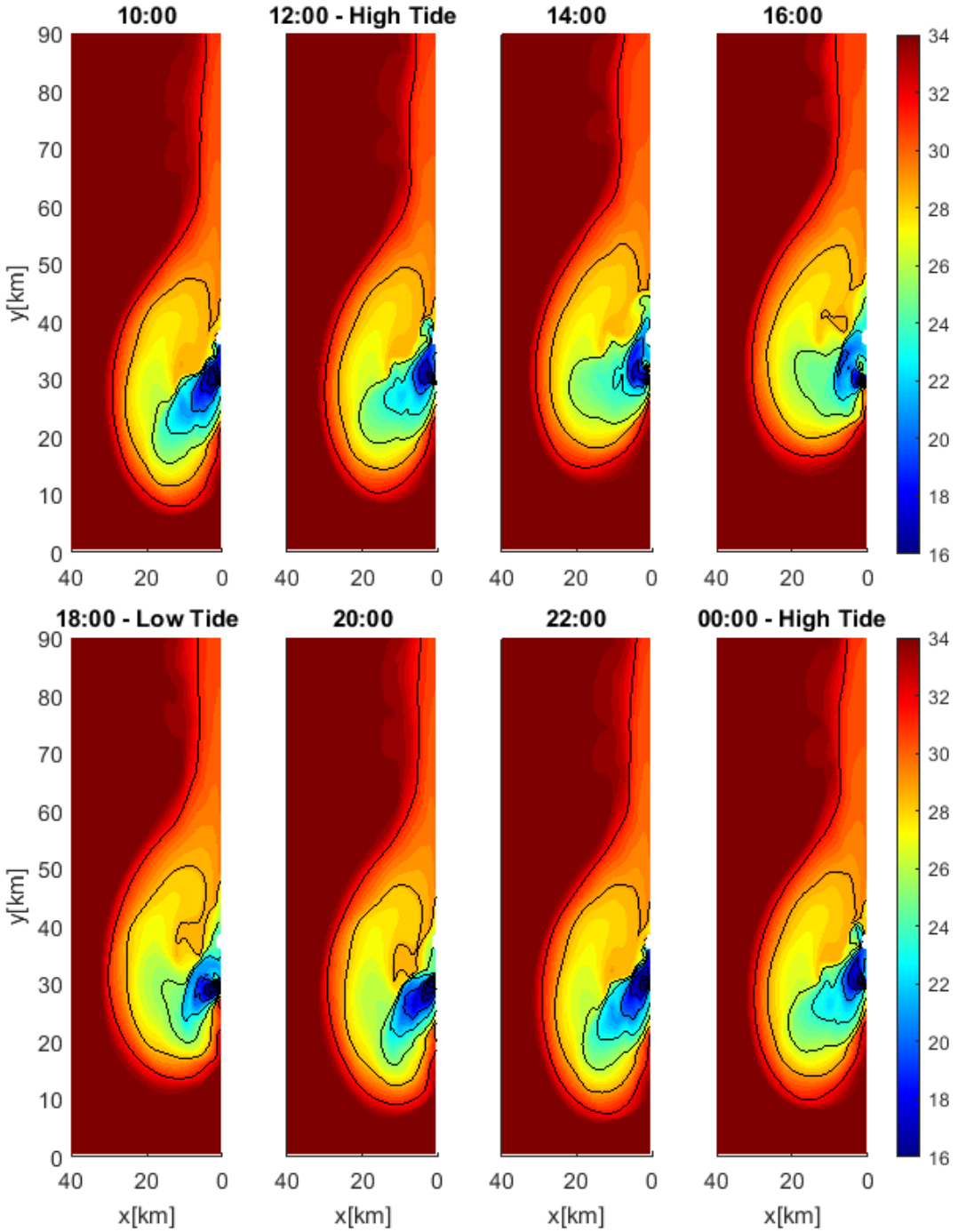

Figure 5.4: Salinity distributions in the surface layer for neap tide simulation including the Sand Engine.

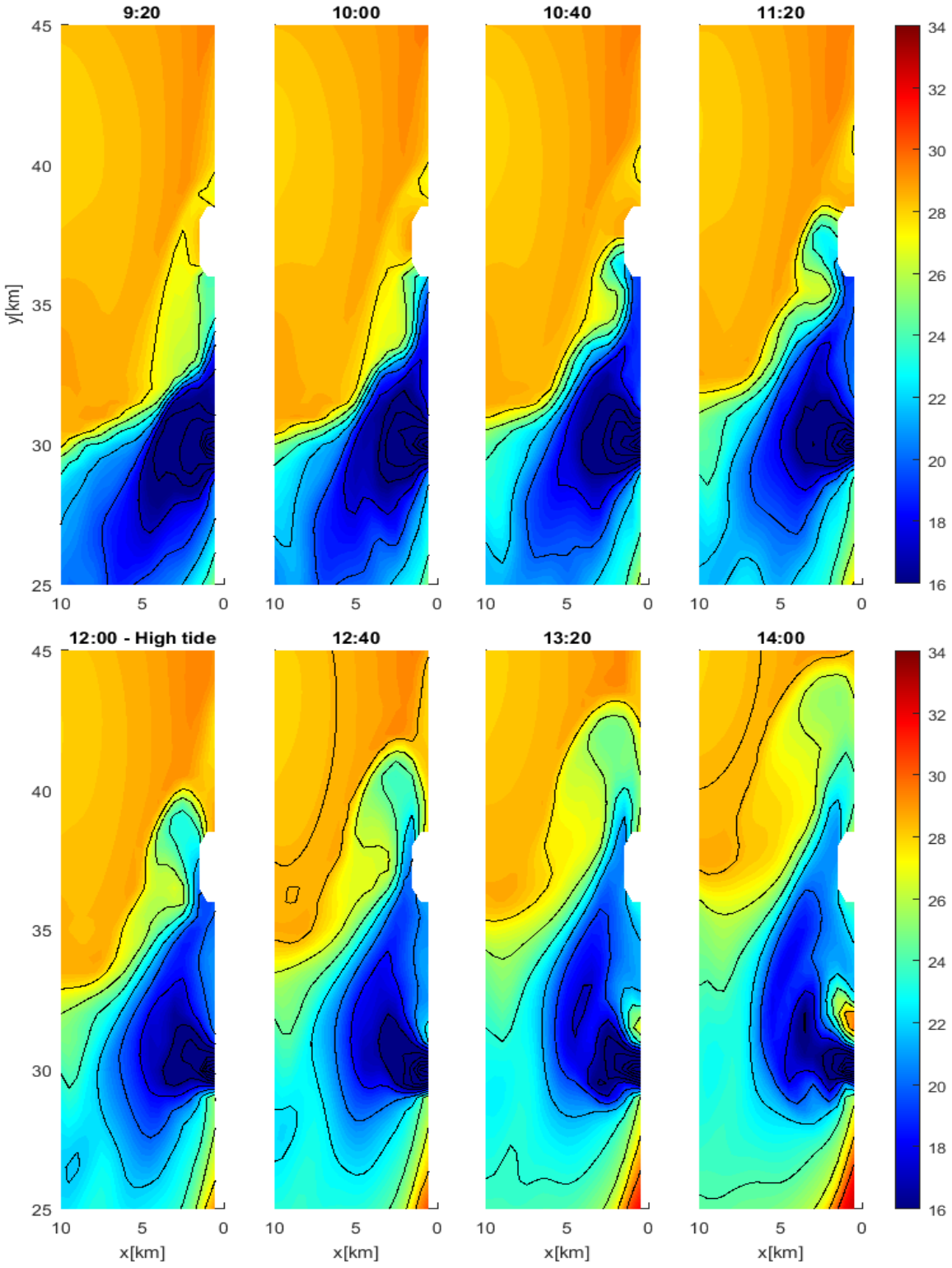

Figure 5.5: Distributions of salinity in an area capturing the Sand Engine and river mouth. It shows the hours around high tide (HT is at 12 a.m.) when a fresh water feature forms at the head of the Sand Engine. It subsequently grows in size in the cross-shore direction and it moves along the coast to the north.

5.1.3. Discussion neap tide simulations

The goal of this section is to attempt to attain the reasons for the changes that have been found when comparing the runs with and without the Sand Engine. Figure 5.5 showed the existence of a fresh water feature near the Sand Engine at high tide. It grows in size, disperses offshore and is transported northwards. Its width is approximately twice the size of the Sand Engine, which would correspond to the estimated size of an eddy in Signell's work (Signell & Geyer, 1991). However the characteristics of the fresh water feature found in the model results do not compare with Signell's tidal flow separation (Signell R. , 1989). The eddy Signell finds is a leeside eddy with an opposite rotary direction where recirculation occurs along the leeside of the headland. This cannot be found in the model results. It is likely that the blunt shape of the Sand Engine plays a role in this. Furthermore Signell and Geyer (1991) do not take into account any density gradients which play a major role in the Rhine ROFI.

What can be seen in Figure 5.5 is that the fresh water feature that occurs is not stationary; it grows and is transported by the tidal currents. It could be very likely that this effect is caused by barotropic currents; i.e. would also be visible when salinity is excluded from the model. However, Figure 5.6 shows that this cannot be the full explanation. In this figure the velocity vectors at 11 a.m. (LT + 5) are plotted for barotropic and baroclinic cases in which the Sand Engine has been included and the baroclinic case where the Sand Engine is excluded. The figure displays this for the surface layer and for depth-layer 10. In Attachment B such figures are plotted for more points in time. To show the magnitude and direction of the velocity vectors in the three different runs, the velocity vectors have been isolated and plotted in one figure: Figure 5.7. Figures plotting such isolated velocity vectors for other points in time are shown in Attachment D.

These figures show one location where deviations from the original model can solely be explained by the barotropic run. That one location is near the bottom-left corner of the Sand Engine. A strong current is found at the corner as the flow has to go around the Sand Engine. This is the strongest current that is found in the area surrounding the Sand Engine and in the same order as the velocity of the river outflow component. This corner current is rather constant over depth and it is the offset of the fresh water feature seen in Figure 5.5.

Further alongshore and offshore the barotropic effect of the Sand Engine diminishes quickly. However in the baroclinic run, a strong deviation is still found until four kilometres offshore; here a strong offshore flow is found, which is several magnitudes larger than in the original model where it is caused by tidal straining.

It is speculated that offshore directed velocity components are being enhanced by the presence of the Sand Engine. These components could well be the resultant velocities of tidal straining. However, in the original model outcomes no strong offshore flow can be detected. It is therefore likely that in the original case without the Sand Engine tidal straining barely occurs in this area. A possible explanation could be the lack of stratification. As explained (section 3.4) stratification is required in order to decouple the velocities in the surface and bottom layer, allowing tidal ellipses to develop. The cross-shore components of these ellipses cause a semidiurnal period of stratification and destratification. It

can be seen that indeed very little stratification occurs at the location of the Sand Engine in the original model (compare the area in the red circles in the two left figures of Figure 5.6).

In the new situation a fresh water lens is advected to the Sand Engine via a barotropic current at the bottom-left corner of the Sand Engine (see Figure 5.6). Here it causes strong local stratification (around 23 PSU at the surface and 33 PSU near the bottom). This strong stratification allows for tidal straining to occur. If tidal straining occurs, offshore velocities are found during the period between low tide (6 a.m.) and high tide (12 a.m.). The period of offshore advection lies within this period; in Figure 5.5 it can be seen that offshore advection occurs until high tide (12 a.m.) up to 5 kilometres from the shoreline, after which the fresh water is only transported in the alongshore direction. This may be an indication of indeed tidal straining being the cause of the offshore spreading of the fresh water.

In Attachment C several time-dependent plots of salinities and cross-shore velocities are plotted for several locations in the vicinity of the Sand Engine. At all locations increased stratification occurs, expressed in a density difference between a near-bottom layer and the surface layer. A newly developed peak in stratification occurs before and at high tide, when the fresh water passage occurs. This peak is associated with relatively large offshore-directed velocities.

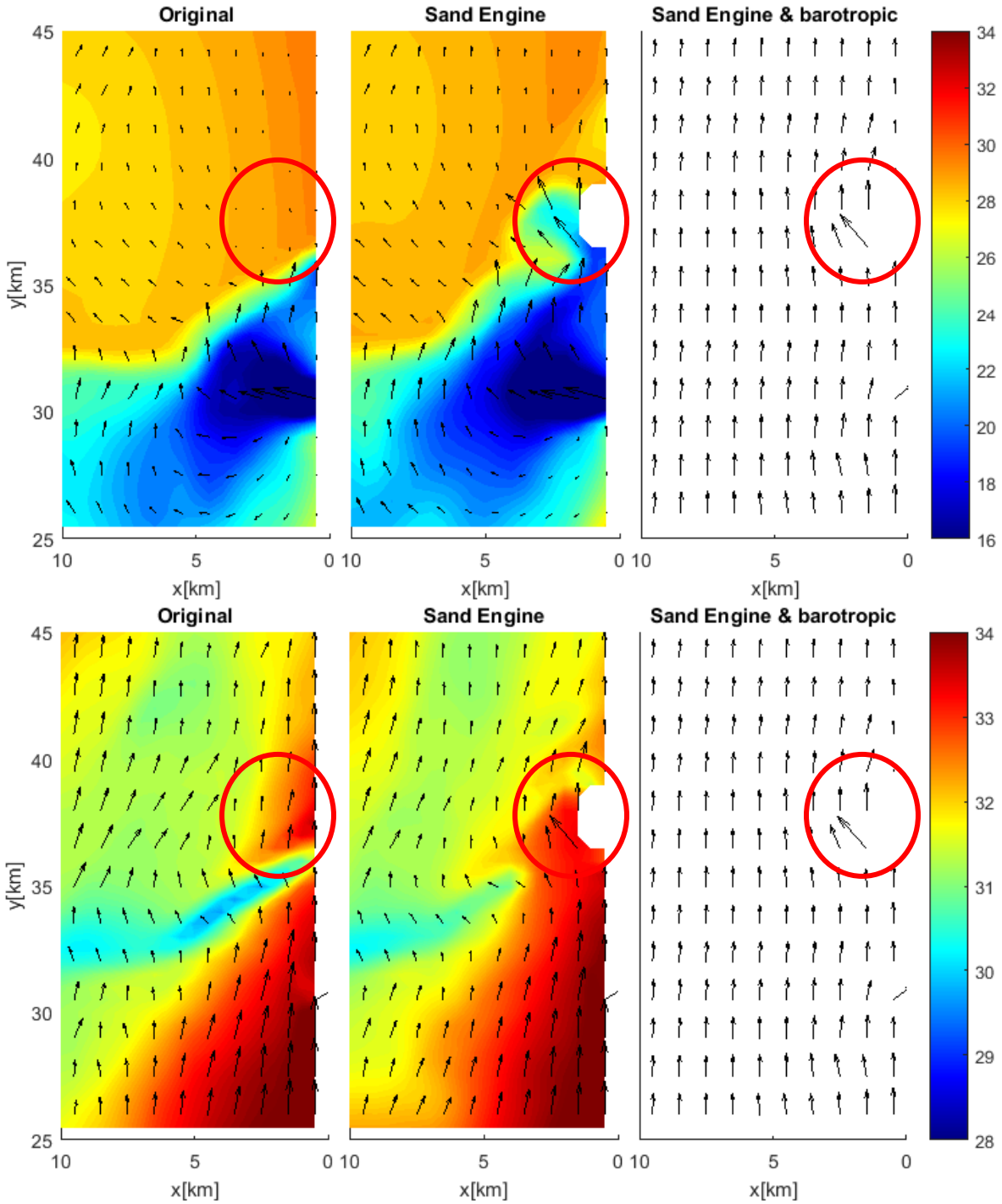

Figure 5.6: Velocity vectors and salinities at 11a.m. (LT+5) plotted for three model setups: the original model without the Sand Engine, and a baroclinic and barotropic model with the Sand Engine implemented. Note the different scales of the colour bar for the surface and bottom layer. *Top panel:* surface layer. *Bottom panel:* layer 10. The red circles indicate the area where large deviations in the velocity field can be found in the baroclinic run in which the Sand Engine is included.

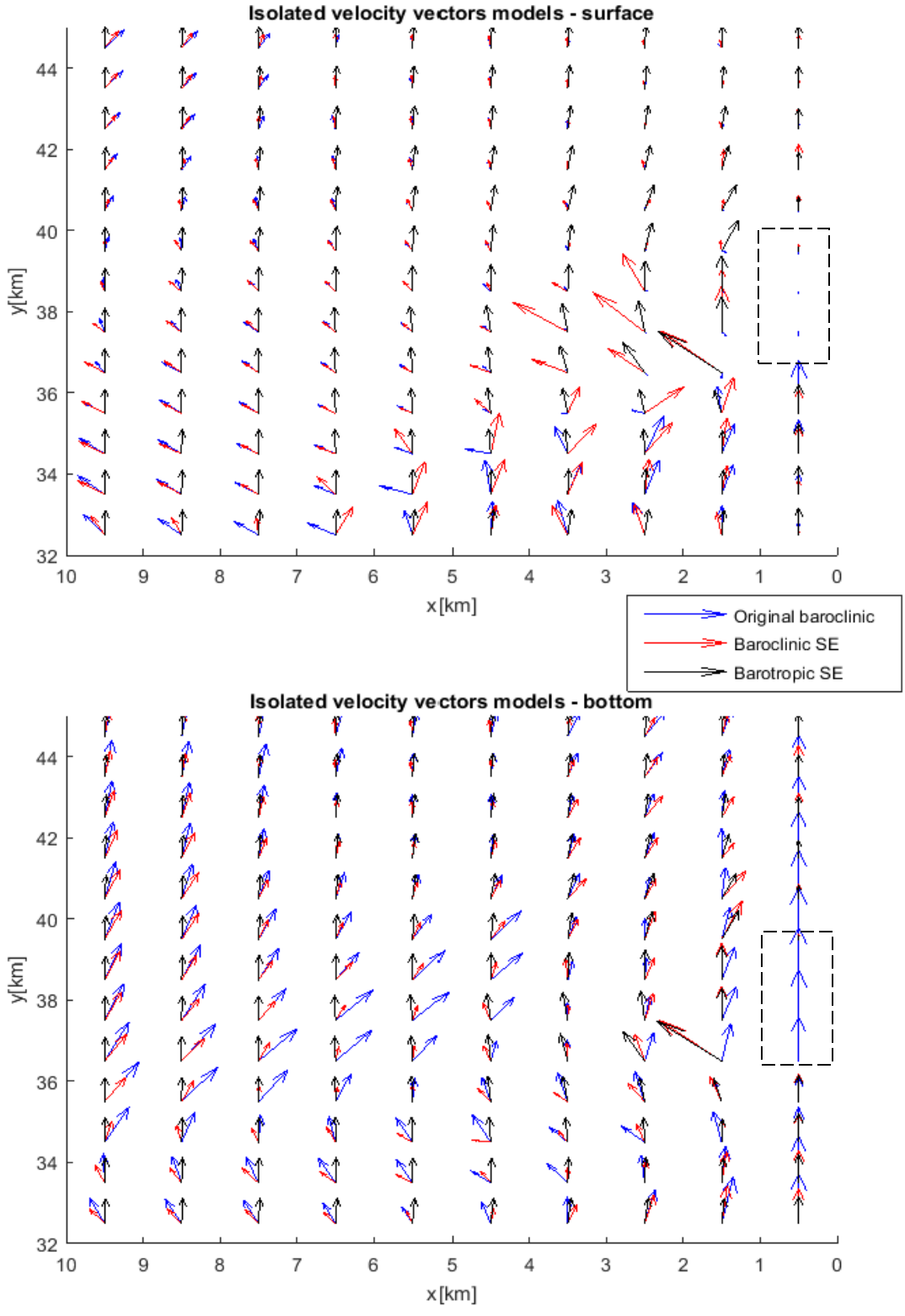

Figure 5.7: Isolated velocity vectors in selected layers in the area around the Sand Engine (LT+5). Top figure: surface layer; bottom figure: 10th sigma layer. Rather strong offshore flow can be detected at the surface which is not caused by a barotropic mechanism. The scaling of the velocity vectors is different for the top and bottom figure, which explains the large size of the blue velocity vectors in the bottom figure.

5.2. Spring tide simulations

The spring tide simulations have much higher energy levels due to a tidal boundary condition with an amplitude of 1.25 meters. This causes increased tidal mixing and thus a smaller and less profound Rhine ROFI which does not stratify on a semi-diurnal timescale. The simulations will again be discussed in three stages. First the original model outcomes will be shown (5.2.1). Subsequently the simulation is presented in which the Sand Engine has been added (5.2.2) and finally the results will be discussed (5.2.3).

5.2.1. Original spring tide simulations

This section discusses the original model outcomes for the spring tide simulation. The time- and depth averaged salinities resulting from this model run were shown in section 4.2. This paragraph discusses the physics in the Rhine ROFI during spring tide. Salinity distributions with a two-hour interval are shown in Figure 5.8 for the entire area of interest.

The more energetic environment clearly disturbs the development of a stable Rhine ROFI, consistent with De Boer (2008). A highly irregular pattern is found. The shape of the ROFI is rather constant over depth. Very little stratification occurs besides a region close to the river mouth (from y = 20km to y = 50 km). This can be concluded when comparing Figure 5.8 to Figure 5.9, which shows the salinity distributions at a larger depth. In general salinities in the Rhine ROFI are lower compared to neap tide conditions. The likely reason is the increased tidal mixing during spring tide.

Furthermore the ROFI does not extend as far offshore as in the neap simulation in the region of the river mouth. The cross-shore width during neap conditions is approximately 35 kilometres, whereas for the spring tide simulation this is only 20 kilometres. This can indicate the weakness of the tidal straining process compared to neap tide conditions. Further northwards though the width of the ROFI grows to nearly 40 kilometres. This is again in contrast with the neap tide simulation where a narrow “tidal river” is formed in the northern direction. The widening of the ROFI in northern direction could for instance be explained by gravitational circulation due to the cross-shore density gradient (see section 3.3). This cross-shore density gradient causes a stationary offshore (freshwater) flow at the surface and onshore flow at the bottom. This does not explain the widening of the ROFI at mid-depths (Figure 5.9). A possible explanation for this can be found in the tidal mixing process (section 3.4): fresh water at the surface disperses downwards.

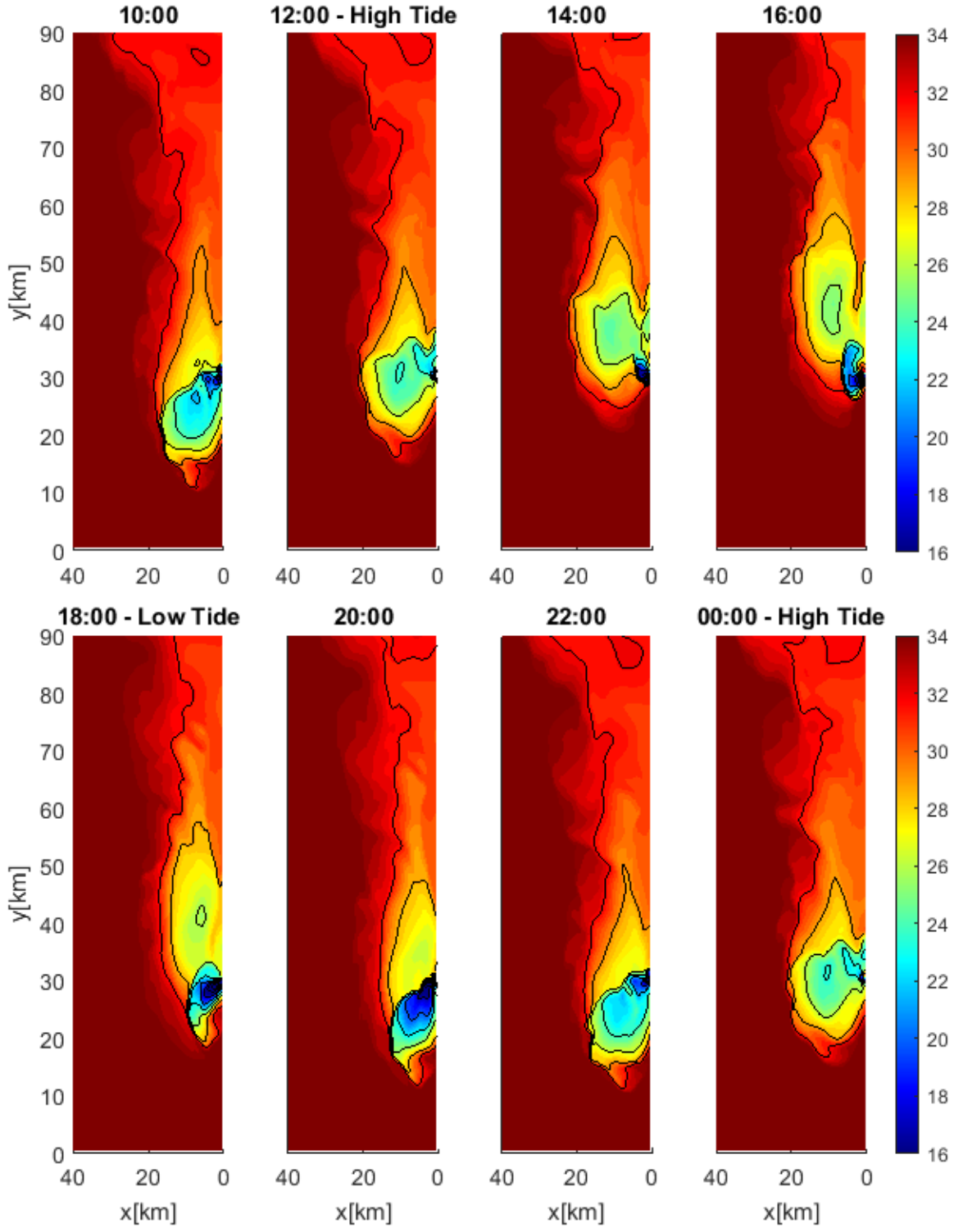

Figure 5.8: Distributions of salinities in the outcomes of the original spring tide model at two hour intervals.

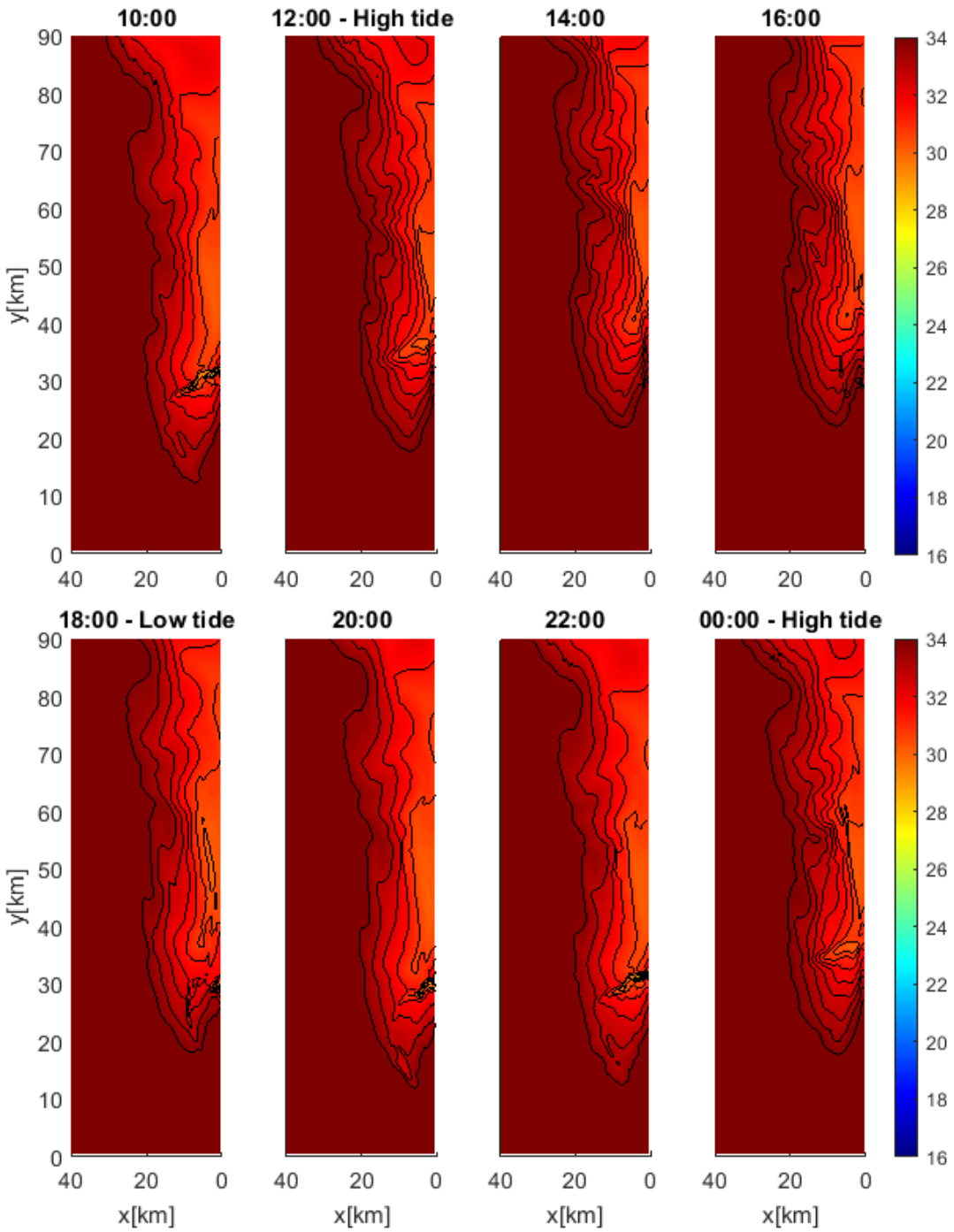

Figure 5.9: Distributions of salinities in the eight sigma-layer.

5.2.2. Spring tide with Sand Engine

In this paragraph the results are discussed when the Sand Engine in the spring tide conditions is included. The model set-up for the implementation of the set-up is discussed in 4.3. The distributions of salinity in the surface layer are plotted in Figure 5.10. Again no problems arise around the boundaries of the model when the Sand Engine is added.

Consistent with neap conditions, no large scale changes of the Rhine ROFI occur when the Sand Engine is added to the model. In detail, see Figure 5.11, some minor but remarkable differences can be identified once more. Similar to neap conditions, the Sand Engine seems to attract a stream of fresh water around high tide (12 a.m. and 12 p.m.). Subsequently between high and low tide the fresh water disperses strongly and instead salt water surfaces around the Sand Engine. This effect of the Sand Engine was not found during the neap tide simulations.

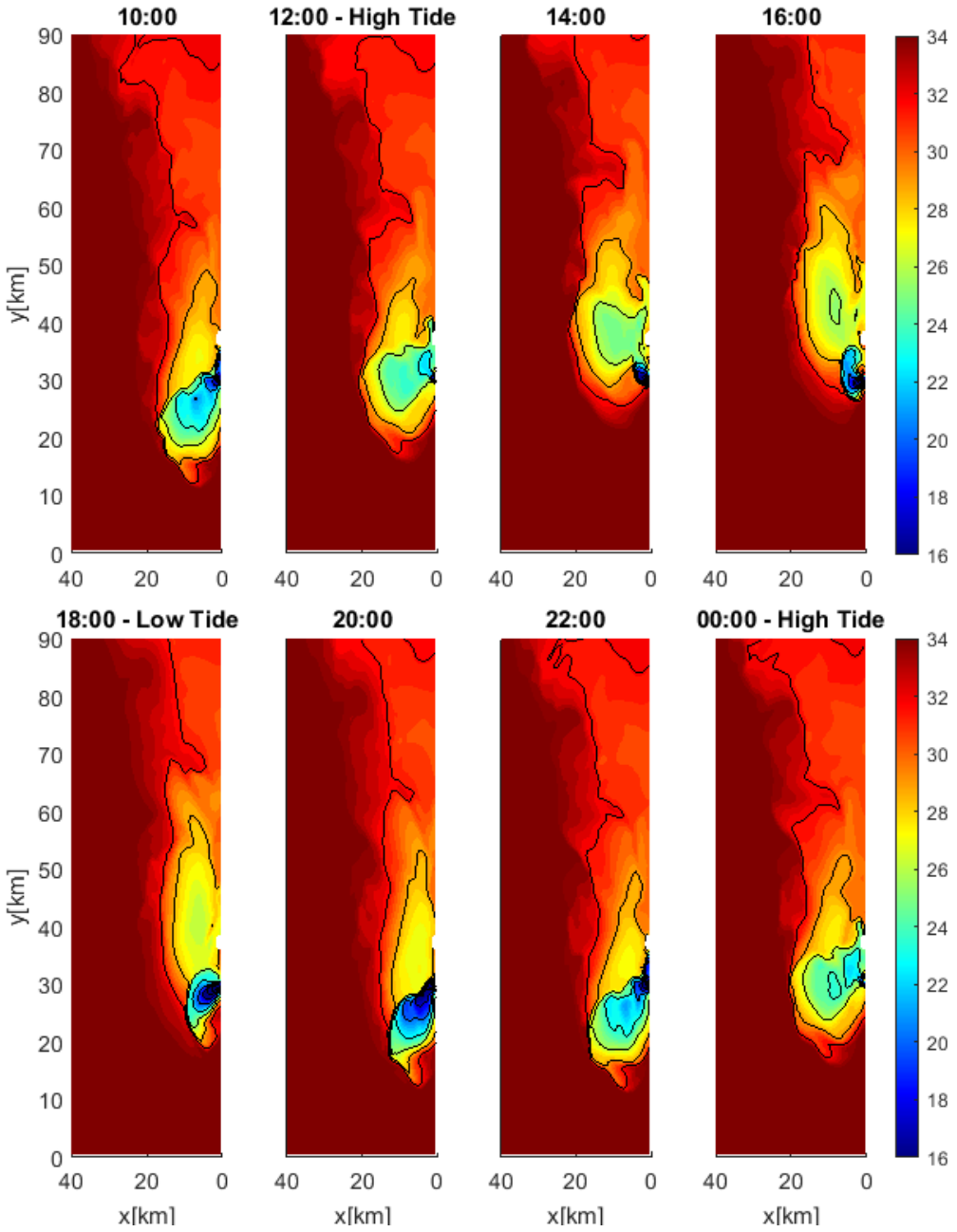

Figure 5.10: Salinity distributions in the surface layer for spring tide simulation including the Sand Engine.

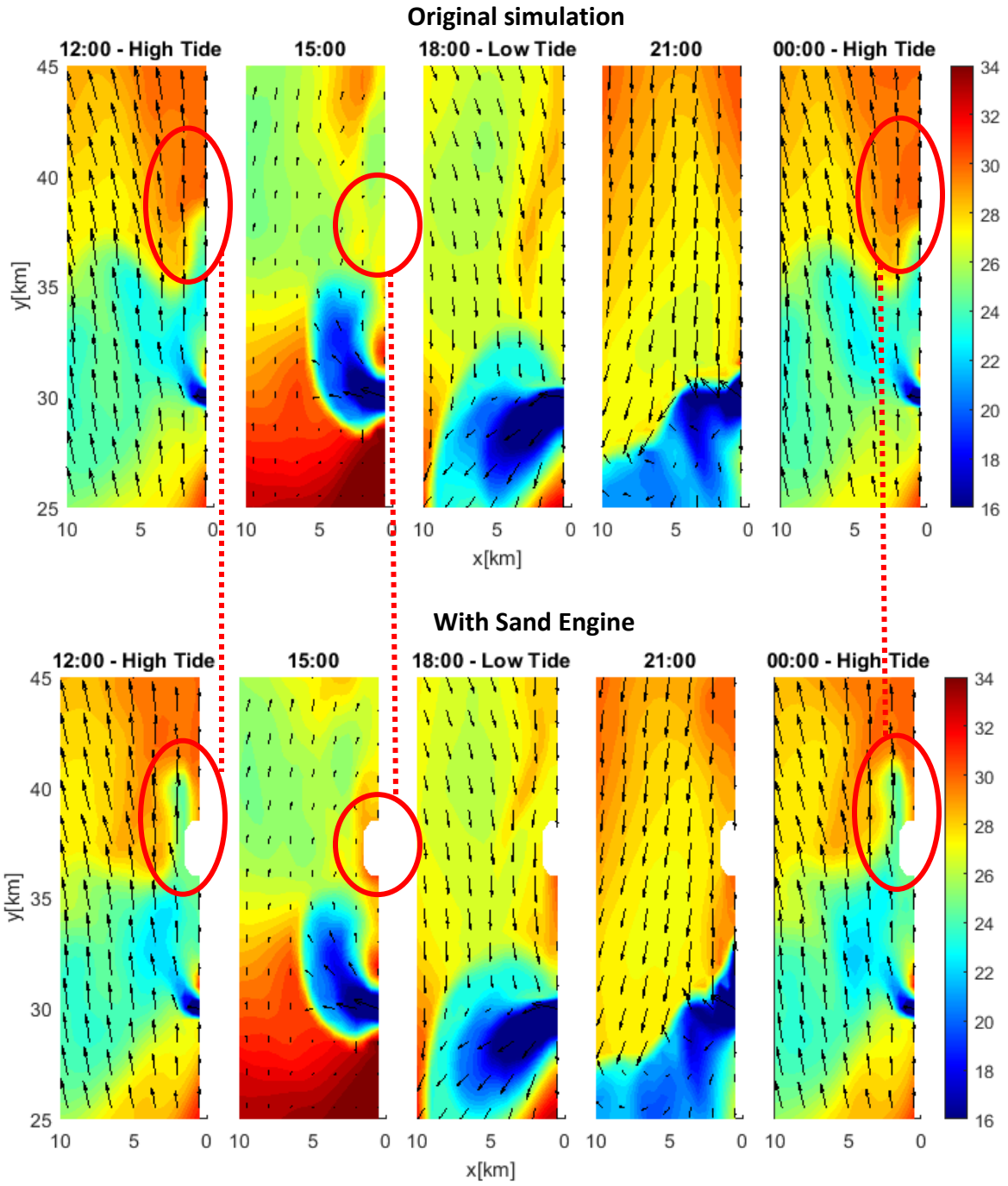

Figure 5.11 Salinity and velocity distributions in a smaller area encapturing the Sand Engine. In the red circles some interesting phenomena have been highlighted which are discussed in "Discussion of spring tide simulations" (section 5.2.3).

5.2.3. Discussion of spring tide simulations

Two remarkable effects of the Sand Engine to the salinity distributions have been identified in section 5.2.2: an alongshore fresh water stream along the Sand Engine at high tide (12 a.m. and 12 p.m.) and saltier water surrounding the Sand Engine between high and low tide (around 3 p.m.). For these two features an explanation is sought.

The fresh water feature is stretched along the alongshore edge of the Sand Engine and continues downstream. This feature probably has the same origin as during neap tide. Again a strong barotropic current (for continuity reasons) is initiated at the south-west corner of the Sand Engine (see Attachment D for the isolated velocity vectors).This current transports water to the area right in front of the Sand Engine. From there on it is transported downstream with the tidal currents. However in contrast with neap conditions, under spring tide conditions the fresh water is not being dispersed offshore (again see Attachment D for the velocity vectors). It is transported strictly alongshore from south to north until it mixes with saltier water.

The most likely explanation is the 'failing' of the tidal straining process. During the highly energetic spring tide little mean stratification exists as relaxation of the horizontal density gradient (gravitational circulation) cannot occur. Therefore the tidal straining effect is also weak (as explained in section 3.4). Stratification is superimposed by the advection of the fresh water in front of the Sand Engine by the strong barotropic current at the southwest corner of the Sand Engine. However, viscosities throughout the water column may remain large enough to prevent decoupling of the velocities in the bottom and surface layer. In that case tidal straining does not occur although a stratified situation emerged. This results in nearly strict alongshore advection of the fresh water.

The other remarkable difference between the original simulation and the simulation with the Sand Engine is the surfacing of saltier water between high and low tide (around 3 p.m.). This salt water feature is not found during neap conditions and is thus unique for high energy conditions. The likely cause is a faster mixing of the fresh water feature after high tide (after 12 p.m.). Still, the barotropic currents at the corners of the Sand Engine cause an offshore flow. To compromise an onshore flow at the bottom has to occur. The combined velocities lead to upwelling of saltier water at the Sand Engine. A more detailed explanation including figures illustrating this phenomenon can be found in Attachment E.

6. Discussion

In this research a very simplified approach and model has been applied in order to gain insight into the effects of the Sand Engine on the Rhine ROFI. The simplified method is a reason for caution as the outcomes must be placed in the right perspective. The most important restraints will be discussed in this chapter before drawing some final conclusions and making recommendations in the next chapter.

In first instance the original model of De Boer was applied. This model is highly simplified. It has (amongst other simplifications) a flat bathymetry with a constant depth, a constant river outflow of 2500 m^3/s and a simplified coastline. The same motivation for the use of this simplified model in this research is applicable as in De Boer's dissertation (2008): the simplification removes a lot of secondary forcing. It thus makes it easier to investigate the processes of interest. The received model was first verified by comparing the outcomes to De Boer's research. It appeared that differences in the salinity distributions arose due to some altered settings. De Boer used his model for different purposes which required different settings (e.g. investigating all mechanisms at the same time and specifically investigating upwelling induced by tidal straining, require different model set-ups). In the end rather arbitrary settings were applied for some physical parameters such as viscosity and friction. It appeared that the ROFI was very sensitive to this.

With the considerations of a simplified bathymetry, the outcomes cannot be directly translated to the real situation. Other factors come into play, which might be dominant. An example is the heat input by solar radiation, as discussed in "*Tide-Stratification Interaction in the Rhine ROFI Coastal Zone*" (De Boer, Pietrzak, & Winterwerp, 2011). However, still valuable conclusions can be drawn within this perspective (De Boer, Pietrzak, & Winterwerp, 2009).

The conclusions on the effect of the implementation of the Sand Engine in the coastline must be placed in the same perspective. For several reasons this research can only be assessed as being exploratory. Many simplifications regarding the Sand Engine have been made. The main simplification is the basic geometry of the Sand Engine in the model. De Boer's model works with a grid with a resolution of 500x500 meters. This limits the possible shape of the Sand Engine in the model to a very blunt shape. In reality this shape is much more streamlined, even in its first phase in 2011. This might very well be the reason for some exaggerated results. As discussed in section 5.1.3 no leeside eddy is found in the results. The appearance of the eddy could be expected from Signell's theory (Signell R. , 1989), see section 3.5. In Signell's work a more realistic streamlined shape is used. This streamlined shape causes a very different type of flow separation in comparison to a blunt shape. Furthermore it might be possible that the leeside eddy cannot be seen on the course grid used in the model as the eddy predicted with Signell's theory would not span across a large number of grid cells.

Nevertheless, the findings of large density gradients and offshore velocities in such a simple model are very valuable. The large temporal changes of the density during one tidal cycle in the vicinity of the Sand Engine might be a very large influence on the local hydrodynamics. For neap tide conditions these density gradients also coincide with widespread offshore velocities; for barotropic conditions only locally a strong offshore current was found, see Figure 5.6 and Figure 5.7. For spring tide conditions no clear

offshore velocity component can be detected, besides the similar barotropic current at the southwest corner of the Sand Engine. Still density differences are large for spring tide conditions.

The widespread offshore component of the velocity vectors in the vicinity of the Sand Engine is also found in measurement campaigns. One of those campaigns was MegaPEX2014 (TUDelft, N.D.). This large scale campaign had multiple purposes within the fields of hydrodynamics, morphology and ecology. The specific target was to gain insight into the (future) development of the Sand Engine. In the measurements and also measurements from earlier campaigns, offshore directed currents were found. In many researches regarding the measurements the effect of densities were not considered (Schlooz, 2012) (Van Ettinger & De Zeeuw, 2010) (Wengrove, Henriquez, De Schipper, Holman, & Stive, 2013).

In a more recent study based on the MegaPEX measurements (Radermacher, Zeelenberg, De Schipper, & Reniers, 2015), very similar flood patterns were described as were found in this research. Specific results were discussed from drifters deployed on October 1st 2014 (Radermacher, Zeelenberg, De Schipper, & Reniers, 2015). A rather low-energy tide was present as the moon was at its first quarter of the moon period (although the lag time is a few days to neap tide) (Maanstanden, 2014). Nearly all drifters were transported at least a few hundred meters offshore, in the same direction as the fresh water feature is dispersed during neap conditions in the model. By speculation, it is thus possible that the offshore currents present during the measurements had a strong baroclinic origin, i.e. not caused by a pure combination of geometry and tide.

7. Conclusions and recommendations

The goal of this research was to explore the influence of the Sand Engine on the Region Of Freshwater Influence (ROFI) of the river Rhine. In a very pragmatic approach this problem has been simplified and analysed using Delft3D-FLOW. Although very simplified, the Sand Engine was succesfully implemented in the model of De Boer (2008).

The most important finding was the development of a fresh water feature around high tide at the location of the Sand Engine during both neap and spring tide conditions. During neap conditions the feature was not only advected downstream but also offshore due to widespread offshore velocity components in front of the Sand Engine. This offshore spreading of the fresh water did not occur during the more energetic spring tide conditions.

For the offshore directed currents to develop several possible mechanisms were identified. A logical cause could be a current with barotropic origin initiated at the southern end of the Sand Engine for continuity reasons as the tide has to propagate around the perturbation. However, it was found that this introduces only a very local offshore directed current at the southwestern tip of the Sand Engine. This local current is likely the offset of the fresh water feature, but is not the cause of its offshore growth. Possible other mechanisms causing the offshore advection are a gravitational circulation due to a cross-shore density gradient or an enhanced tidal straining. If tidal straining would indeed be the cause of the offshore advection it would explain why offshore advection of the freshwater feature does not occur during spring tide. During spring tide tidal straining is weakened or even neglectable.

During one tidal cycle very large differences in salinities at the Sand Engine can be found both during neap and spring tide. During spring tide even salinization occurs between high and low tide after the fresh water feature has been dispersed or mixed. These large differences in salinities may seriously influence local hydrodynamics and ecology. Maximum offshore currents of 0.2 m/s were found, which contribute to geometry-induced offshore currents (Schlooz, 2012). Together such offshore currents could seriously harm swimmer safety at the Sand Engine (Van Ettinger & De Zeeuw, 2010).

As a very pragmatic approach was applied in this thesis there is room for additional research. This research has shown the possible importance of taking into account salinities and densities in hydrodynamic research in this specific area. A lot of the topics discussed in this research are entailed with uncertainty. As the physics and phenomena influencing the Rhine ROFI have been identified (De Boer, 2008), more detailed research can be undertaken. One of the possible topics is the effect of perturbations, which has been dealt with in this thesis. This thesis can be seen as a preliminary research for more advanced research on the topic. It is therefore recommended to look at the problem with more detail and increase the complexity and accuracy of the model along the way. Some recommendations are:

- *Develop a model in which the Sand Engine can be implemented more accurately*. In the course grid applied in this research it could only be represented by a rectangular block. When the shape of the Sand Engine is modelled, the outcomes in the salinity and velocity distributions are likely

to correspond more closely to reality. Furthermore it can then also be tested how different shapes of perturbations in the coastline effect the baroclinic conditions.

- *Test the effects of the Sand Engine in a more realistic mode of the Rhine ROFII*. If in future research the Rhine ROFI is modelled more accurately it might be very important to implement the Sand Engine from the start. In this research a simplified bathymetry was used with a constant depth of 20 meters, similar to De Boer (2008). Depth variations also contribute to the velocity field and thus also the salinity distributions. In the same line of thought the sloping edges of the Sand Engine will also play a role. The depth is reduced for an area larger than what is implemented in this research (which is only the emerged area of the Sand Engine). This may increase the area of the Rhine ROFI on which the Sand Engine may have an effect.

- *Add water temperatures to the model*. In this research only baroclinic effects due to salinity have been tested. However, the Rhine ROFI also has a large contrast in temperatures with the surrounding areas. Temperature can be regarded as a passive tracer (De Kok, De Valk, Van Kester, De Goede, & Uittenbogaard, 2001), but may enhance the density gradients and as of such the baroclinic currents (De Boer, Pietrzak, & Winterwerp, 2011). In the current model a certain temperature for the river outflow could be set and solar heat input can be added to evaluate the effect of temperature.

- *Run a model for an entire tidal period.* The model applied in this research had two fixed (separate) tidal conditions: neap and spring tide. It may be interesting to see how the fresh water feature at the Sand Engine changes for different moments in the tidal period; e.g. until when in the tidal period the fresh water is advected offshore as well as downstream.

- *Run a separate model in which the Maasvlakte 2 is added instead of the Sand Engine.* Implementing the Maasvlakte 2 into the model was beyond the scope of this research. However being the most radical perturbation in the Holland coast, it is likely to be a very influencing factor to the Rhine ROFI. Therefore it is recommended to perform a similar or more in-depth research on the effects of the Maasvlakte 2.

Bibliography

De Boer, G. (2008). *On the interaction between tides and stratification in the Rhine Region of Freshwater Influence.* Doctoral Dissertation.

De Boer, G., Pietrzak, J., & Winterwerp, H. (2011). Tide-stratification interaction in the Rhine ROFI coastal zone. *In: Heip, C. et al. (Ed.) (2011). Aspects of coastal research in contribution to LOICZ in the Netherlands and Flanders (2002-2010). LOICZ Research & Studies, 38: pp. 61-69*.

De Boer, G., Pietrzak, J., & Winterwerp, J. (2009). SST observations of upwelling induced by tidal straining in the Rhine ROFI. *Continental shelf research, 29*, 263-277.

De Kok, J., De Valk, C., Van Kester, J., De Goede, E., & Uittenbogaard, R. (2001). Salinity and temperature stratification in the Rhine plume. *Estuarine, Coastal and Shelf Science, 53*, 467-475.

Google Maps. (2016). *Location Sand Engine*. Retrieved May 11, 2016, from https://www.google.nl/maps/@52.0253246,4.1832283,11.25z

Keulegan, G., & Carpenter, L. (1958). Forces on Cylinders and plates in an oscillating fluid. *Journal of Research of the National Bureau of Standards, 60*.

Maanstanden. (2014). *Maanstanden 2014*. Retrieved September 13, 2016, from Maanstanden-Info: http://www.maanstanden-info.nl/maanstanden-2014.html

Oostdam, B. (2001). *Index for Coastal Hazards*. Retrieved May 12, 2016, from http://isis.uwimona.edu.jm/uds/GEOHAZARDS_2001/coastal2001/tides-page2.html

Radermacher, M., Zeelenberg, W., De Schipper, M., & Reniers, A. (2015). Field Observations of Tidal Flow Separation at a Mega-Scale Beach Nourishment. In P. Wang, J. Rosati, & J. Cheng (Ed.), *The Proceedings of Coastal Sediments 2015* (pp. 253-264). San Diego, USA: World Scientific Publishing Company.

Savenije, H. H. (2012). *Salinity and tides in alluvial estuaries* (Second Edition ed.). Delft: Delft University of Technology.

Schlooz, G. (2012). *Convex coastline induced rip currents at the Sand Engine.* TUDelft.

Signell, R. (1989). *Tidal Dynamics and Dispersion Around Coastal Headlands.* Massachusetts Instute of Technology - Woods Hole Oceanographic Institution, Joint Program in Physical Oceanography.

Signell, R. P., & Geyer, W. R. (1991, February 15). Transient Eddy Formation Around Headlands. *Journal of Geophysical Research, 96*(C2), 2561-2575.

Simpson, J., & Souza, A. (1995, April 15). Semidiurnal switching of stratification in the region of freshwater influence of the Rhine. *Journal of Geophysical Research Atmospheres, 100*(C4), 7037-7044.

Simpson, J., Bos, W., Schirmer, F., Souza, A., Rippeth, T., Jones, S., et al. (1993). Periodic stratification in the Rhine ROFI in the North Sea. *Oceanologica ACTA, 16*(1), 23-32.

Simpson, J., Brown, J., Matthews, J., & Allen, G. (1990, June). Tidal straining, Density currents, and stirring in the Control of Estuarine Stratification. *Estuaries, 13*(2), 125-132.

Taylor, G. (1921). Tidal oscillations in gulfs and rectangular basins. *Proceedings of the London Mathematical Society, XX(2)*, 148-81.

TUDelft. (N.D.). *MegaPEX2014*. Retrieved September 13, 2016, from TUDelft; Coastal Engineering: http://www.citg.tudelft.nl/en/about-faculty/departments/department-of-hydraulic-engineering/sections/coastal-engineering/research/nemo/megapex2014/

Van Ettinger, H., & De Zeeuw, R. (2010). *Prognose zwemveiligheid Zandmotor - Stromingen en bodemontwikkeling.* Projectbureau Pilot Zandmotor.

Van Eyck, B. Luchtfoto Maeslantkering. *Luchtfoto van de gesloten Maeslantkering in de nieuwe Waterweg nabij Hoek van Holland.* Rijkswaterstaat, https://beeldbank.rws.nl.

Van Houdth, J. *131001 ZANDMOTOR 1 oktober 2013-52.* Rijkswaterstaat.

Visser, M. (1993). *On the transport of fine sediment in the Netherlands coastal zone.* Universiteit Utrecht, faculty of physics and astronomy.

Wengrove, M., Henriquez, M., De Schipper, M., Holman, R., & Stive, M. (2013). Monitoring morphology of the sand engine leeside using ARGUS' cBATHY . *Coastal Dynamics 2013: 7th International Conference on Coastal Dynamics.* Arcachon, France: Bordeaux University.

Attachments

Attachment A. Tidal straining in the 'Coastal river' during neap tide

To prove tidal straining being one of the mechanisms causing the stratification, Figure A.1 plots salinities and velocities in a cross-section in the 'coastal river' three hours after low tide. In the coastal river the physics become more two-dimensional as there is less alongshore variation. In the figures the tidal straining effect can clearly be distinguished in a ten-kilometre wide band close to the coast. Decoupling of surface and bottom velocities occurs, inducing a cross shore velocity shear, which is a characteristic of tidal straining. The findings are similar to what is found in theory (section 3.4).

A location-dependent variation is found in the tidal straining mechanism. This has been illustrated in Figure A.2. For all three locations a semi-diurnal variation of stratification is found. However, peaks occur at different times. Furthermore it can be seen that more mechanisms are in play. At kilometre y=50, only onshore velocities occur. It is likely that a mean onshore velocity is the cause of this and that the semidiurnal oscillation is due to tidal straining.

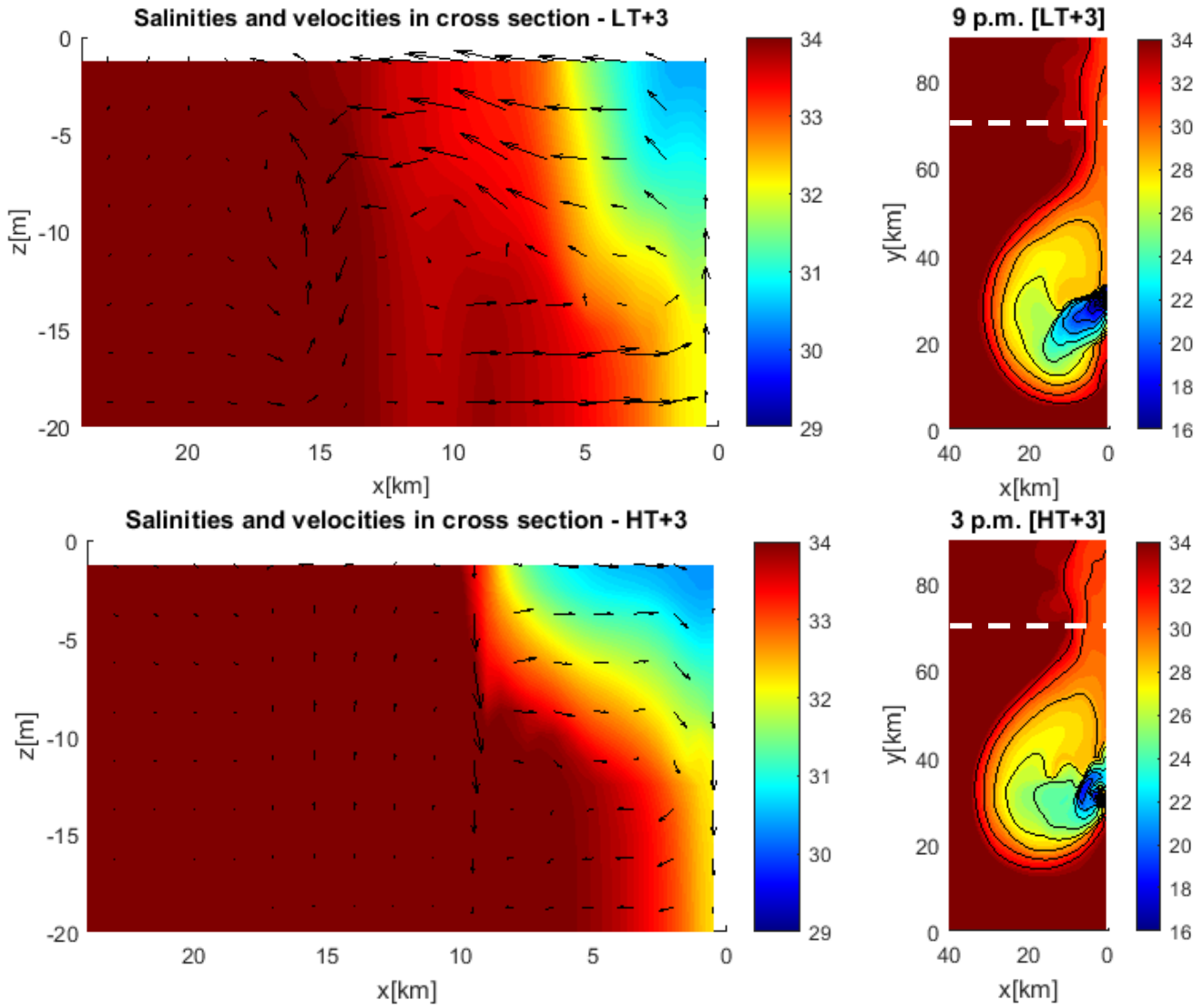

Figure A.1: Salinities and velocities in cross-section (left figures) at location shown in the figures on the right. Note the different color scale in the left figures compared to the right figures. The vertical velocities have been scaled by a factor 250 as those are several magnitudes smaller than the horizontal velocities. In both plots the cross-shore tidal straining effect can be distinguished which causes the semi-diurnal cycle of stratification and destrafication. Upwelling and downwelling at the land border occurs which is also an indication of the cross-shore tidal straining effect.

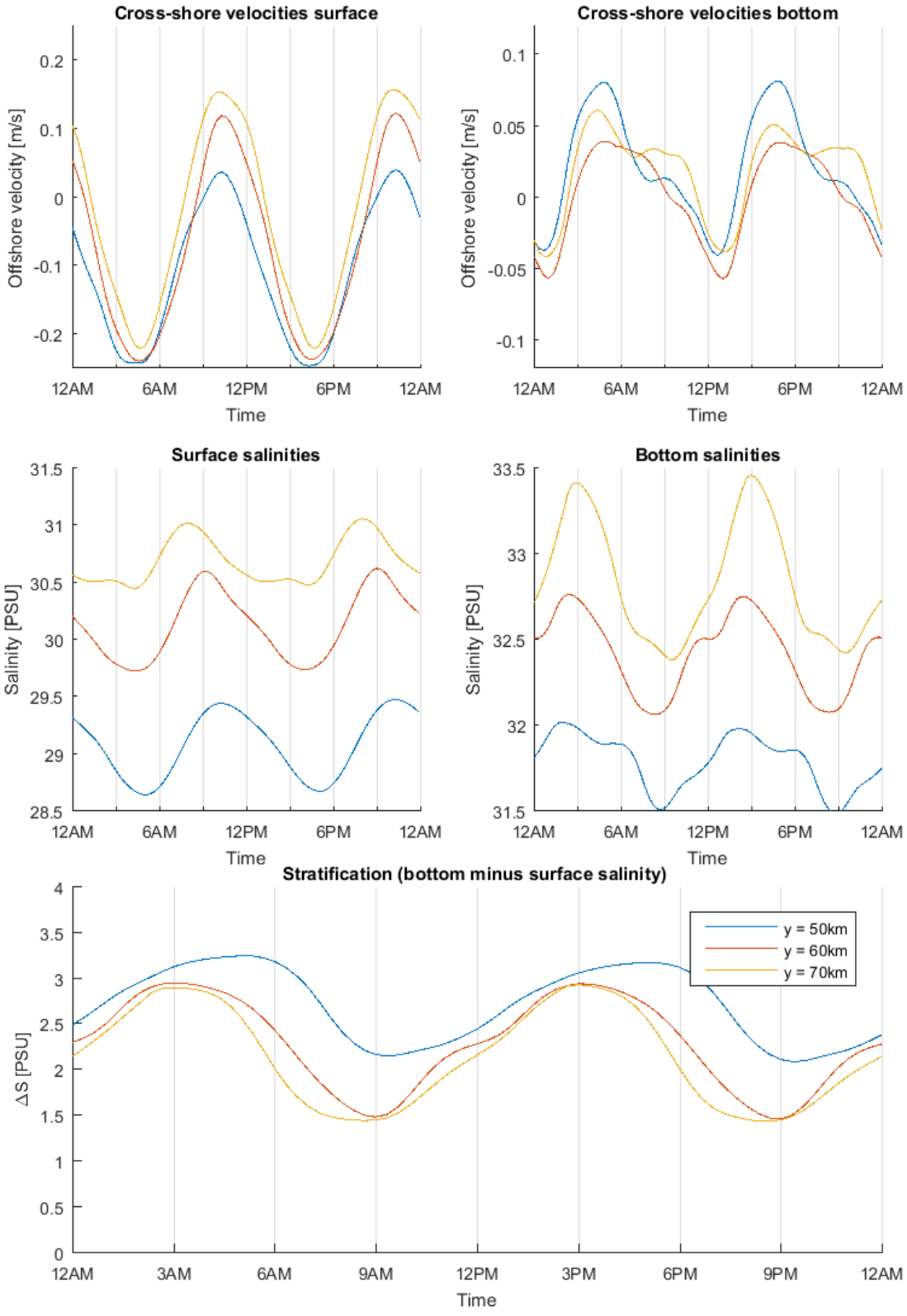

Figure A.2: Salinities and cross-shore velicities at different locations in the 'Coastal River'

Attachment B. Comparison of salinities and velocities for neap tide models

This attachment plots several figures comparing the salinities and velocities found in the various models. The figures are as follows:

- Figure B.1: 10 a.m. (HT-2)
- Figure B.2: 11 a.m. (HT-1)
- Figure B.3: 12 p.m. (HT)
- Figure B.4: 1 p.m. (HT+1)
- Figure B.5: 2 p.m. (HT+2)

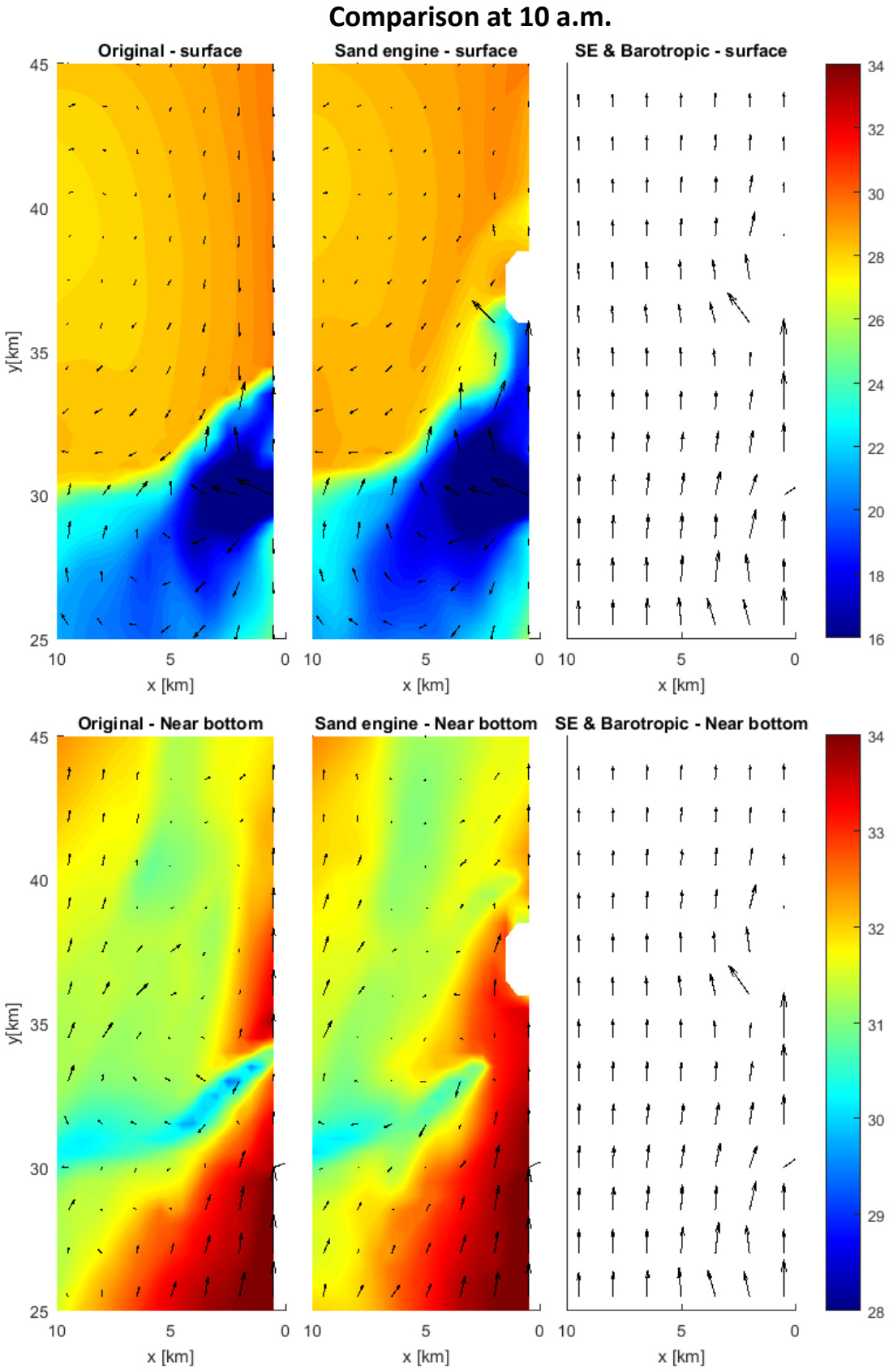

Figure B.1: Salinities and velocities at 10 a.m.

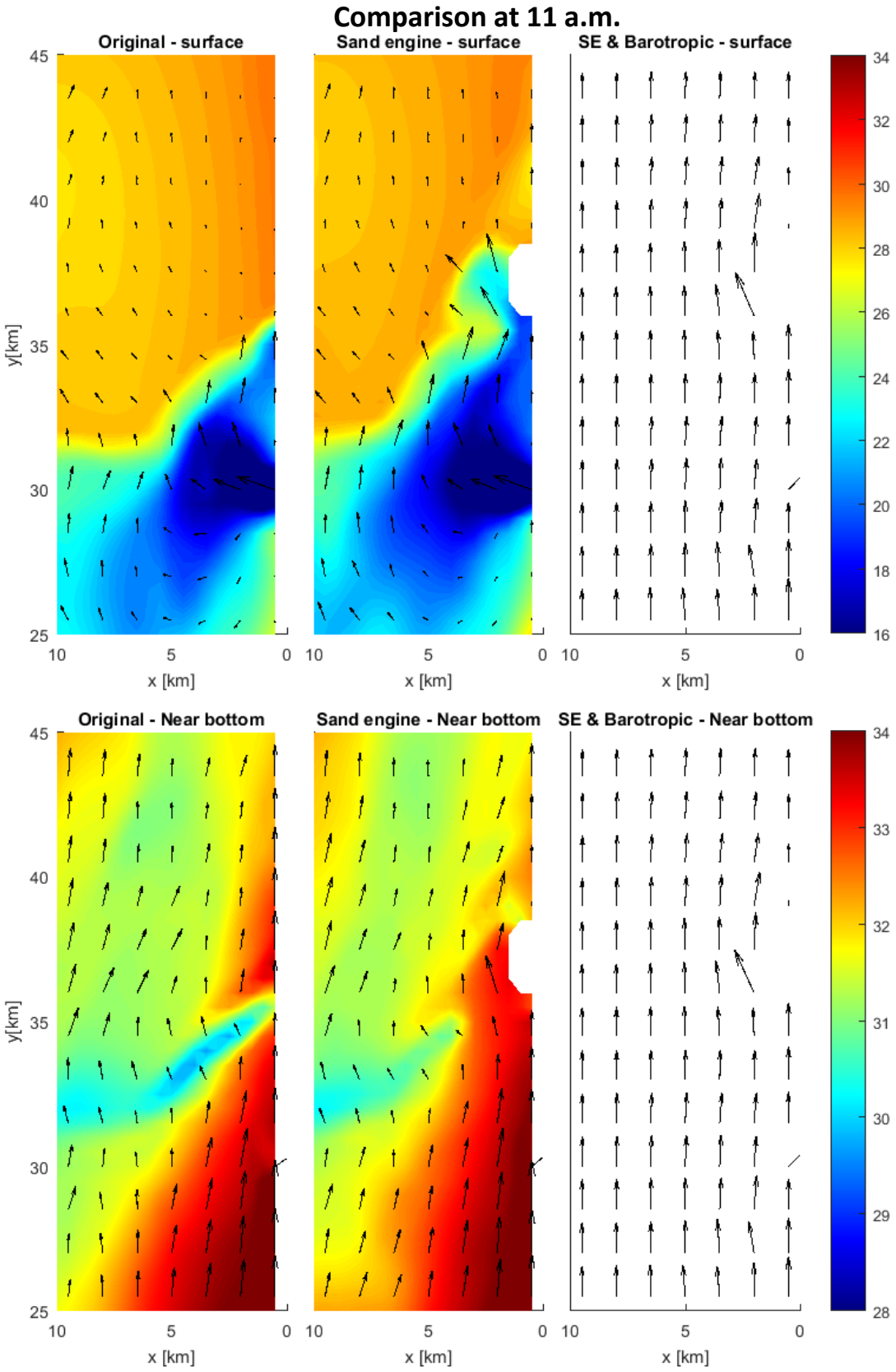

Figure B.2: Salinities and velocities at 11 a.m.

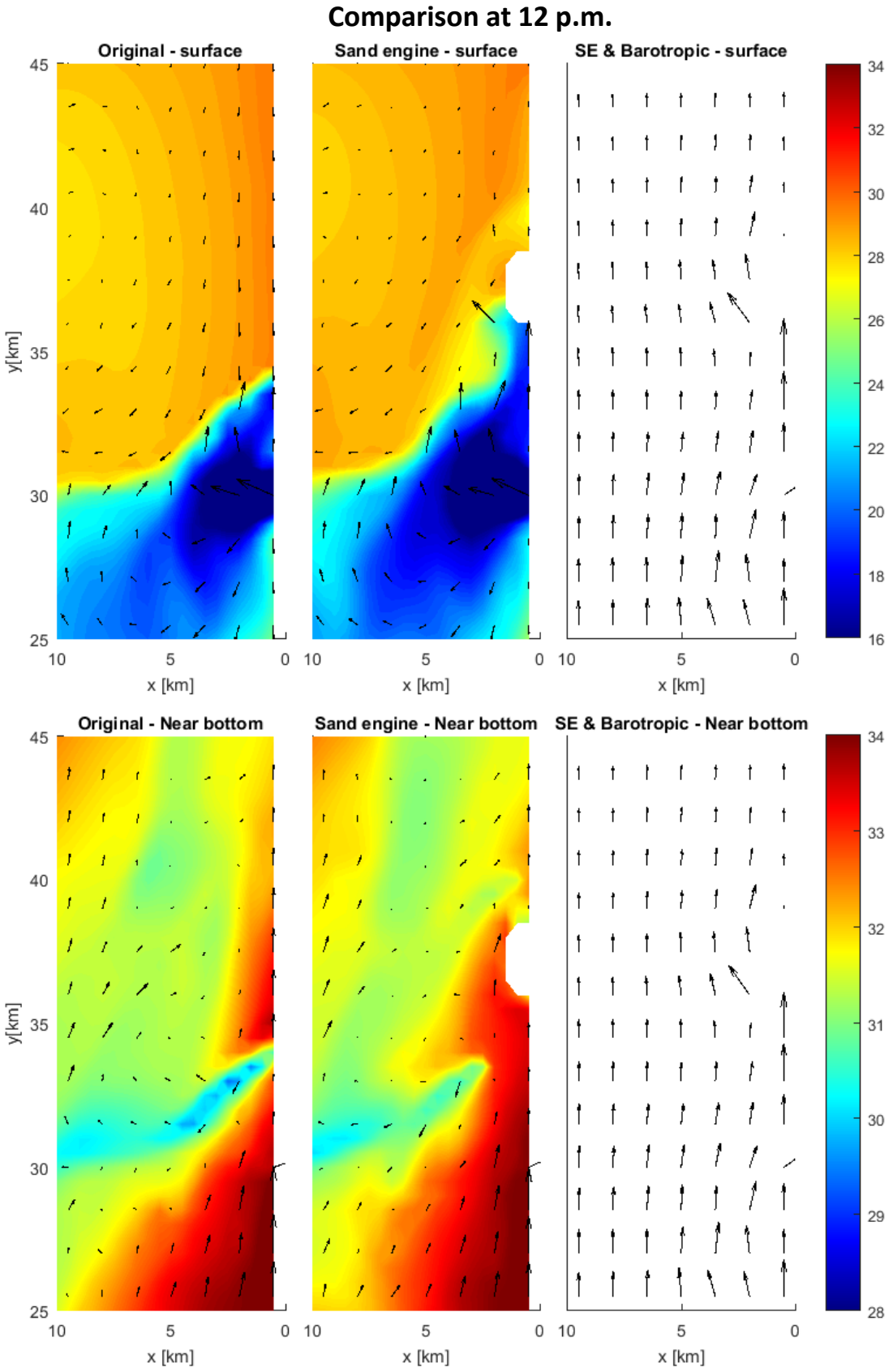

Figure B.3: Salinities and velocities at 12 p.m.

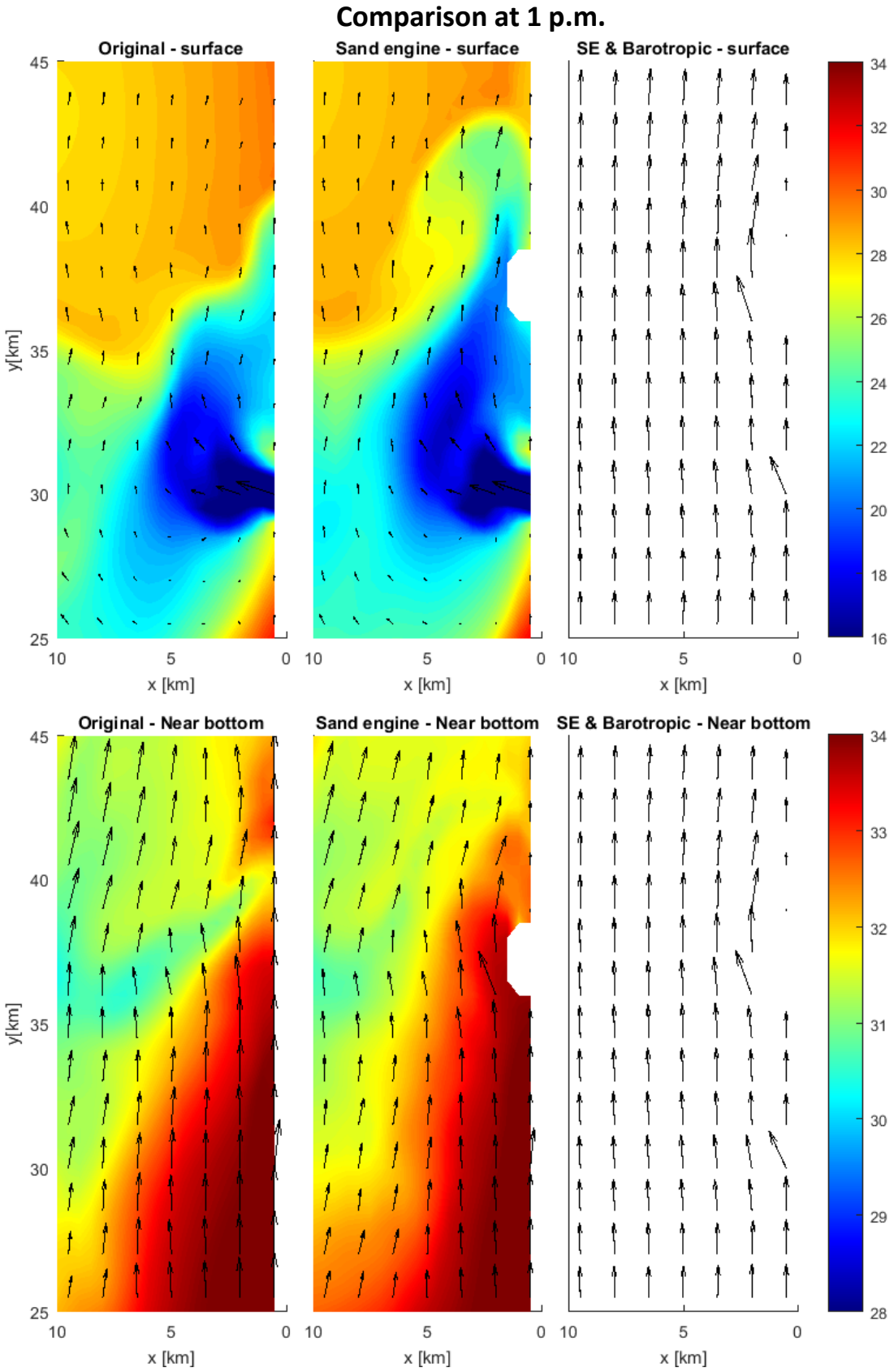

Figure B.4: Salinities and velocities at 1 p.m.

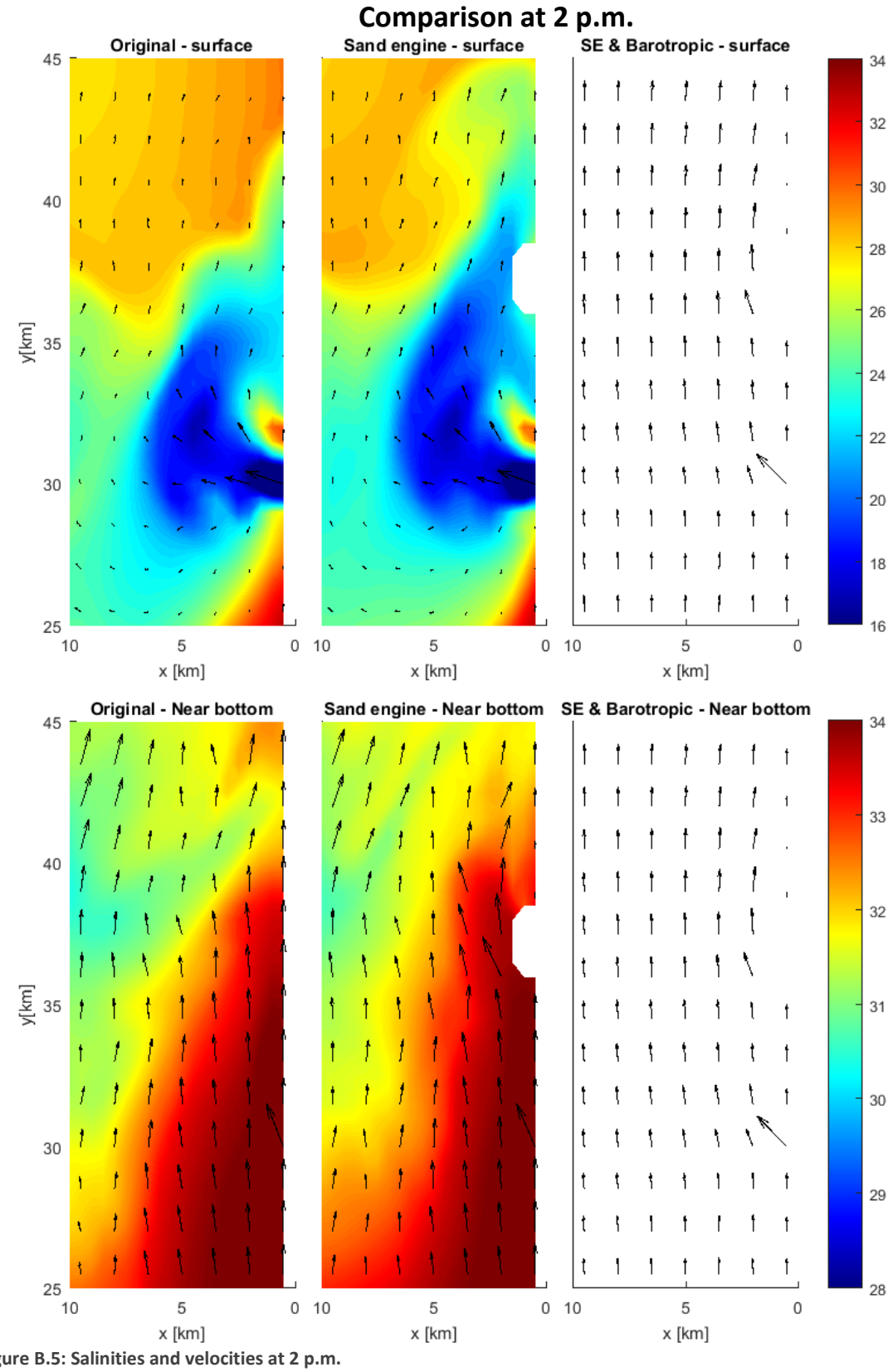

Figure B.5: Salinities and velocities at 2 p.m.

Attachment C. Time series of cross-shore velocities and salinities near the Sand Engine during neap tide

This attachment will show various figures of cross-shore velocities and salinities in locations near the Sand Engine. The locations are indicated in Figure C.1 below.

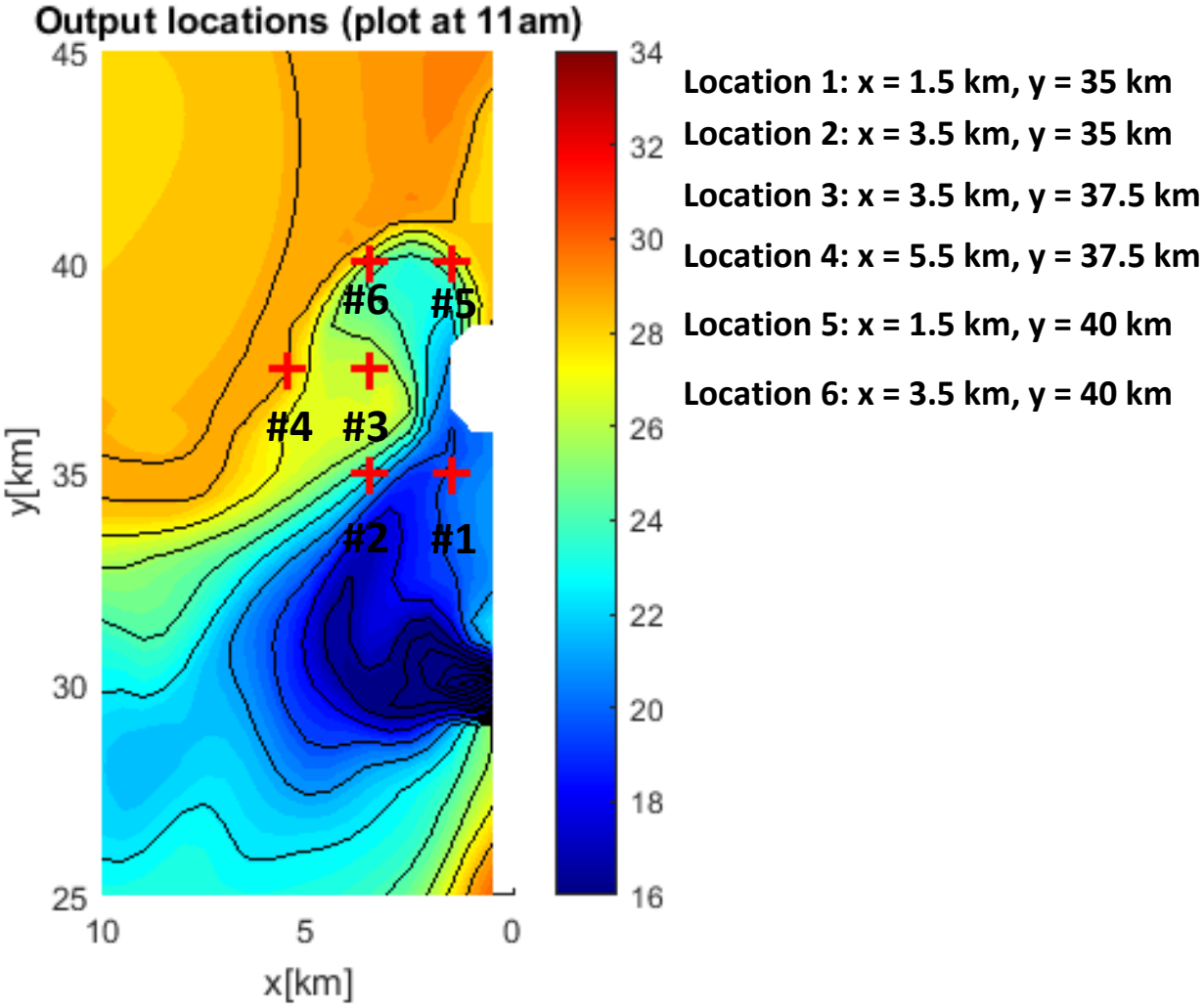

Figure C.1: Output locations near the Sand Engine for which time series of salinities and cross-shore velocities are plotted

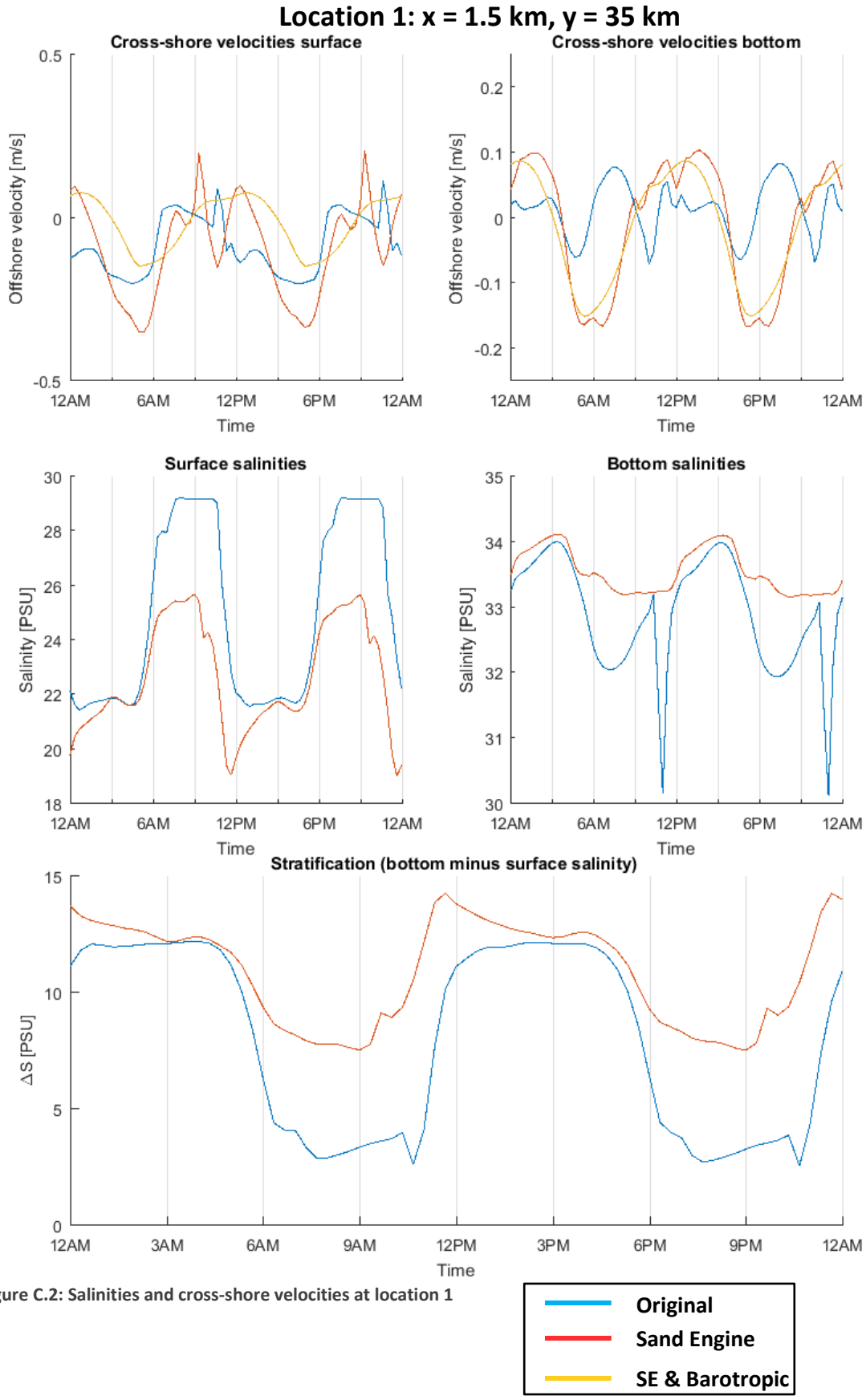

Figure C.2: Salinities and cross-shore velocities at location 1

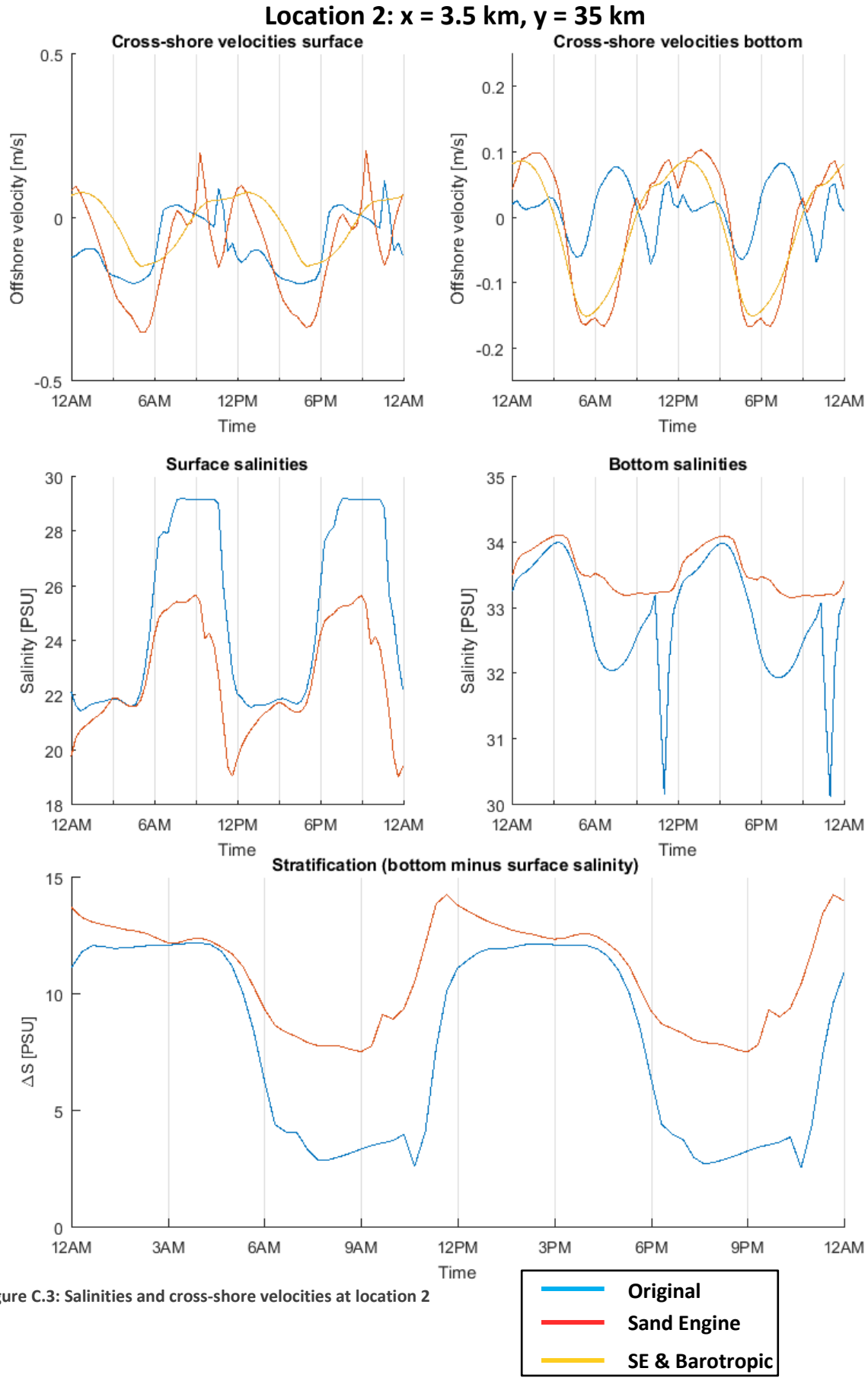

Figure C.3: Salinities and cross-shore velocities at location 2

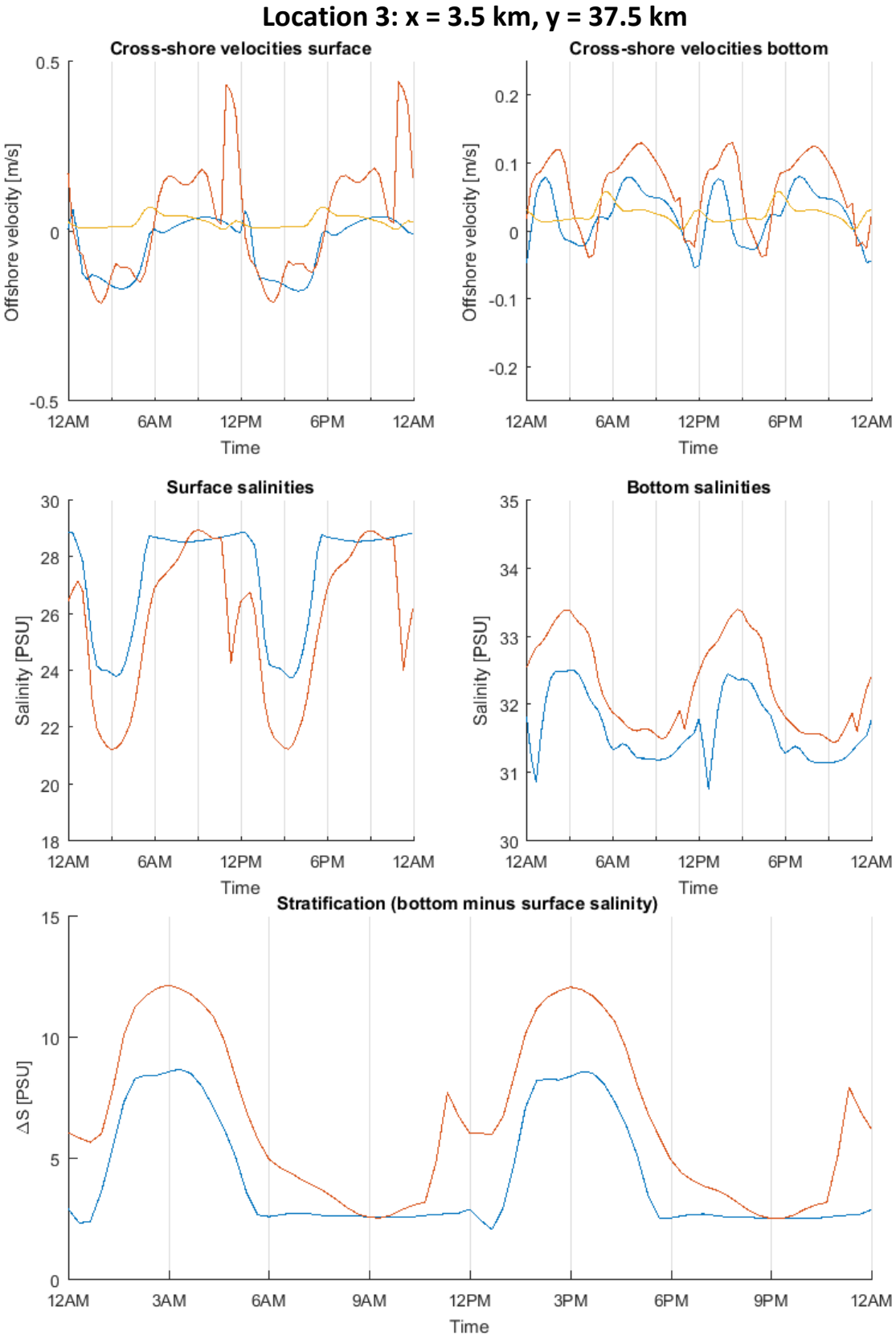

Figure C.4: Salinities and cross-shore velocities at location 3

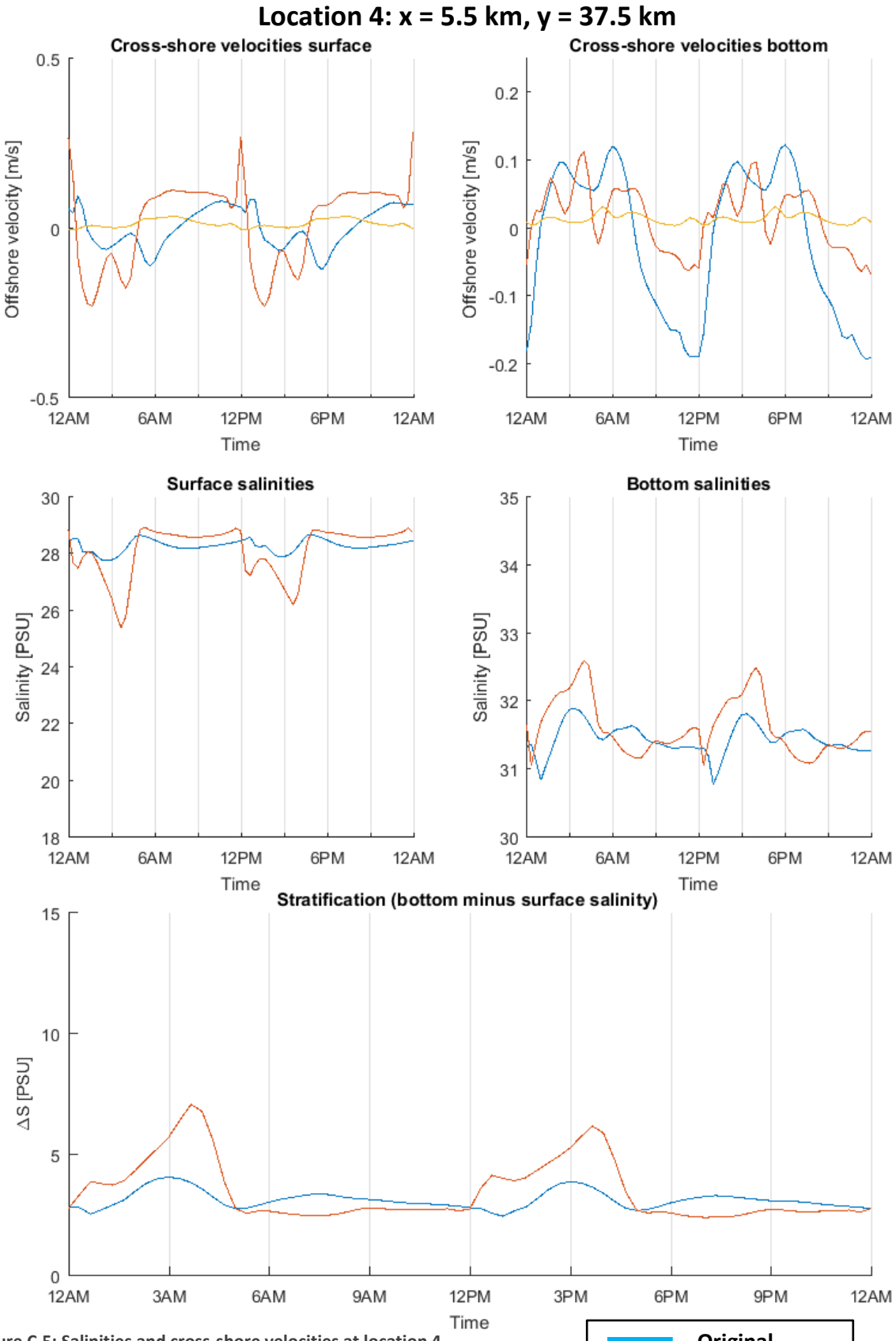

Figure C.5: Salinities and cross-shore velocities at location 4

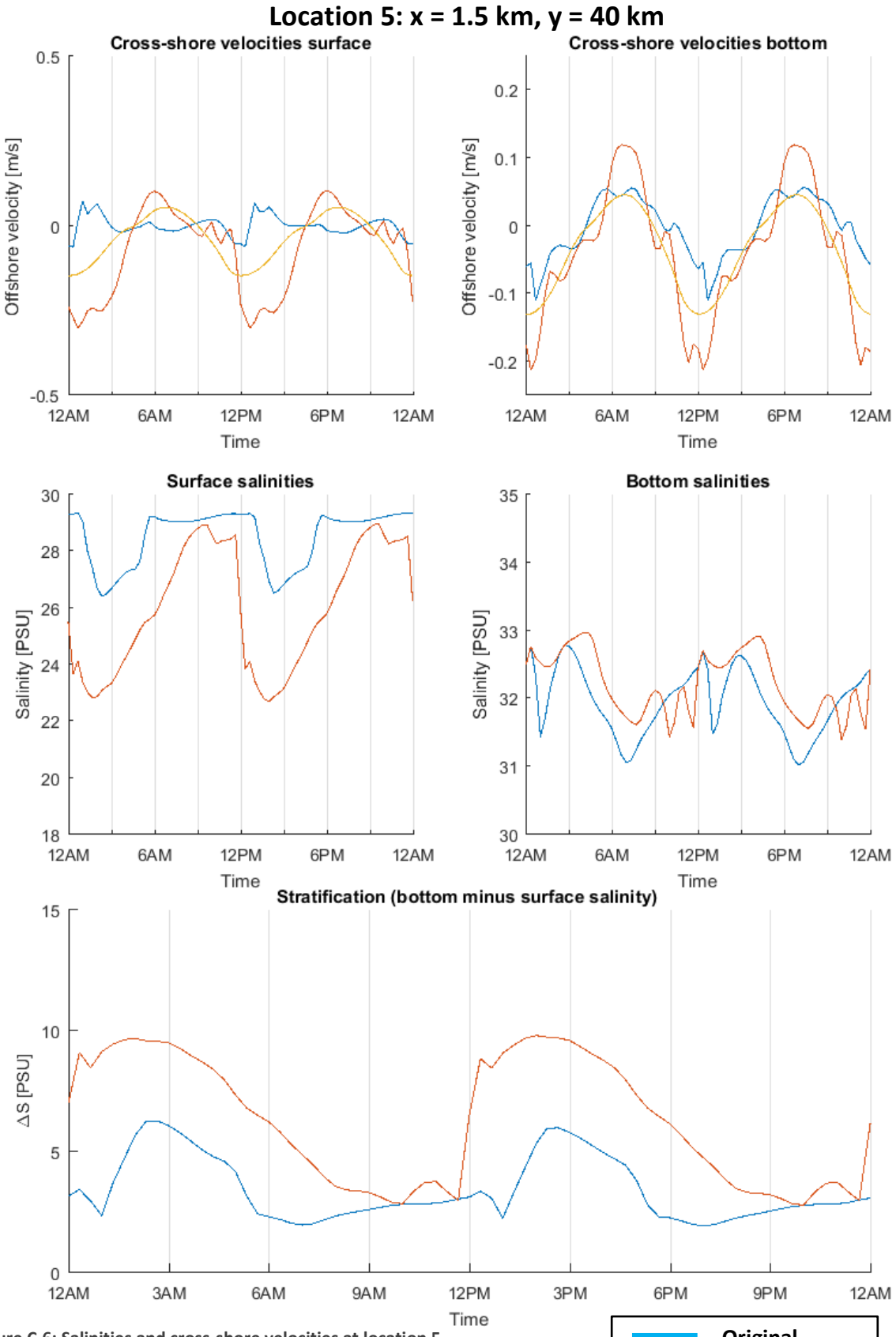

Figure C.6: Salinities and cross-shore velocities at location 5

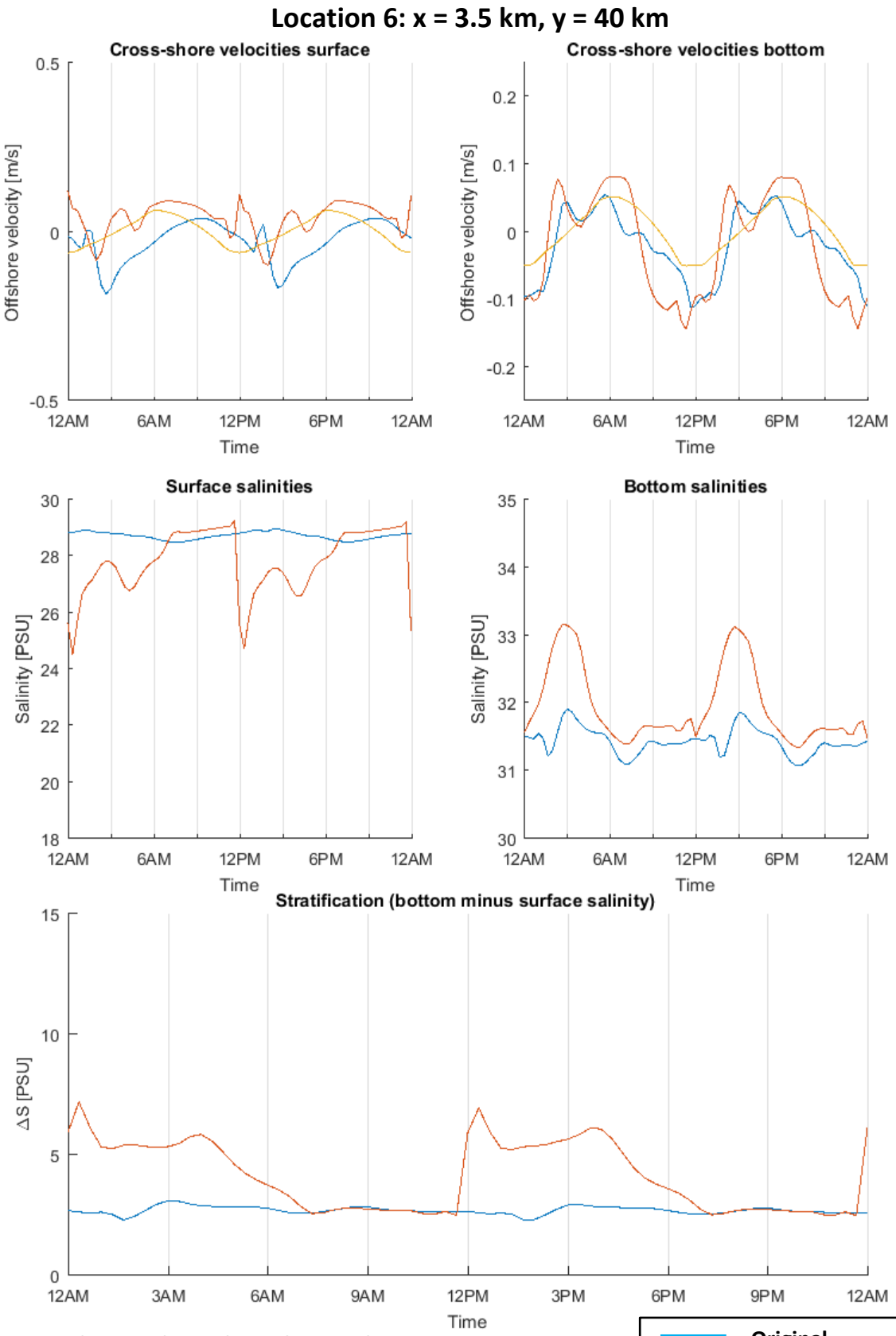

Figure C.7: Salinities and cross-shore velocities at location 6

Attachment D. Velocity distributions around high tide near the Sand Engine for neap and spring tide

This attachment will show figures with isolated velocity vectors. In the top figures the velocity vectors are plotted for the surface layer whereas the bottom figures show the velocity vectors in the 10th sigma layer (over half-way the water depth). The scaling of the vectors is different for the two figures, the same length of an arrow indicates a larger velocity in the top figure compared to the bottom figure. This is due to the large differences in velocity magnitudes over depth.

The following figures are plotted:

- Figure D.1: Velocity vectors for neap tide at 11AM (LT+5). Similar to Figure 5.7.
- Figure D.2: Velocity vectors for neap tide at 12PM (HT).
- Figure D.3: Velocity vectors for neap tide at 1PM (HT+1).
- Figure D.4: Velocity vectors for neap tide at 2PM (HT+2).
- Figure D.5: Velocity vectors for spring tide at 11AM (LT+5).
- Figure D.6: Velocity vectors for spring tide at 12PM (HT).
- Figure D.7: Velocity vectors for spring tide at 1PM (HT+1).
- Figure D.8: Velocity vectors for spring tide at 2PM (HT+2).

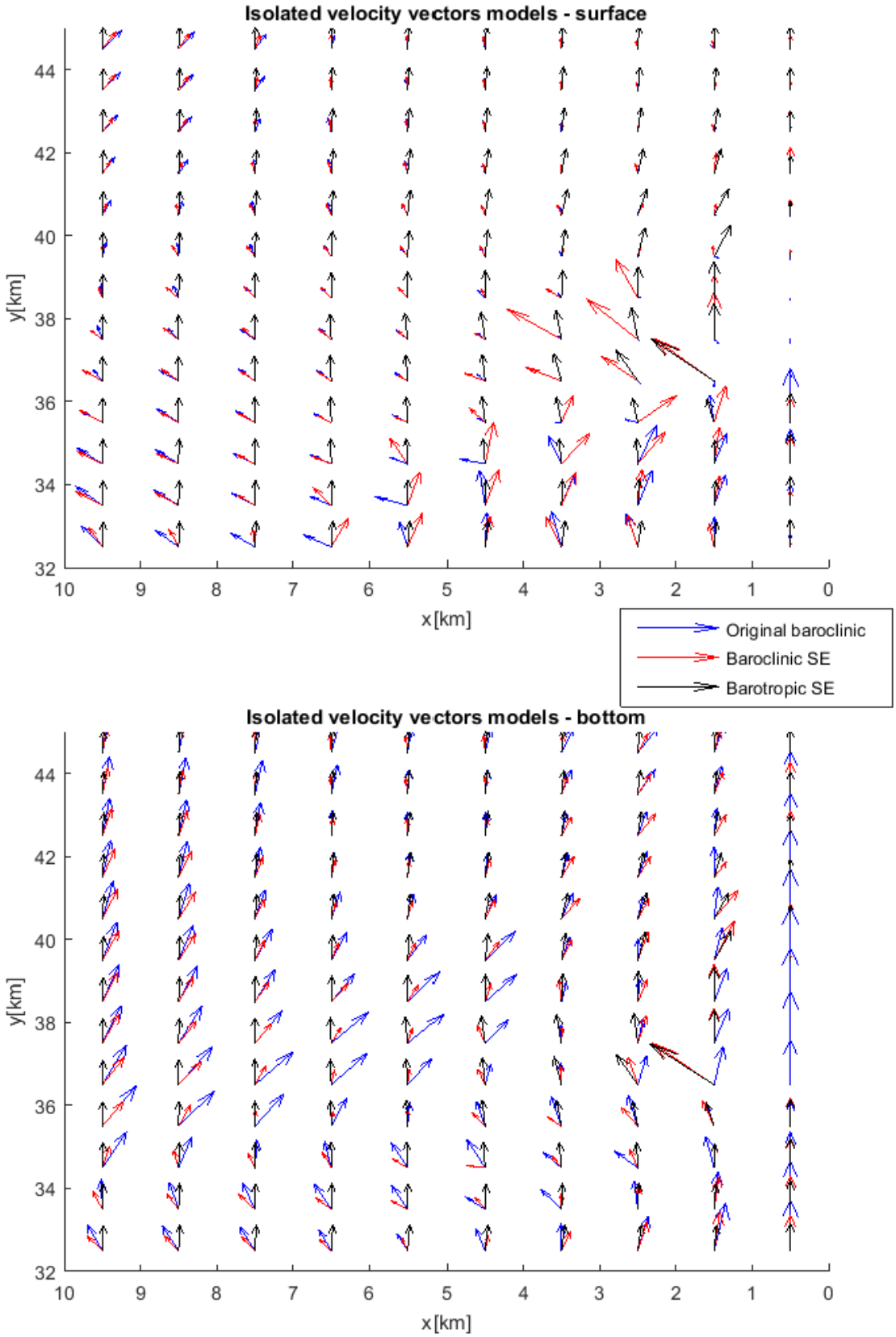

Figure D.1: Velocity vectors for neap tide at 11AM (LT+5).

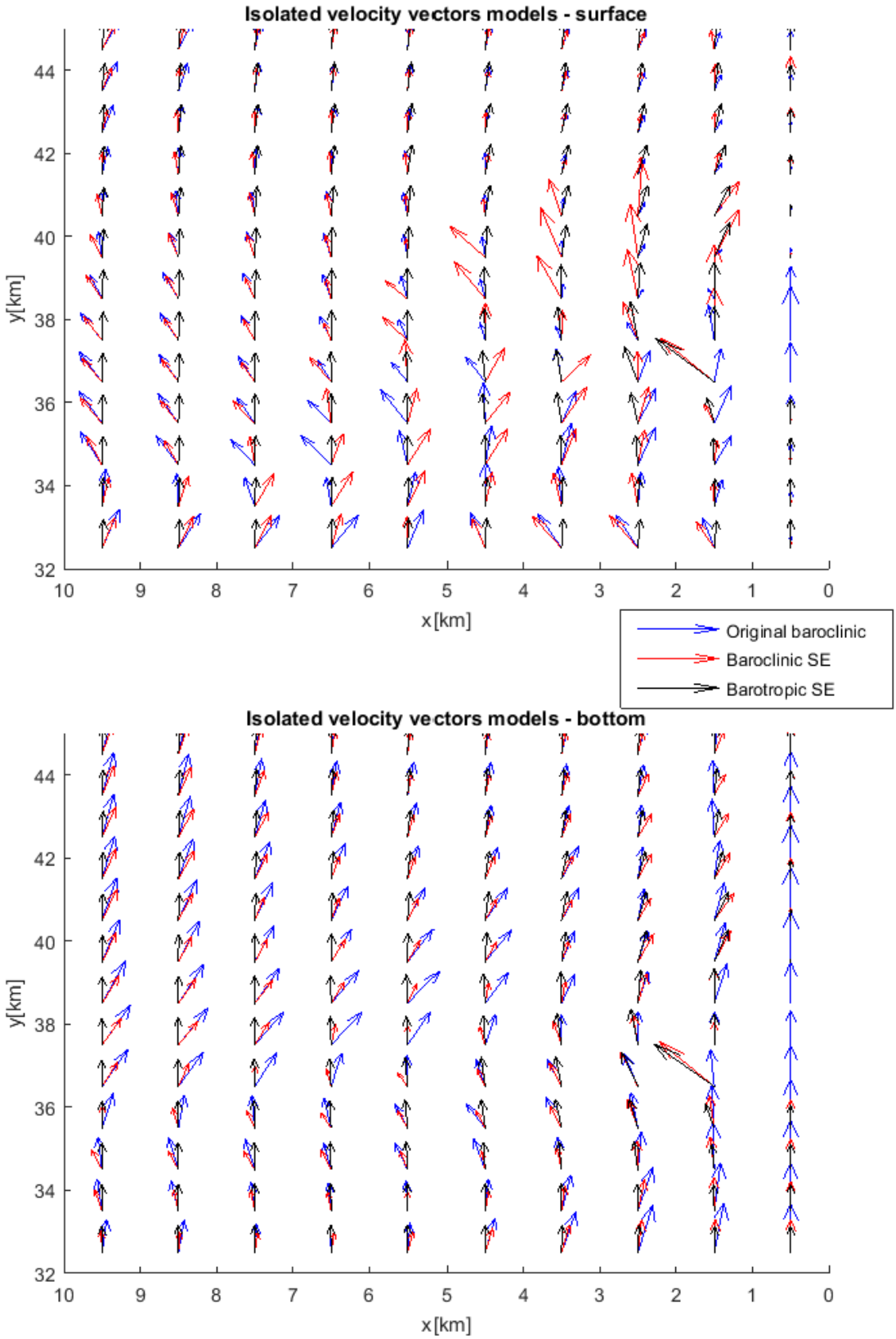

Figure D.2: Velocity vectors for neap tide at 12PM (HT).

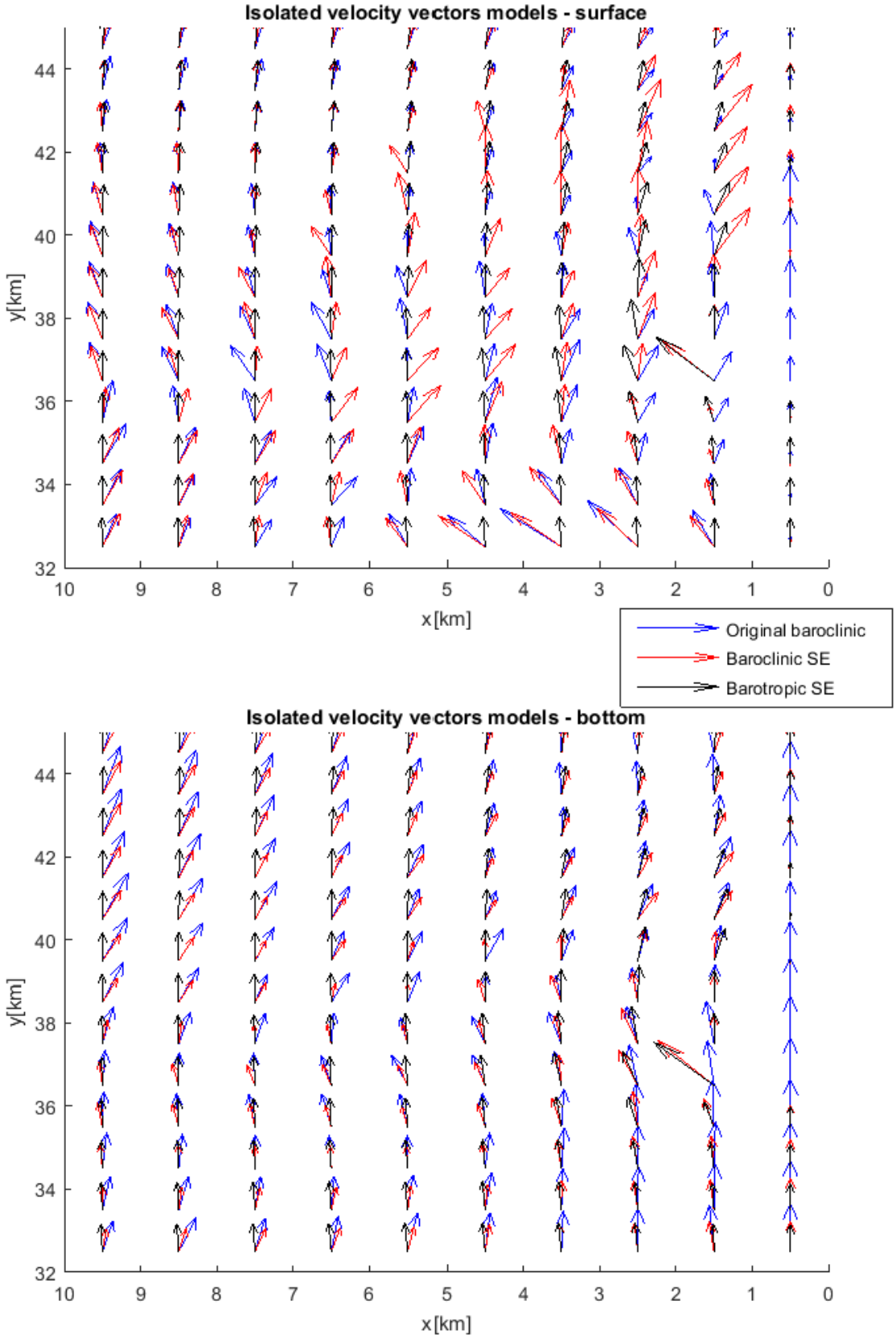

Figure D.3: Velocity vectors for neap tide at 1PM (HT+1).

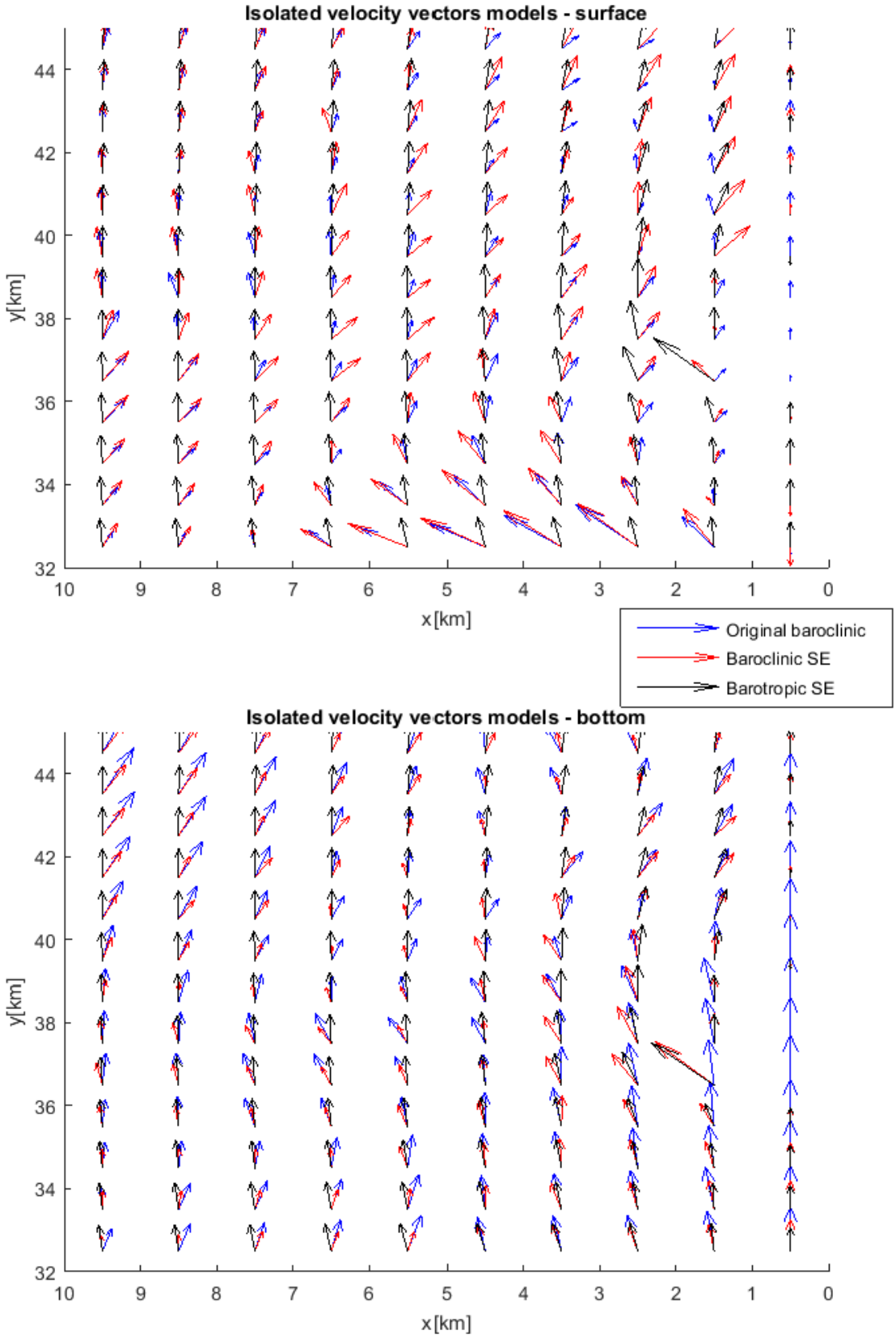

Figure D.4: Velocity vectors for neap tide at 2PM (HT+2).

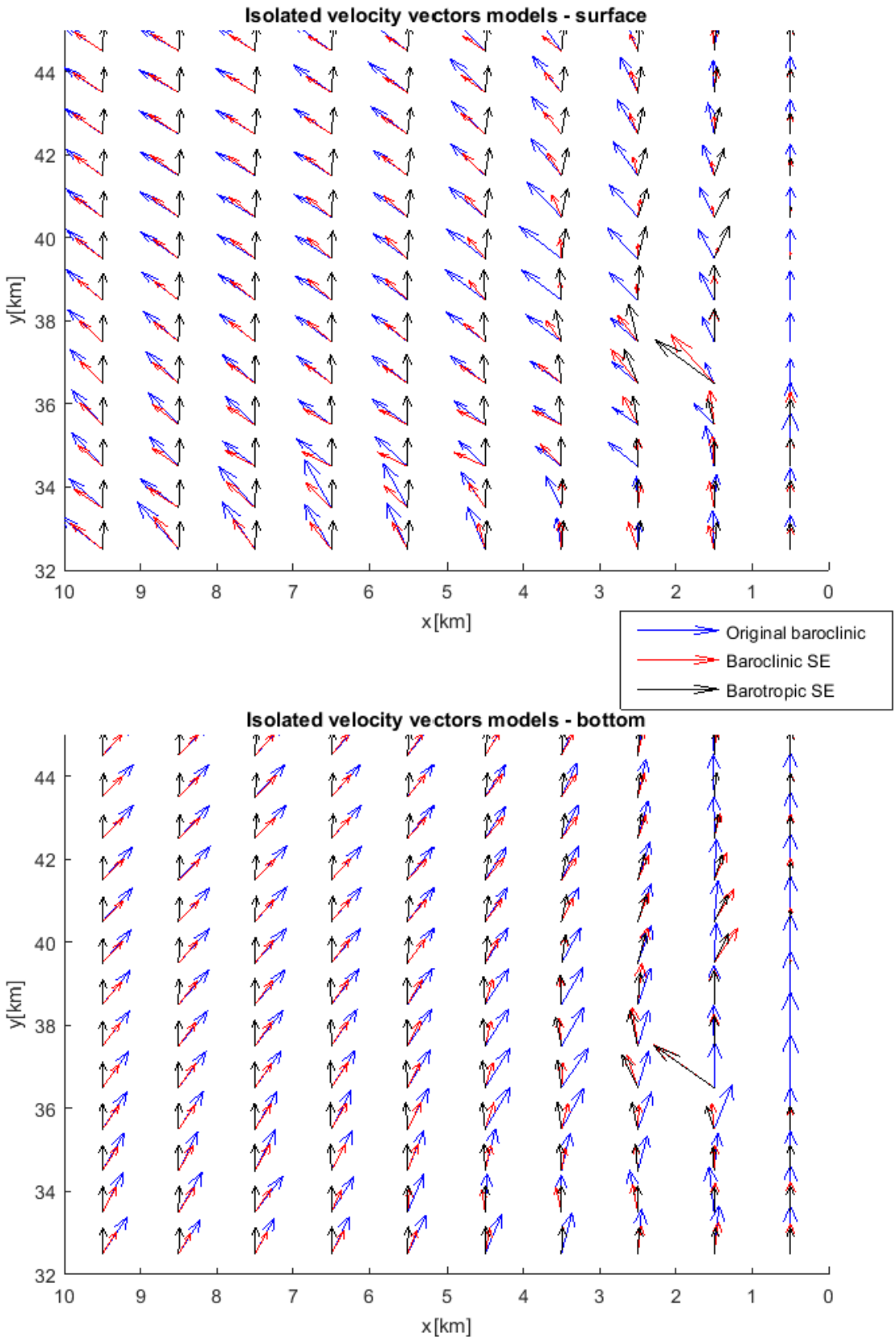

Figure D.5: Velocity vectors for spring tide at 11AM (LT+5).

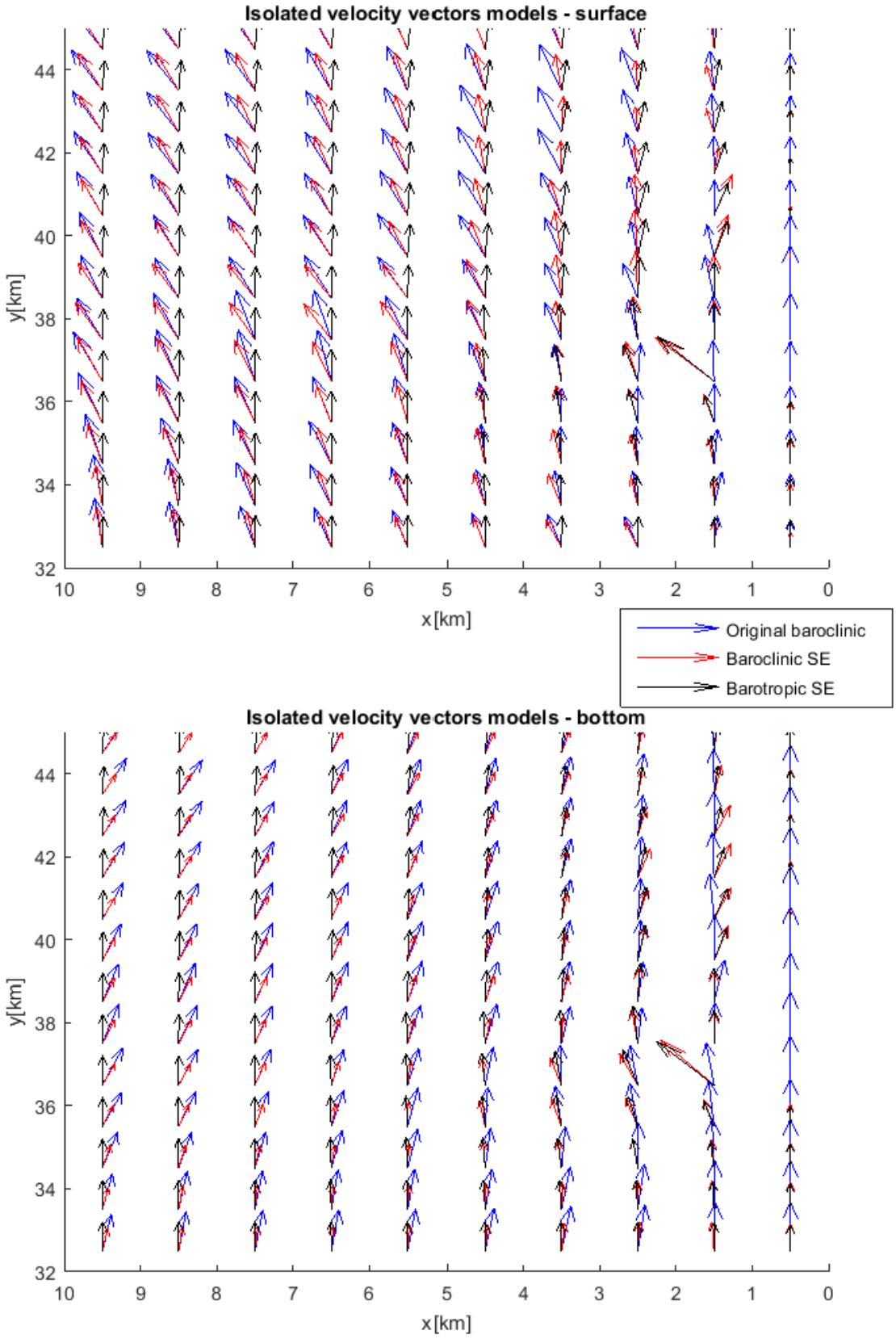

Figure D.6: Velocity vectors for spring tide at 12PM (HT).

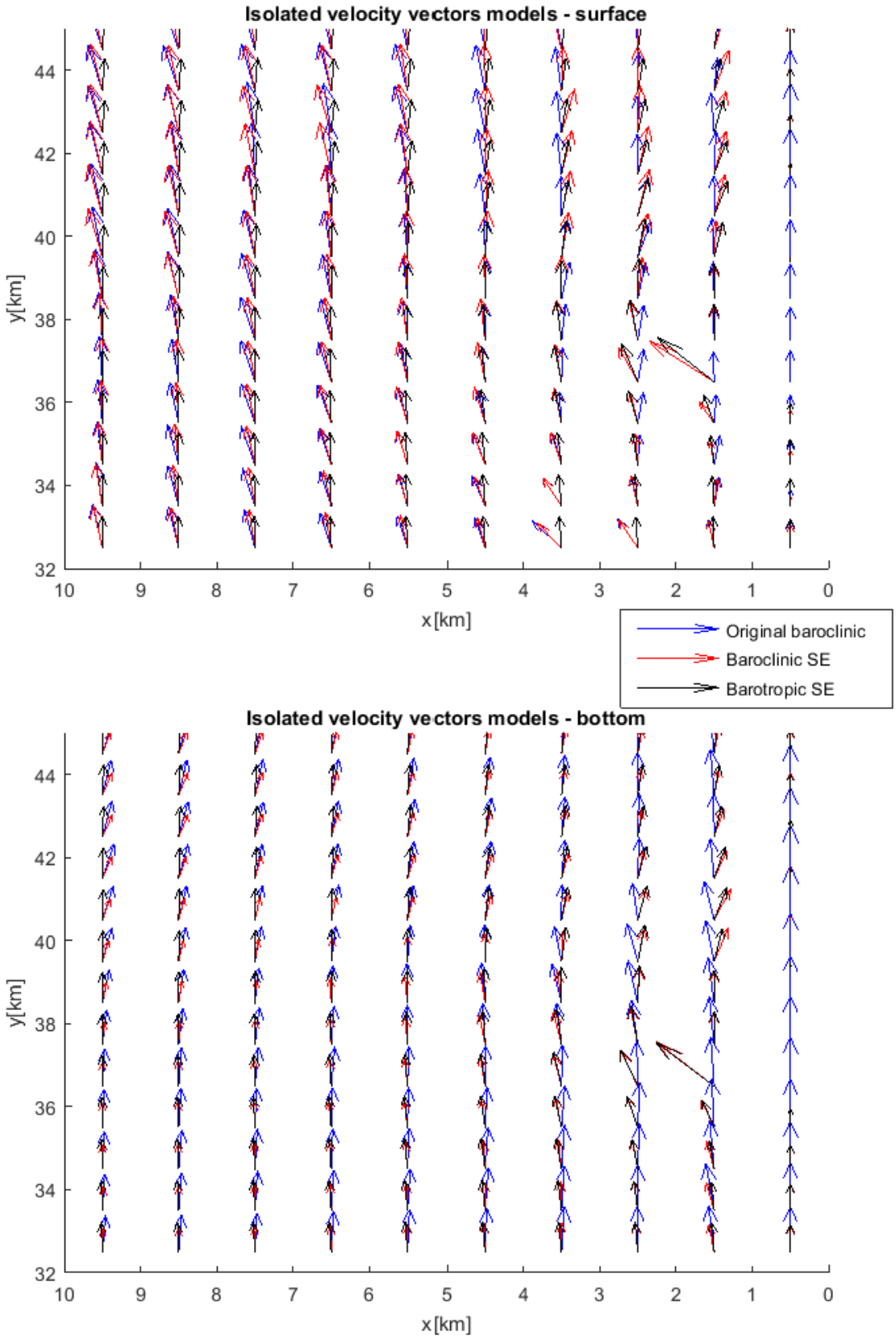

Figure D.7: Velocity vectors for spring tide at 1PM (HT+1).

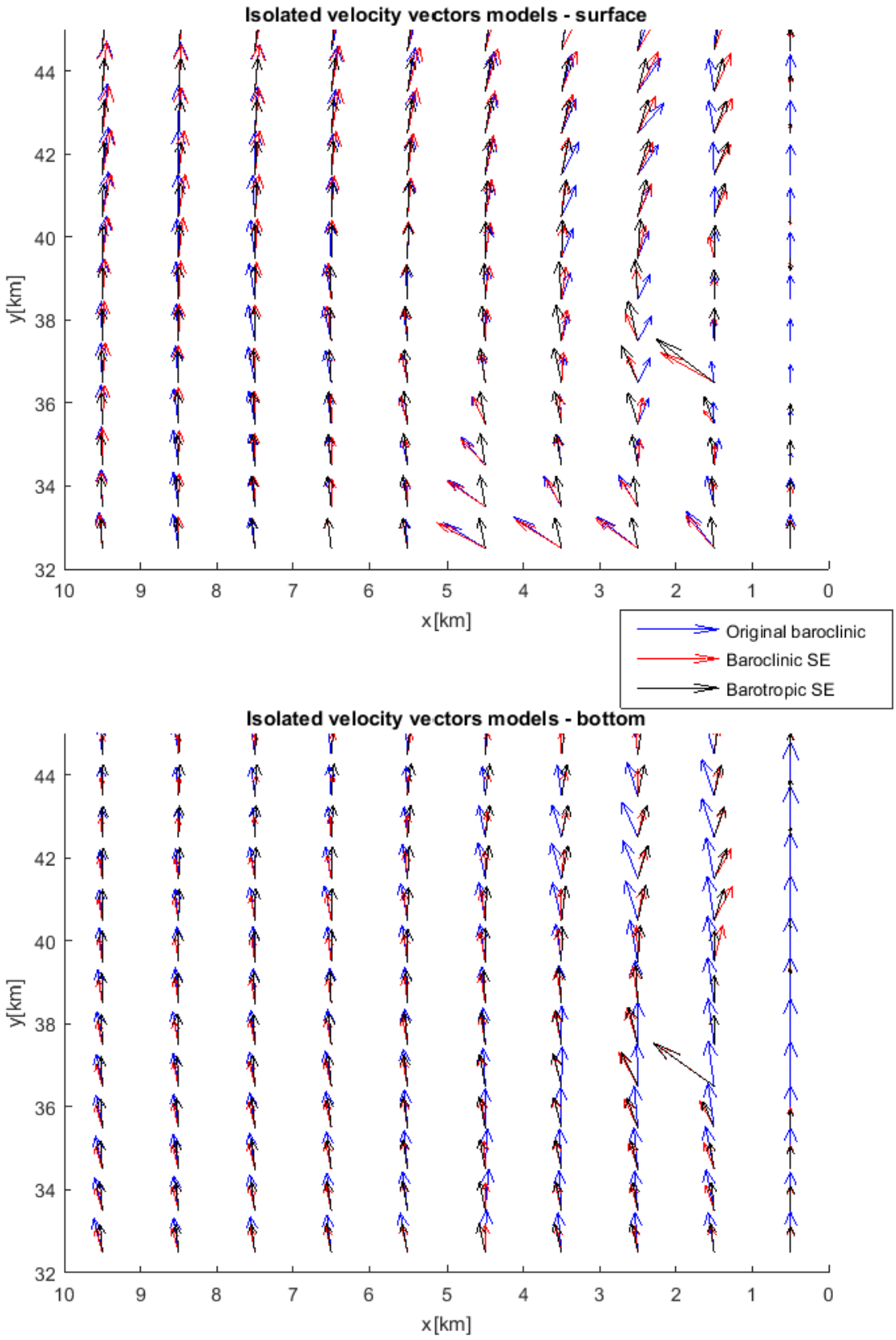

Figure D.8: Velocity vectors for spring tide at 2PM (HT+2).

Attachment E. Salinization of the surface water near the Sand Engine during spring tide conditions

In section 5.2.3 the appearance of salty water around the Sand Engine was discussed. This attachment will go into more detail. Figure E.1 plots the salinities in time such that the development of the salinization can be seen.

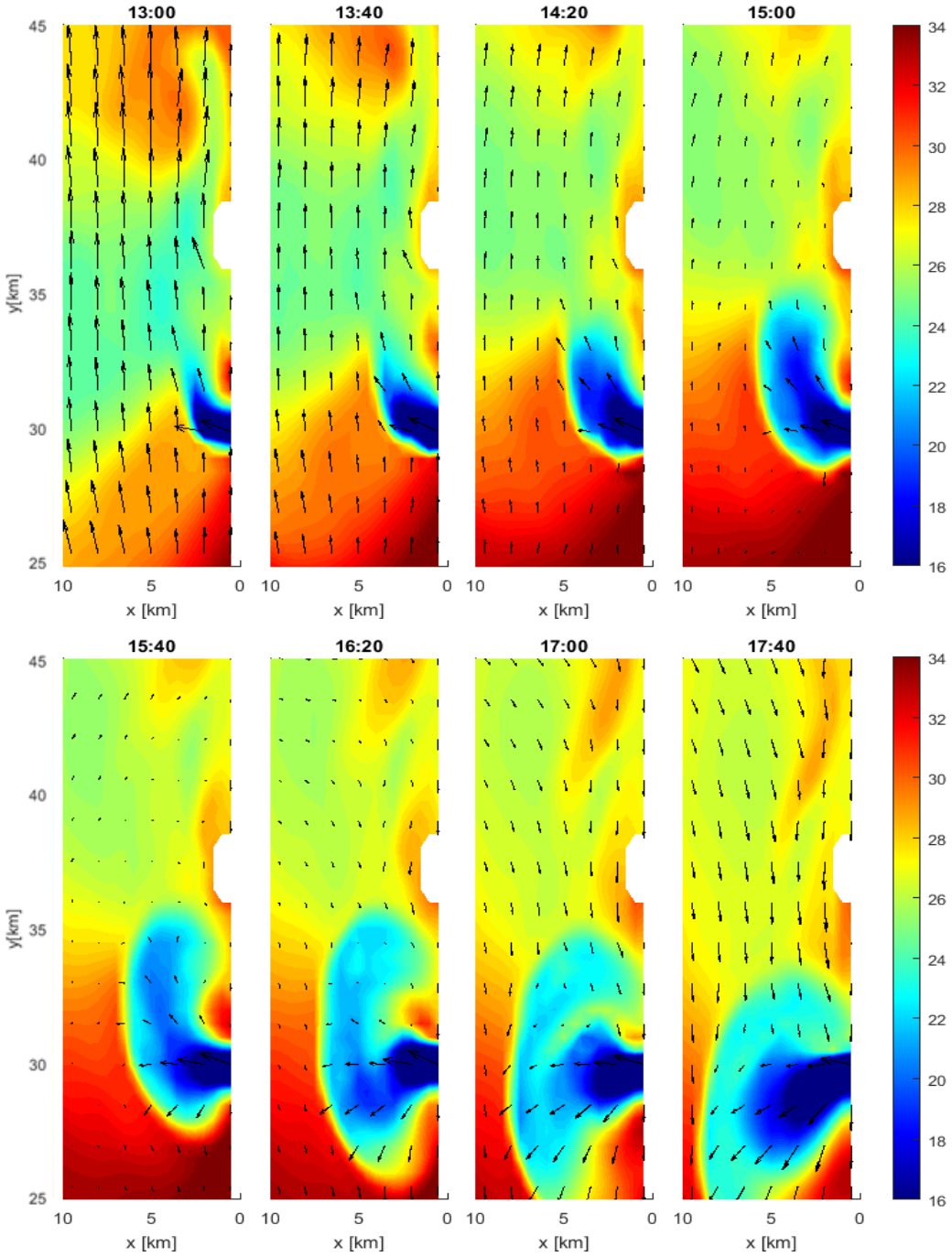

Figure E.1: Plots of salinities and velocities in time showing the salinization of the area surrounding the Sand Engine

The first step in the appearance of this feature is the mixing of the fresh water feature found around high tide. Traces of this fresh water feature can still be seen three kilometres north of the Sand Engine, where rather low salinities can be distinguished. The mixing of the fresh water during spring conditions is in contrast with neap conditions where the fresh water sustains (e.g. in Figure 5.4 it can be seen that at low tide fresh water still surrounds the Sand Engine). The higher energy levels during spring conditions allow for the tidal mixing to occur.

Once an "average" salinity has been reached the possibility is gained to increase the salinity even further. This is only possible with ongoing tidal propagation towards the north. These tidal currents get deflected in the offshore direction due to the presence of the Sand Engine (for continuity reasons the flow is pushed offshore, similar to the reason of the offspring of the fresh water feature). The cross-shore current is strongest at the surface as the tidal flow velocities are also largest at the surface. This cross-shore component at the southwest corner of the Sand Engine persists as long as the tidal flow is in northern direction. From a mass balance it can be concluded that upwelling has to occur at the land boundary. As the deeper water is much saltier (compare Figure 5.8 and Figure 5.9), the surface layer also becomes saltier. The mechanism is schematized in Figure E.2 below.

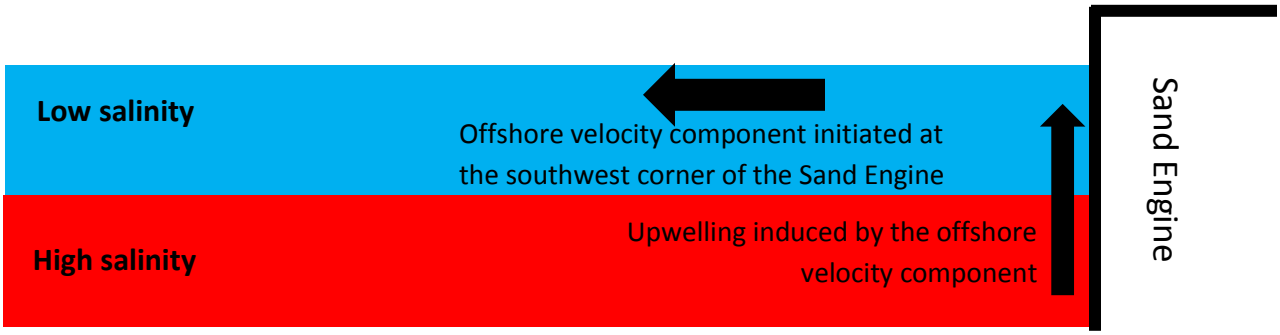

Figure E.2: Simplified schematization of the likely cause of the salinization around the Sand Engine between high and low tide (3 p.m.).

The confidence in this mechanism indeed being the cause of the momentary salinization is enhanced by Figure E.3. In this figure vertical velocities and cross-shore velocities have been plotted for a cross-section at the location of the Sand Engine (km 37.5 in y-direction of the model). The two left plots show the velocities of the original simulation whereas the right two figures show the velocities for the model including the Sand Engine. A clear transition can be seen from onshore to offshore velocities at the surface near the edge of the Sand Engine. Rather strong upwelling can also be distinguished at the new land border (upper right figure).

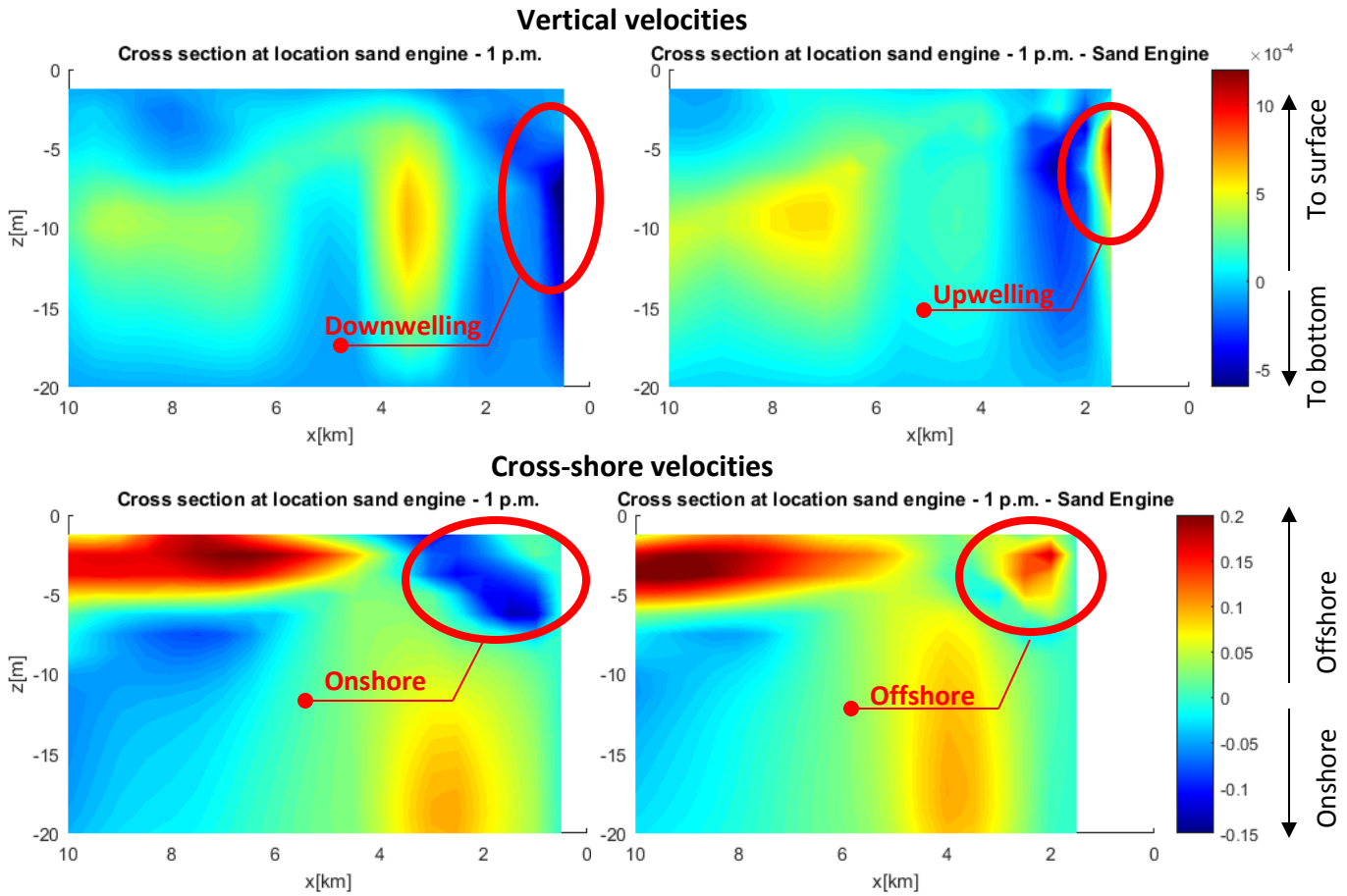

Figure E.3: Figures explaining the salinities in the surface layer surrounding the Sand Engine. Cross-plots are shown at kilometre 37.5 at 1 p.m. *Top left panel*: vertical velocities without the Sand Engine. *Top right panel*: vertical velocities with the Sand Engine. *Bottom left panel*: cross shore velocities without the Sand Engine. *Bottom right panel*: cross shore velocities with the Sand Engine. Upwelling induced by (barotropic) offshore velocities starts at 1 p.m. At depth salinities are higher and thus due to the upwelling the salinity increases near the surface.